




Review

# Layered Oxygen-Deficient Double Perovskites as Promising Cathode Materials for Solid Oxide Fuel Cells

Andrei I. Klyndyuk <sup>1,\*</sup>, Ekaterina A. Chizhova <sup>1</sup>, Dzmitry S. Kharytonau <sup>2</sup> and Dmitry A. Medvedev <sup>3,4</sup>

- <sup>1</sup> Department of Physical, Colloid and Analytical Chemistry, Organic Substances Technology Faculty, Belarusian State Technological University, Sverdlova 13a, 220006 Minsk, Belarus; chizhova@belstu.by
- <sup>2</sup> Jerzy Haber Institute of Catalysis and Surface Chemistry, Polish Academy of Sciences, Niezapominajek 8, 30-239 Krakow, Poland; dmitry.kharitonov@ikifp.edu.pl
- <sup>3</sup> Laboratory of Electrochemical Devices Based on Solid Oxide Proton Electrolytes, Institute of High Temperature Electrochemistry, Ural Branch of Russian Academy of Sciences, 620660 Ekaterinburg, Russia; dmitrymedv@mail.ru
- <sup>4</sup> Hydrogen Energy Laboratory, Ural Federal University, 620002 Ekaterinburg, Russia
- \* Correspondence: klyndyuk@belstu.by

**Abstract:** Development of new functional materials with improved characteristics for solid oxide fuel cells (SOFCs) and solid oxide electrolysis cells (SOECs) is one of the most important tasks of modern materials science. High electrocatalytic activity in oxygen reduction reactions (ORR), chemical and thermomechanical compatibility with solid electrolytes, as well as stability at elevated temperatures are the most important requirements for cathode materials utilized in SOFCs. Layered oxygen-deficient double perovskites possess the complex of the above-mentioned properties, being one of the most promising cathode materials operating at intermediate temperatures. The present review summarizes the data available in the literature concerning crystal structure, thermal, electrotransport-related, and other functional properties (including electrochemical performance in ORR) of these materials. The main emphasis is placed on the state-of-art approaches to improving the functional characteristics of these complex oxides.

**Keywords:** SOFCs; SOECs; layered perovskite; double perovskite; cobaltites; oxygen deficiency; cathode materials; thermal expansion; thermal stability; electrical transport; electrochemistry; energy conversion



**Citation:** Klyndyuk, A.I.; Chizhova, E.A.; Kharytonau, D.S.; Medvedev, D.A. Layered Oxygen-Deficient Double Perovskites as Promising Cathode Materials for Solid Oxide Fuel Cells. *Materials* **2022**, *15*, 141. <https://doi.org/10.3390/ma15010141>

Academic Editor: Enrico Negro

Received: 28 November 2021

Accepted: 22 December 2021

Published: 25 December 2021

**Publisher's Note:** MDPI stays neutral with regard to jurisdictional claims in published maps and institutional affiliations.



**Copyright:** © 2021 by the authors. Licensee MDPI, Basel, Switzerland. This article is an open access article distributed under the terms and conditions of the Creative Commons Attribution (CC BY) license (<https://creativecommons.org/licenses/by/4.0/>).

## 1. Introduction

Fuel cells (FCs) are electrochemical devices in which the chemical energies of different fuels (including fossil fuels) can be directly and effectively converted into electrical energy in one stage [1,2]. In FCs the restrictions of the Carnot cycle are absent; therefore, the thermodynamic efficiency of these devices may reach 90% and higher [3] depending on their composition, interval of working temperatures, etc. These devices are categorized into different groups which consider geometrical design [1], fuel (hydrogen, biomass, hydrocarbons, alcohols, etc.) [2], used electrolyte (proton-conducting membranes, oxygen- and proton-conducting solid oxide fuel cells (SOFCs), etc.) [3], and operating temperature range (low-temperature, intermediate-temperature, and high-temperature FCs), etc. Taking into account peculiarities of the SOFC's design, they can be divided into typical asymmetrical (A-SOFCs, in which the cathode and the anode are made of different materials) and symmetrical (S-SOFCs, in which the cathode and the anode materials are the same) derivatives [4]. Typically, SOFCs are divided into three groups according to their operation temperatures (and the solid electrolyte used in them): high-temperature SOFCs (HT-SOFCs, 1073–1273 K, and ZrO<sub>2</sub>- or CeO<sub>2</sub>-based solid electrolytes), intermediate-temperature SOFCs (IT-SOFCs, 873–1073 K, and LaGaO<sub>3</sub>-based solid electrolytes), and low-temperature SOFCs (LT-SOFCs, < 873 K, and δ-Bi<sub>2</sub>O<sub>3</sub> or Bi<sub>4</sub>V<sub>2</sub>O<sub>11</sub>-based solid electrolytes) [5–10]. Usually, oxygen-ion-conducting solid electrolytes are widely used in SOFCs (such as the above

mentioned electrolytes and others [5–10]), but recently increasing attention has been paid to proton-conducting BaCeO<sub>3</sub>- and BaZrO<sub>3</sub>-based solid electrolytes [2,8,10,11], which exhibit some advantages over oxygen-ionic electrolytes, especially at intermediate and low temperatures.

Despite essential progress, which recently has been achieved in the development of individual SOFCs materials (electrolytes, anodes, cathodes, collectors, and sealants) [3,6–10,12–20] and the production and testing of SOFCs [1,2,7,21–23], some urgent challenges still exist. One of the most important of these challenges is the search for, development of, and study of new electrode materials, which possess high stability, thermal and chemical compatibility, and improved electrochemical performance towards cathode and electrode reactions occurring in SOFCs. Regarding anodes (fuel electrodes), this problem was partially solved by the development of a new class of anode materials based on double perovskite molybdates SrMMoO<sub>6</sub> (M = Ni, Mg, and Fe) and their derivatives, including cermets [4,24,25]. Discussing the cathodes (oxygen or air electrodes), one of the most interesting and promising materials for IT-SOFCs are the layered oxygen-deficient double perovskites, LnBaM<sub>2</sub>O<sub>6-δ</sub> (Ln—rare-earth element; M—3d-metal), which have been intensively studied with this aim for last two decades [4,8–10]. Due to the high tolerance of perovskite structure, these complex oxides can be formed at different combinations of their constituents, demonstrating outstanding thermal, electrotransport-related, magnetic, electrochemical, and other properties. As a result, these double perovskites can be used as working elements of chemical gas sensors, high-temperature thermoelectrics, cathode materials of IT-SOFCs, etc. [26].

The present article provides an overview of peculiarities of the crystal structure, physicochemical properties, and electrochemical performance of layered oxygen-deficient perovskites as cathode materials of SOFCs, as well as ways and methods of improving the functional characteristics of these materials.

## 2. Cathode Materials for IT-SOFCs: Past, Present, and Future

An ideal cathode material for a SOFC must possess [27–33]: (a) high electronic (*n*- or *p*-type) conductivity (in an oxidizing atmosphere, preferably, more than 10<sup>2</sup> S cm<sup>-1</sup>); (b) thermal and chemical compatibility with solid electrolytes and interconnectors; (c) enough large porosity to provide fast diffusion of gaseous oxygen through a cathode to a triple-phase cathode–solid electrolyte–gas phase interface; (d) high stability in an oxidizing atmosphere; (e) high catalytic activity in an oxygen reduction reaction (ORR); and (f) low cost.

Typical cathode materials utilized in SOFCs are perovskites (ABO<sub>3</sub>) of light rare-earth elements (REE), 3d-metals (usually, Mn, Fe, Co, and Ni), and their solid solutions and composites [4,6–10,27,34–39]. Among all cathode materials, Co-based perovskites and their derivatives received enormous research interest and played an integral role in the development and commercialization of IT-SOFCs [14,21,26,39]. Figure 1 shows the crystal structures of perovskites and other complex oxides possessing mixed ionic–electronic conductivity (MIEC), which have been used as cathode materials for SOFCs operating in different temperature intervals. A common strategy for tuning their functional properties is the partial heterovalent substitution of A- or/and B-site cations in their structure, mostly to enhance electrical conductivity and to lower the value of the thermal expansion coefficient (TEC). To decrease the electrode polarization losses at reduced operating temperatures, the addition of noble metals (Pd, Ag, and Pt) to the cathode material is used as well [27]. To increase the compatibility of these compounds with the solid electrolyte, they are often used in the form of composites.

During the investigation of ABO<sub>3</sub> perovskite solid solutions, a new class of oxide materials (named layered oxygen-deficient double perovskites (LODPs)), LnBa(M',M'')<sub>2</sub>O<sub>6-δ</sub> (Ln is REE; M', M'' are 3d-metals) (cation-ordered phases), was purposefully designed. Their electrochemical performance is reported to be better than that of the parent perovskites. Therefore, these phases are currently considered as being very promising cathode

materials, especially for IT-SOFCs [4,6,8–10,34,35,40,41] and have been intensively studied both as single materials and SOFCs components [42].

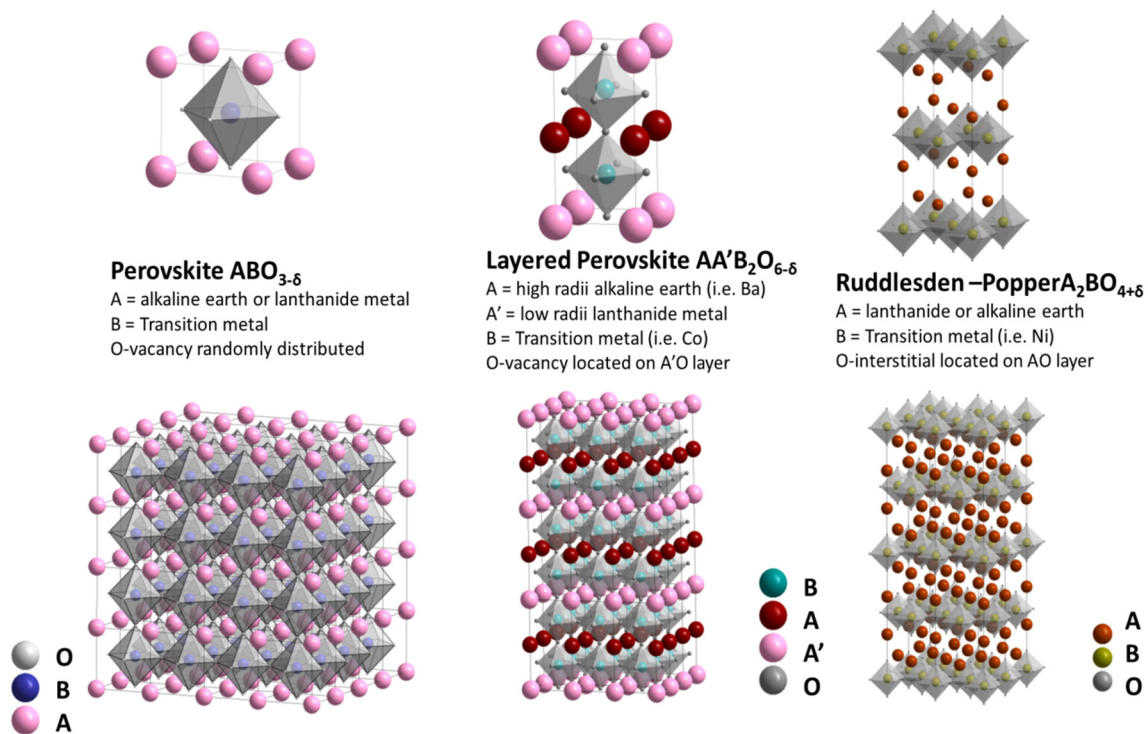


**Figure 1.** Crystal structures of perovskite, double perovskite, and Ruddlesden–Popper phase (Reproduced from [40] with permission from the Royal Society of Chemistry).

Another group of cathode materials includes complex oxides with so-called Ruddlesden–Popper (RP) phases (layered oxides) with a general formula of  $A_{n+1}B_nO_{3n+1}$ . These compounds, for example,  $Ln_2NiO_{4+\delta}$  ( $Ln = La, Pr, Nd$ ), and their solid solutions possess high diffusivity of interstitial oxygen ions, comparatively low TEC values, and high enough electrical conductivity, which also makes them promising for SOFCs applications [6,8,10,27,40]. Other RP phases, such as  $(Sr,La)_3(Fe,Co)_2O_{7-x}$  ( $n = 2$ ) and  $(La,Sr)_4(Fe,Co)_3O_{10-x}$  ( $n = 3$ ) showed good electrocatalytic activity in ORR in single cell measurements [6].

Recently, it has been shown that effective cathodes for proton-conducting SOFCs operating at low and intermediate temperatures are  $Ba(Ce,Zr)O_3$ -based solid solutions doped with transition elements in high concentration. These phases demonstrate excellent chemical compatibility with typical proton-conducting solid electrolytes due to the similarity of their compositions [43,44]. These compounds belong to the triple-conducting oxides (TCOs) [45–47], in which transport species are simultaneously protons, oxygen ions, and electrons (holes). The advantage of TCOs as cathode materials for proton-conducting SOFCs is that both protons from the solid electrolyte and oxygen species adsorbed from the air may migrate through the bulk and over the surface of the cathode, which extends the reaction area over the whole electrode. We should note that LODPs, such as  $LnBa_{0.5}Sr_{0.5}Co_{1.5}Fe_{0.5}O_{5+\delta}$  ( $Ln = Pr, Nd$ ), when used as cathodes for proton-conducting SOFCs, also belong to the class of TCOs [9,44]. According to [48], triple conductivity in LODPs can appear due to the formation of impurity phases, which should be taken into account for the development of new TCOs.

Very interesting and promising materials for use in SOFCs are high-entropy ceramics (HECs, Figure 2), which are solid solutions of inorganic compounds (including metal oxides) with one or more Wyckoff site shared by equal or near-equal atomic ratios of five (or occasionally four) constituting elements [49,50]. The so-called compositionally complex ceramics (CCCs) include, besides HECs, medium-entropy and/or non-equimolar

compositions [51]. It has been shown recently that medium- and high-entropy perovskite oxides, such as  $\text{Sr}(\text{Fe}_\alpha\text{Ti}_\beta\text{Co}_\gamma\text{Mn}_\zeta)\text{O}_{3-\delta}$  [52],  $(\text{La},\text{Sr})(\text{Co},\text{Cr},\text{Fe},\text{Mn},\text{Ni})\text{O}_{3-\delta}$  [53,54], and  $(\text{La},\text{Pr},\text{Nd},\text{Sm},\text{Ba},\text{Sr})(\text{Co},\text{Fe},\text{Ni},\text{Cu})\text{O}_{3-\delta}$  [55] demonstrate lower TECs with a lack of visible contribution from the chemical expansion effect and a more stable and much lower polarization resistance compared with the conventional cathode materials. These peculiarities make such materials very attractive for electrochemical applications.

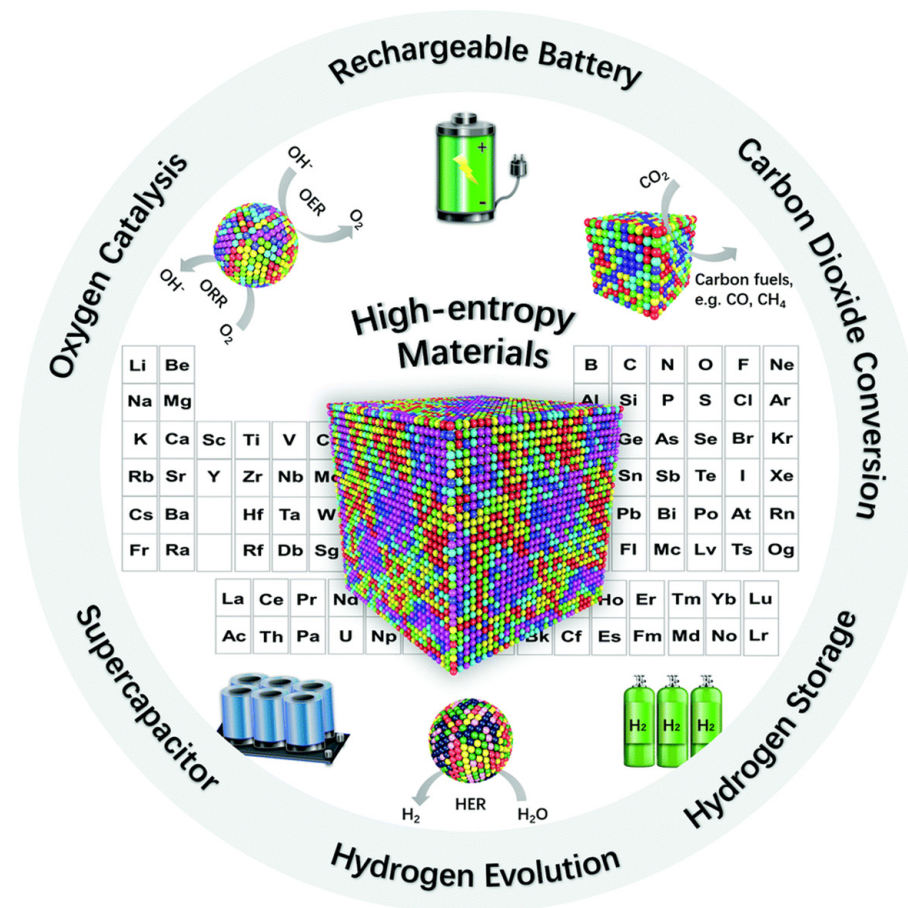
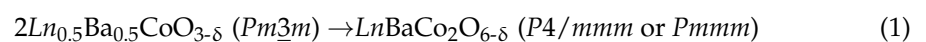


**Figure 2.** Fields of using high-entropy materials for energy conversion and storage purposes (Reproduced from [49] with permission from the Royal Society of Chemistry).

### 3. Crystal Structure, Phase Transitions, and Physicochemical and Functional Properties of Layered Oxygen-Deficient Double Perovskites

The crystal structure of  $\text{LnBa}(M',M'')_2\text{O}_{6-\delta}$  LODPs, consisting of alternating  $(-\text{BaO}-)$ ,  $(-M'M'')\text{O}_2-$  and  $\text{LnO}_{1-\delta}$  layers, is formed due to the ordering of oxygen vacancies,  $\text{Ln}$ , and  $\text{Ba}$  atoms in the structure of oxygen deficient  $\text{Ln}M'(M'')\text{O}_{3-\delta}$  perovskites according to Equation (1):



A structural phase transition occurs at such an arrangement: cubic perovskite structure ( $Pm\bar{3}m$ ) transforms into a tetragonal ( $P4/mmm$ ) or an orthorhombic ( $Pmmm$ ) structure (Figure 3). A different character of oxygen-vacancy ordering, as well as the ordering of  $M'$  and  $M''$  ions, may result in the fact that LODPs crystallize in other space groups (SGs), such as  $P\bar{1}$ ,  $P2$ , or  $Ammm$  [26]; nevertheless,  $P4/mmm$  or  $Pmmm$  are the most typical ones.



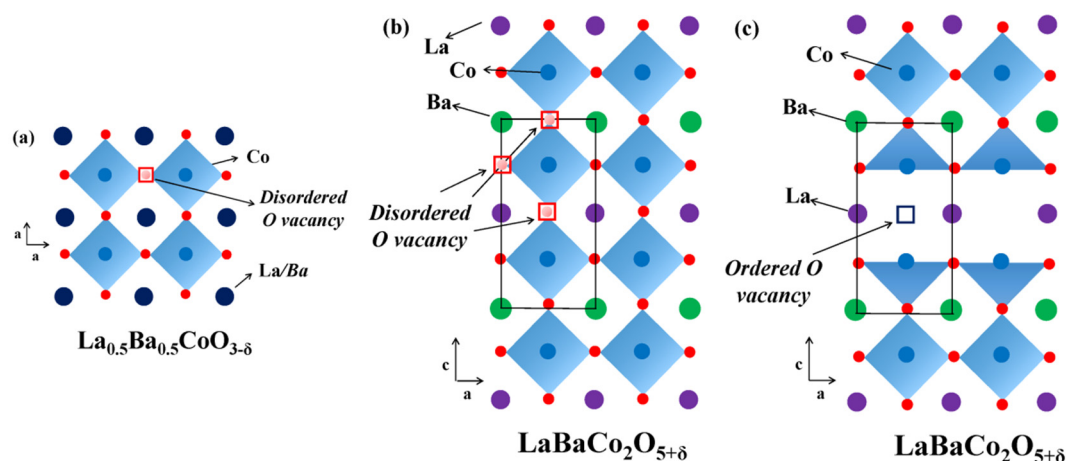


**Figure 3.** Crystal structures of (a) cubic  $Pm\bar{3}m$  single perovskite  $\text{La}_{0.5}\text{Ba}_{0.5}\text{CoO}_{3-\delta}$ ; (b) tetragonal  $P4/mmm$  ordered A-site cation and disordered oxygen-vacancy double perovskite  $\text{LaBaCo}_2\text{O}_{5+\delta}$ ; (c) orthorhombic  $Pmmm$  both an ordered A-site cation and ordered oxygen-vacancy double perovskite  $\text{LaBaCo}_2\text{O}_{5+\delta}$  (reproduced with permission from [56]. Copyright 2016, Multidisciplinary Digital Publishing Institute).

This transition usually occurs at high temperatures and low oxygen partial pressures and may proceed through the formation of an intermediate product with a complex domain structure, which has a strong affinity with oxygen and may exchange it with an atmosphere at relatively low temperatures (ca. 340 K) [57].

Oxygen content variation in LODPs results in a change in their structure, which takes place at different temperatures depending on the cationic composition and oxygen partial pressure. For example,  $\text{GdBaCo}_{2-x}\text{Fe}_x\text{O}_{6-\delta}$  ( $0 \leq x \leq 0.4$ ) perovskites undergo a  $Pmmm$ – $P4/mmm$  phase transition at approximately 730–760 K [58]. Layered cobaltites of REE and barium undergo the dielectric-metal transition, in which their electrical conductivity increases by several orders of magnitude. This is caused by a change in the spin state of the cobalt ions [26,59]. At high temperatures, these phases are paramagnetic, but at cooling LODPs become antiferro-, ferri-, or ferromagnetic [26,60–62] due to a different type of ordering of magnetic moments of the transition metal ions in their structure.

Electrical conductivity values of LODPs vary widely depending on their cationic composition and oxygen nonstoichiometry [26,58,60,62–67]. For compounds which contain light REEs and possess small oxygen deficiencies, electrical conductivity is approximately  $10^3 \text{ S cm}^{-1}$  (such phases are metal-like conductors). On the contrary, for compounds composed of heavy REE and possessing large oxygen deficiency, conductivity is approximately  $10^{-8} \text{ S cm}^{-1}$ , which is typical for dielectrics.

Large values of both the Seebeck coefficient and the electrical conductivity of several layered cobaltites [58,68], ferrocobaltites [62,69], ferrocuprates [69–72], and other LODPs [73] make them promising candidates for use in high-temperature thermoelectrogenerators (TEGs) for effective conversion of heat into electrical energy.

Double perovskites  $\text{LnBaCo}_2\text{O}_{5+\delta}$  ( $\text{Ln} = \text{Eu}, \text{Gd}, \text{and Sm}$ ) containing weakly-bonded oxygen ( $\delta$ ) and cobalt ions in different oxidation states ( $\text{Co}^{2+}$ ,  $\text{Co}^{3+}$ ,  $\text{Co}^{4+}$ ) demonstrate certain photocatalytic activity during the degradation of Congo Red, which indicates that they may be promising photocatalysts for the oxidation (degradation) of organic substances [74].

To be used in high-temperature devices, such as SOFCs, solid oxide electrolysis cells (SOECs), TEGs, and other applied directions, LODPs must possess a good thermomechanical and chemical compatibility with other components of these devices [75]. The first condition of thermomechanical compatibility is the similarity of their TEC values with those of the typical solid electrolytes used in SOFCs. The TEC values for some typical LODPs are set out in Table 1. As can be seen, for the layered perovskites with only Co

atoms in B-site, the TEC values vary within ca.  $(17–24) \times 10^{-6} \text{ K}^{-1}$ ; the measured TECs are much higher than those of the commonly used  $\text{ZrO}_2$ -,  $\text{CeO}_2$ -, and  $\text{LaGaO}_3$ -based solid electrolytes (as a rule, between  $(10–13) \times 10^{-6} \text{ K}^{-1}$ ) [5].

**Table 1.** TEC values of some layered oxygen-deficient perovskites.

Compound (Space Group)	TEC $10^6, \text{K}^{-1}$	Temperature Interval, K	Refs.
NdBaCoFeO <sub>5+δ</sub> ( <i>P4/mmm</i> )	16.6	300–653	[62]
	26.5	653–1100	
SmBaCoFeO <sub>5+δ</sub> ( <i>P4/mmm</i> )	13.6	300–518	[62]
	19.3	518–1100	
GdBaCoFeO <sub>5+δ</sub> ( <i>P4/mmm</i> )	12.9	300–553	[62]
	19.9	553–1100	
SmBaCo <sub>2</sub> O <sub>5+δ</sub> ( <i>Pmmm</i> )	21.2	293–1173	[63]
SmBaCoCuO <sub>5+δ</sub> ( <i>Pmmm</i> )	15.0	293–1173	[63]
NdBaCo <sub>2</sub> O <sub>5+δ</sub> ( <i>P4/mmm</i> )	19.7	293–1173	[63]
NdBaCoCuO <sub>5+δ</sub> ( <i>P4/mmm</i> )	16.5	293–1173	[63]
NdBaCo <sub>2</sub> O <sub>5+δ</sub> ( <i>P4/mmm</i> )	18.3	300–530	[64]
	23.8	530–1300	
NdBaCo <sub>1.8</sub> Fe <sub>0.2</sub> O <sub>5+δ</sub> ( <i>P4/mmm</i> )	18.8	300–530	[64]
	21.9	530–1300	
NdBaCo <sub>1.6</sub> Fe <sub>0.4</sub> O <sub>5+δ</sub> ( <i>P4/mmm</i> )	18.9	300–530	[64]
	21.9	530–1300	
NdBaCo <sub>1.4</sub> Fe <sub>0.6</sub> O <sub>5+δ</sub> ( <i>P4/mmm</i> )	18.3	300–530	[64]
	22.1	530–1300	
NdBaCo <sub>1.2</sub> Fe <sub>0.8</sub> O <sub>5+δ</sub> ( <i>P4/mmm</i> )	18.4	300–530	[64]
	21.9	530–1300	
PrBaCo <sub>2</sub> O <sub>6-δ</sub> ( <i>Pmmm</i> )	16.8	298–473	[66]
	21.6	473–1273	
NdBaCo <sub>2</sub> O <sub>6-δ</sub> ( <i>Pmmm</i> )	16.3	298–473	[66]
	21.6	473–1273	
NdBaCo <sub>2</sub> O <sub>6-δ</sub> ( <i>Pm3m</i> )	11.9	298–473	[66]
	22.6	473–1273	

The TEC values of layered oxygen-deficient double cobaltites decline when the REEs' ionic radii decrease, as well as when a partial substitution of cobalt with iron (at small doping levels) or copper occurs (Table 1). Both of these strategies are effective in improving the thermomechanical properties of LODPs. Molecular dynamics simulations have shown [76], that variations in the cationic composition or/and oxygen nonstoichiometry of layered oxygen-deficient double cobaltites is the other effective way to reduce the TEC values of these materials.

The TEC values of LODPs sharply increase at high temperatures (above ca. 500–700 K) due to the beginning of the evolution of weakly-bonded oxygen from their crystal structures into the environment. Therefore, the expansion of these phases at high temperatures is determined by both thermal and chemical factors [26,58,62,75].

The chemical expansion coefficient (CEC) values of some LODPs are provided in Table 2. As can be seen, these values vary within 0.5–2.6%, exhibiting a strong anisotropy; simultaneous chemical expansion along the *a*-axis (in the *ab*-plane) and chemical contraction along the *c*-axis (out-of-plane) take place during the evolution of weakly-bonded oxygen. According to [58,77], the former occurs due to an increase in the average radii of cobalt ions due to their reduction, but the latter occurs due to the change in the coordination environment of REE and cobalt ions.

**Table 2.** CEC values of some layered oxygen-deficient perovskites.

Compound (Space Group)	CEC 10 <sup>3</sup>	Direction	Refs.
NdBaCoFeO <sub>5+δ</sub> ( <i>P4/mmm</i> )	11.04	in-plane	[62]
	−17.27	out-of-plane	
	4.59	volume	
SmBaCoFeO <sub>5+δ</sub> ( <i>P4/mmm</i> )	20.72	in-plane	[62]
	−18.00	out-of-plane	
	23.94	volume	
GdBaCoFeO <sub>5+δ</sub> ( <i>P4/mmm</i> )	17.78	in-plane	[62]
	−12.36	out-of-plane	
	25.97	volume	
LaBaCuFeO <sub>5+δ</sub> ( <i>Pm3m</i> )	9.20	volume	[78]
LaBa <sub>0.75</sub> Sr <sub>0.25</sub> CuFeO <sub>5+δ</sub> ( <i>Pm3m</i> )	7.55	volume	[78]
PrBaCuFeO <sub>5+δ</sub> ( <i>P4/mmm</i> )	8.72	volume	[78]
LaBaCoFeO <sub>5+δ</sub> ( <i>Pm3m</i> )	17.3	volume	[79]
LaBaCoCuO <sub>5+δ</sub> ( <i>Pm3m</i> )	15.7	volume	[79]
PrBaCuFeO <sub>5+δ</sub> ( <i>P4/mmm</i> )	12.0	volume	[80]

A serious drawback of layered cobaltites is their degradation in CO<sub>2</sub>-containing atmospheres. For example, Zhu et al. [81] have studied the degradation features of PrBaCo<sub>2</sub>O<sub>5+δ</sub> in CO<sub>2</sub>-containing atmospheres. They found a considerable decrease in the electrochemical activity of PrBaCo<sub>2</sub>O<sub>5+δ</sub> electrodes due to the formation of insulating BaCO<sub>3</sub> particles at the PrBaCo<sub>2</sub>O<sub>5+δ</sub> surface.

On the other side, efficient cathodes of SOFCs should provide a large oxygen exchange rate between the atmosphere and the surface of the cathode and enough high oxygen mobility. Therefore, both bulk and surface chemistry in the oxygen exchange kinetics of MIEC layered perovskites are very important. It was found [82] that the surfaces of PrBaCo<sub>2</sub>O<sub>5+δ</sub> and GdBaCo<sub>2</sub>O<sub>5+δ</sub> LODPs can significantly change in their local chemical composition and can exchange by oxygen with the atmosphere even at ambient temperature.

Perry and Ishihara [83] summarized the main directions of improving the efficiency and durability of oxygen electrodes (including those based on LODPs) in SOFCs. Concerning the bulk chemistry, the areas of “electro-chemo-mechanics” are (1) the enhancement in transport and surface reactivity through the strain-state tailoring (mechano-electrical and mechano-electrochemical coupling) and (2) the mitigation of deleterious chemical expansion during operation, induced by stoichiometry changes (chemo-mechanical coupling). Regarding the surface chemistry and oxygen surface exchange kinetics, the main areas of interest are (1) clarifying the rate-limiting steps and mechanisms of oxygen incorporation/excorporation with atomistic insight; (2) exploiting the unique properties of hetero-interfaces, grain boundaries, and other large surface defects; (3) identifying the optimal composition for the outermost atomic monolayers; and (4) studying how to control the outermost chemistry in operating conditions via bulk and surface chemical tailoring.

Oxygen mobility in materials used in SOFCs and catalytic membranes was comparatively discussed in detail in [84]. The results of the investigation of chemical compatibility between different oxide electrodes and solid electrolytes in SOFCs are provided in [85]. Concerning LODPs, cathode materials such as LnBaCo<sub>2</sub>O<sub>5+δ</sub> (Ln = Pr and Gd) possess poor chemical compatibility with (Ce,Sm)O<sub>2-δ</sub> (SDC) and (Ce,Gd)O<sub>2-δ</sub> (GDC) above 1173 K and are prone to chemical reactions with the formations of BaCeO<sub>3</sub>, BaCoO<sub>3</sub>, and Sm<sub>2</sub>CuO<sub>4</sub>. The composite material of the LODP cathode with (La,Sr)(Cr,Mn)O<sub>3</sub> (LSCM) is stable below 1273 K without any obvious secondary phase formation. However, chemical interactions in this material may occur above 1473 K. Chemical reactions between the LODP cathode and Ba(Zr,Y)O<sub>3-δ</sub> (BZY) or Ba(Zr,Y,Yb)O<sub>3-δ</sub> (BZYYb) proton conductors were not observed. However, GdBaCo<sub>2</sub>O<sub>5+δ</sub> reacts with YSZ at 973 K with the formation of BaZrO<sub>3</sub>. Doping

with Fe, Cu, and Nb at the B-site of  $R\text{BaCo}_2\text{O}_{5+\delta}$  ( $R = \text{Pr}$  and  $\text{Y}$ ) can effectively improve chemical compatibility between the LODP cathodes and SDC or GDC solid electrolytes.

Figure 4 shows the XRD results for  $\text{YBaCoCuO}_{5+\delta}$  (YBCC) and  $\text{YBaCo}_{2/3}\text{Fe}_{2/3}\text{Cu}_{2/3}\text{O}_{5+\delta}$  (YBCFC), which were calcined at 1223 K for 10 h in air mixtures with different solid electrolytes (SDC, GDC, and LSCM). No impurities or shifts of diffraction peaks were observed for compositions containing YBCC (Figure 4a), indicating that this compound is chemically compatible with the studied electrolytes. On the contrary, small amounts of  $\text{Sm}_2\text{CuO}_4$  and  $\text{Gd}_2\text{CuO}_4$  impurity phases in the YBCFC–SDC and YBCFC–GDC mixtures were observed (Figure 4b), showing that the YBCFC material is incompatible with SDC and GDC electrolytes. However, the absence of impurity phases in the YBCFC–LSCM mixture indicates that YBCFC presents good chemical compatibility with LSCM solid electrolytes below 1223 K.

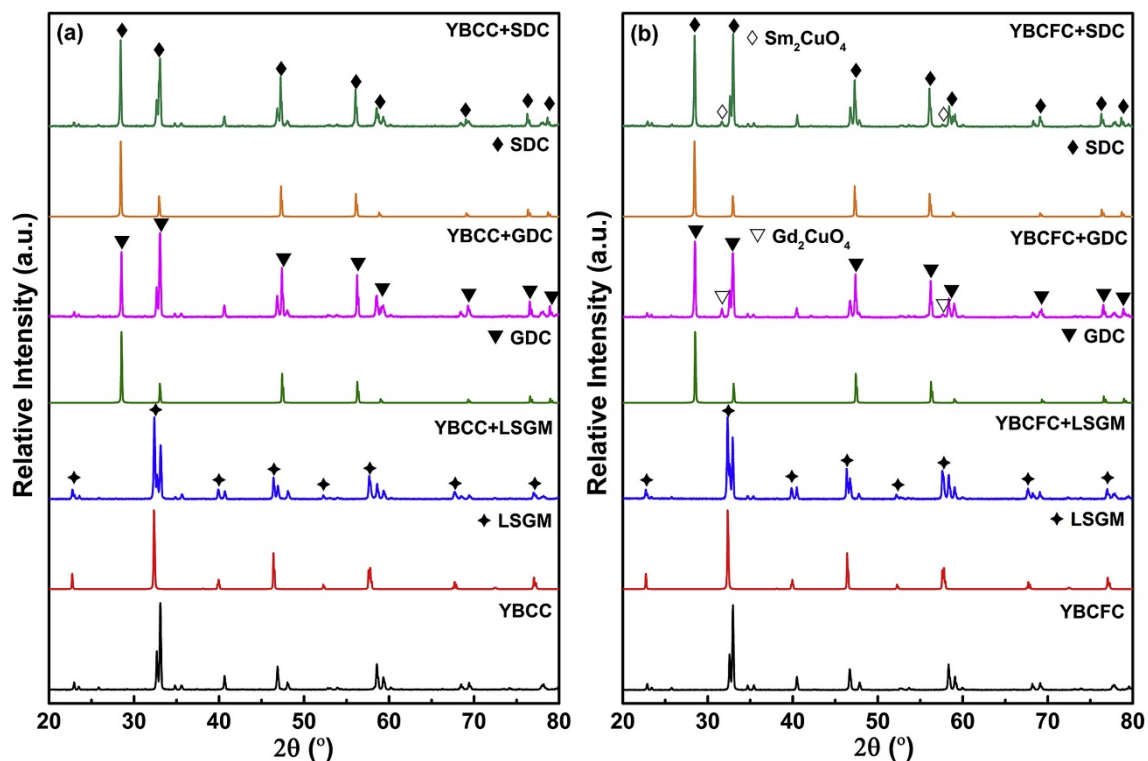


**Figure 4.** XRD patterns of the samples: YBCCO–SDC, YBCCO –GDC, and YBCCO –LSGM: (a) YBCFC–SDC, YBCFC–GDC, and YBCFC–LSGM (b) calcined at 1123 K for 10 h in air (reproduced with permission from [86]. Copyright 2019, Elsevier).

Tsvetkov et al. [87] found that  $\text{PrBaCo}_2\text{O}_{5+\delta}$  and SDC experienced the interdiffusion of Pr and Sm at 1273 K; the formation of  $\text{BaCeO}_3$  had high electrical resistivity. Diffusion of praseodymium into the electrolyte resulted in an increase in its electronic conductivity, which led to a decrease in the open-circuit voltage and even the short circuit of the cell [88]. The formation of the  $\text{BaCeO}_3$  phase also increased the ohmic and polarization resistance of the components of the electrochemical cell.

The  $\text{NdBaFe}_{1.9}\text{Mn}_{0.1}\text{O}_{5+\delta}$  cathode material showed good chemical compatibility with the  $\text{BaZr}_{0.1}\text{Ce}_{0.7}\text{Y}_{0.2}\text{O}_{3-\delta}$  (BZCY) electrolyte at a temperature of 1173 K [89]. In [90], it was shown that  $\text{Sr}_2(\text{Co},\text{Nb})\text{FeO}_{5+\delta}$  double perovskites do not react with  $\text{La}_{0.9}\text{Sr}_{0.1}\text{Ga}_{0.8}\text{Mg}_{0.2}\text{O}_3$  (LSGM) at 1273 K in air, indicating the good chemical compatibility of these compounds.



## 4. Electrochemical Performance of Layered Oxygen-Deficient Perovskites

### 4.1. Layered Cobaltites of REEs and Barium

The main advantages of layered oxygen-deficient cobaltites as cathodes for SOFCs are their superior electronic and ionic conductivity, as well as their higher electrocatalytic activity towards the ORR, especially in the IT-temperature range [8–10,34,35,40]. Table 3 summarizes the electrochemical performance of REE–barium layered cobaltites.

**Table 3.** Performance (ASR: area specific resistance, MPD: maximal power density) of SOFCs based on REE–barium layered double cobaltites.

Cathode	Electrolyte	ASR, $\Omega \text{ cm}^2$ (T, K)	MPD, $\text{mW cm}^{-2}$ (T, K)	Refs.
GdBaCo <sub>2</sub> O <sub>5+<math>\delta</math></sub>	Ce <sub>0.2</sub> Gd <sub>0.2</sub> O <sub>2-<math>\delta</math></sub>	0.534 (918)	–	[91]
GdBaCo <sub>2</sub> O <sub>5+<math>\delta</math></sub>	YSZ	0.25 (998)	250 (1073) 500 (1073) *	[92]
PrBaCo <sub>2</sub> O <sub>5+<math>\delta</math></sub>	GDC	0.23 (873)	–	[93]
LaBaCo <sub>2</sub> O <sub>5+<math>\delta</math></sub>	LSCM	–	516 (1073)	[94]
GdBaCo <sub>2</sub> O <sub>5+<math>\delta</math></sub>	LSCM	–	443 (1073)	[94]
PrBaCo <sub>2</sub> O <sub>5+<math>\delta</math></sub>	SDC	–	866 (923)	[95]
NdBaCo <sub>2</sub> O <sub>5+<math>\delta</math></sub>	SDC	0.08 (973)	–	[96]
YBaCo <sub>2</sub> O <sub>5+<math>\delta</math></sub>	YSZ	2.03 (1053)	–	[97]
PrBaCo <sub>2</sub> O <sub>5+<math>\delta</math></sub>	BaCe <sub>0.5</sub> Zr <sub>0.3</sub> Y <sub>0.16</sub> Zn <sub>0.04</sub> O <sub>3-<math>\delta</math></sub>	0.12 (973)	361 (973)	[98]
LaBaCo <sub>2</sub> O <sub>5+<math>\delta</math></sub>	Gd <sub>0.1</sub> Ce <sub>0.9</sub> O <sub>1.95</sub>	0.0086 (1073)	–	[99]

\* With an intermediate porous YSZ layer introduced between the solid electrolyte and the cathode.

According to this table, layered cobaltites exhibit good electrochemical activity with the lowest ASR value of  $0.0086 \Omega \text{ cm}^2$  at 1073 K reached for the LaBaCo<sub>2</sub>O<sub>5+ $\delta$</sub>  cathode. This is much lower than values taken for commonly used LODPs. The ASR value for the NdBaCo<sub>2</sub>O<sub>5+ $\delta$</sub>  cathode is  $0.08 \Omega \text{ cm}^2$  at 973 K, under a cathodic applied voltage of  $-0.1 \text{ V}$  [96]. The activation energy of the interface conductivity of these materials varied within  $\sim 110 \text{ kJ mol}^{-1}$  and  $160 \text{ kJ mol}^{-1}$ , decreasing with an increase in the applied voltage ( $E$ ), since the diffusion process was more easily affected by the increase in  $E$  than the charge transfer process.

The highest power density values were obtained for PrBaCo<sub>2</sub>O<sub>5+ $\delta$</sub> , which reached  $866 \text{ mW cm}^{-2}$  at 923 K for the cell  $(-)\text{NiO} | \text{Ce}_{0.8}\text{Sm}_{0.2}\text{O}_{1.9} | \text{PrBaCo}_2\text{O}_{5+\delta}(+)$  and  $361 \text{ mW cm}^{-2}$  at 973 K for the cell  $(-)\text{NiO} + \text{BaCe}_{0.5}\text{Zr}_{0.3}\text{Y}_{0.16}\text{Zn}_{0.04}\text{O}_{3-\delta} | \text{BaCe}_{0.5}\text{Zr}_{0.3}\text{Y}_{0.16}\text{Zn}_{0.04}\text{O}_{3-\delta} | \text{PrBaCo}_2\text{O}_{5+\delta}(+)$  (Figure 5). It is interesting to note that the electrochemical performance of this material in SOFCs containing oxygen-ion conducting solid electrolytes is essentially higher than that in SOFCs with the proton-conducting electrolyte.

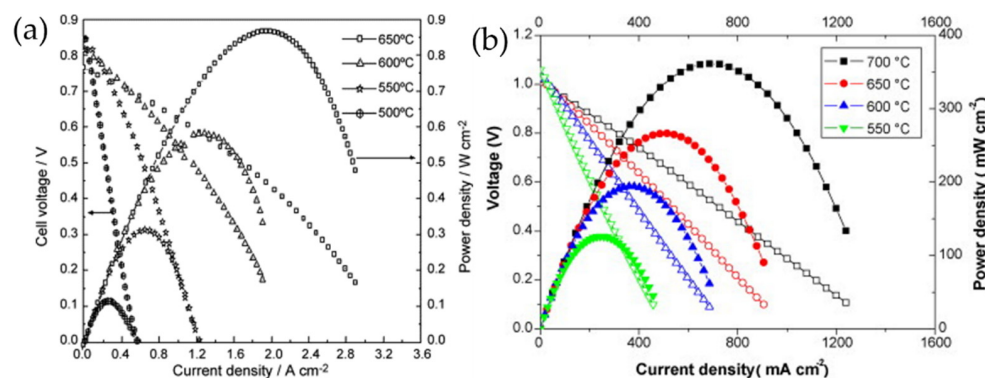


**Figure 5.** Performances of the cell with PrBaCo<sub>2</sub>O<sub>5+ $\delta$</sub>  cathode and (a) oxygen-ion-conducting Ce<sub>0.8</sub>Sm<sub>0.2</sub>O<sub>1.9</sub> electrolyte (reproduced with permission from [69]. Copyright 2008, Elsevier) and (b) proton-conducting BaCe<sub>0.5</sub>Zr<sub>0.3</sub>Y<sub>0.16</sub>Zn<sub>0.04</sub>O<sub>3- $\delta$</sub>  electrolyte (reproduced with permission from [98]. Copyright 2010, Elsevier).

As a whole, the overall electrochemical performance of the ordered oxygen-deficient double perovskites is reported to be higher than for A-site disordered phases. However, the performance of  $LnBaCo_2O_{5+\delta}$  cathodes usually deteriorates with decreases in the  $Ln^{3+}$  ionic radius, partly due to a decrease in oxygen content [94,99–101]. The reported ASR values for the  $La_{0.5}Ba_{0.5}CoO_{3-\delta}$  and  $LaBaCo_2O_{5+\delta}$  cathodes at 873 K were equal to 11.5 and 7.4  $\Omega\text{ cm}^2$ , respectively, with activation energy values of 0.90 and 0.97 eV, respectively [102].

The electrocatalytic activity and stability of  $LnBaCo_2O_{5+\delta}$  ( $Ln = La, Pr, Nd, Sm, Eu,$  and  $Gd$ ) perovskites in the hydrogen evolution reaction (HER) were studied in [103]. It was found, from the DFT calculations, that  $LnBaCo_2O_{5+\delta}$  phases exhibit an optimal free energy combination for the  $H_2O$  adsorption/dissociation and  $-OH/H^*$  desorption, which open up the opportunity for the development of new perovskite-based energy materials.

#### 4.2. A-Site-Deficient and A-Site-Substituted $LnBaCo_2O_{5+\delta}$ Layered Perovskites

An effective way to improve functional properties of the discussed layered perovskites is through the creation of a cation deficiency in their A-sublattice (both in REE and barium positions) and partial isovalent substitution of barium with smaller alkaline-earth elements (AEEs), such as strontium or calcium. Table 4 summarizes some results obtained for SOFCs based on such double perovskites.

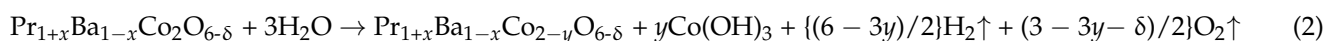
Single-phase materials are formed at a relatively small deficiency of REE (8 mol.% for Pr [104], 5–10 mol.% for Sm [105,106]). The formation of REE-vacancies in the  $Ln_{1-x}BaCo_2O_{5+\delta}$  phases leads to an increase in their lattice constants and decreases their oxygen content. This results in a decrease of their electrical conductivity, and improvement of their electrochemical performance (particularly, to the essential lowering of ASR and increasing of PD [105–107]), at least at a low REE deficiency level (approximately 5 mol.%).

The crystal structure of  $LnBa_{1-x}Co_2O_{5+\delta}$  is retained at  $x \leq 0.15$ , 0.08–0.10 and 0.05 for  $Ln = La$  [108], Pr [109,110], and Nd [111], respectively. The formation of a barium deficiency slightly affects the lattice constants of LODPs [111] but results in a decrease in the oxygen content [111], their TECs [109,110], and electrical conductivity [108–111].

A paramount electrochemical performance of 1.03  $W\text{ cm}^{-2}$  at 973 K was observed in the anode-supported  $NiO-Ce_{0.9}Gd_{0.1}O_{1.95} | Ce_{0.9}Gd_{0.1}O_{1.95} | PrBa_{0.94}Co_2O_{5+\delta}$  SOFC [110]. Improvement of functional properties was also observed for Ba-deficient solid solutions, such as  $Pr_{0.5}Ba_{0.25-x}Ca_{0.25}CoO_{3-\delta}$  [112] and  $PrBa_{0.5-x}Sr_{0.5}Co_2O_{5+\delta}$  [113].

The addition of potassium results in a higher cation deficiency in the  $PrBa_{1-x}Co_2O_{5+\delta}$  perovskites, improving bulk oxygen transport [114]. However, the cobalt content at the surface of these samples was found to have decreased as well, causing the deterioration of their electrochemical performance towards the surface oxygen exchange.

Inter-substitution of praseodymium by barium in  $Pr_{1+x}Ba_{1-x}Co_2O_{6-\delta}$  leads to the formation of double-phase composites comprising orthorhombic  $PrBaCo_2O_{6-\delta}$  (SG  $Pmmm$ ) and  $PrCoO_3$  (SG  $Pnma$ ) for  $x = 0.2$  and 0.8 [115]. The triple-phase boundary reaction suggests the formation of  $Co(OH)_3$  along with the  $H_2$  gas evolution during the electrochemical dissolution of these composite electrodes with  $H_2O$  inreaction (2).



The sample with  $x = 0.6$  showed a higher ORR rate with more intense  $H_2$  gas evolution compared with the others.

Lu et al. [116], using the conventional solid-state reactions method, synthesized an A-site deficient double perovskite  $PrBa_{0.94}Co_2O_{5+\delta}$  (A-PBC) and then created nanorods of simple perovskite ( $PrCoO_3$ ) on the surface of its particles via an in situ exsolution process, which resulted in the formation of a heterostructured simple perovskite nanorod-decorated double perovskite cathode (SPN-A-PBC). High electrocatalytic activity of the SPN-A-PBC cathode toward ORR was found, achieving apolarization resistance of about 0.025  $\Omega\text{ cm}^2$  at 973 K in air. The anode-supported single cell with the SPN-A-PBC cathode reached a power density of 1.1  $W\text{ cm}^{-2}$  at 973 K and a superior steady operation over 120 h at a loading voltage of 0.6 V (Figure 6). This electrode also exhibited a good tolerance to  $CO_2$ ;

when tested in air with 6 vol.% CO<sub>2</sub> at 973K, it maintained a stable polarization resistance of about 0.078 Ω cm<sup>2</sup>.

**Table 4.** Performance (ASR: area specific resistance, MPD: maximal power density) of SOFCs based on A-site deficient and A-site substituted REE-barium layered double cobaltites.

Cathode	Electrolyte	ASR, Ω cm <sup>2</sup> (T, K)	MPD, mW cm <sup>-2</sup> (T, K)	Refs.
Pr <sub>0.95</sub> BaCo <sub>2</sub> O <sub>5+δ</sub>	Ce <sub>0.9</sub> Gd <sub>0.1</sub> O <sub>1.95</sub>	0.054 (923)	–	[104]
Nd <sub>0.96</sub> BaCo <sub>2</sub> O <sub>5+δ</sub>	Ce <sub>0.9</sub> Gd <sub>0.1</sub> O <sub>1.95</sub>	0.043 (973)	600 (973)	[105]
Sm <sub>0.95</sub> BaCo <sub>2</sub> O <sub>5+δ</sub>	GDC	0.038 (1023)	–	[106]
Sm <sub>0.90</sub> BaCo <sub>2</sub> O <sub>5+δ</sub>	Ce <sub>0.9</sub> Gd <sub>0.1</sub> O <sub>2-δ</sub>	0.035 (973)	–	[107]
LaBa <sub>0.90</sub> Co <sub>2</sub> O <sub>5+δ</sub>	Ce <sub>0.9</sub> Gd <sub>0.1</sub> O <sub>1.95</sub>	0.023 (973)	–	[108]
PrBa <sub>0.92</sub> Co <sub>2</sub> O <sub>5+δ</sub>	Ce <sub>0.9</sub> Gd <sub>0.1</sub> O <sub>1.95</sub>	0.093 (873)	–	[109]
PrBa <sub>0.94</sub> Co <sub>2</sub> O <sub>5+δ</sub>	Ce <sub>0.9</sub> Gd <sub>0.1</sub> O <sub>1.95</sub>	0.042 (873)	1030 (973)	[110]
NdBa <sub>0.90</sub> Co <sub>2</sub> O <sub>5+δ</sub>	Ce <sub>0.9</sub> Gd <sub>0.1</sub> O <sub>2</sub>	0.1 (973)	–	[111]
Pr <sub>0.5</sub> Ba <sub>0.245</sub> Ca <sub>0.25</sub> Co <sub>3-δ</sub>	Ce <sub>0.9</sub> Gd <sub>0.1</sub> O <sub>1.95</sub>	–	2080 (1073)	[112]
PrBa <sub>0.42</sub> Sr <sub>0.5</sub> Co <sub>2</sub> O <sub>5+δ</sub>	La <sub>0.8</sub> Sr <sub>0.2</sub> Ga <sub>0.8</sub> Mg <sub>0.2</sub> O <sub>3-δ</sub>	0.082 (1023)	–	[113]
PrBa <sub>0.5</sub> Sr <sub>0.5</sub> Co <sub>2</sub> O <sub>5+δ</sub>	Ce <sub>0.9</sub> Gd <sub>0.1</sub> O <sub>2-δ</sub>	0.286 (873)	–	[117]
Pr <sub>0.9</sub> Ca <sub>0.1</sub> Ba <sub>0.8</sub> Ca <sub>0.2</sub> Co <sub>2</sub> O <sub>5+δ</sub>	SDC	0.069 (973)	712 (1073)	[118]
NdBa <sub>0.5</sub> Sr <sub>0.5</sub> Co <sub>2</sub> O <sub>5+δ</sub>	SDC	0.09 (1073)	341 (1073)	[119]
NdBa <sub>0.5</sub> Sr <sub>0.25</sub> Ca <sub>0.25</sub> Co <sub>2</sub> O <sub>5+δ</sub>	Sm <sub>0.2</sub> Ce <sub>0.8</sub> O <sub>1.9</sub>	0.062 (1073)	812 (1073) *	[120]
NdBa <sub>0.75</sub> Ca <sub>0.25</sub> Co <sub>2</sub> O <sub>5+δ</sub>	GDC	0.066 (873)	2114 (873)	[121]
GdBa <sub>0.5</sub> Sr <sub>0.5</sub> Co <sub>2</sub> O <sub>5+δ</sub>	BaCe <sub>0.5</sub> Zr <sub>0.3</sub> Y <sub>0.16</sub> Zn <sub>0.04</sub> O <sub>3-δ</sub>	0.15 (973)	350 (973)	[122]
YBa <sub>0.5</sub> Sr <sub>0.5</sub> Co <sub>2</sub> O <sub>5+δ</sub>	La <sub>0.9</sub> Sr <sub>0.1</sub> Ga <sub>0.8</sub> Mg <sub>0.115</sub> Co <sub>0.085</sub> O <sub>2.85</sub>	–	650 (1073)	[123]
YBa <sub>0.8</sub> Sr <sub>0.2</sub> Co <sub>2</sub> O <sub>5+δ</sub>	Ce <sub>0.9</sub> Gd <sub>0.1</sub> O <sub>2-δ</sub>	0.21 (973)	–	[124]
Pr <sub>0.5</sub> Sm <sub>0.5</sub> Ba <sub>0.5</sub> Sr <sub>0.5</sub> Co <sub>2</sub> O <sub>5+δ</sub>	Ce <sub>0.9</sub> Gd <sub>0.1</sub> O <sub>2</sub>	0.10 (973)	–	[125]

\* For the single cell containing the composite NdBa<sub>0.5</sub>Sr<sub>0.25</sub>Ca<sub>0.25</sub>Co<sub>2</sub>O<sub>5+δ</sub>–Sm<sub>0.2</sub>Ce<sub>0.8</sub>O<sub>1.9</sub> cathode.

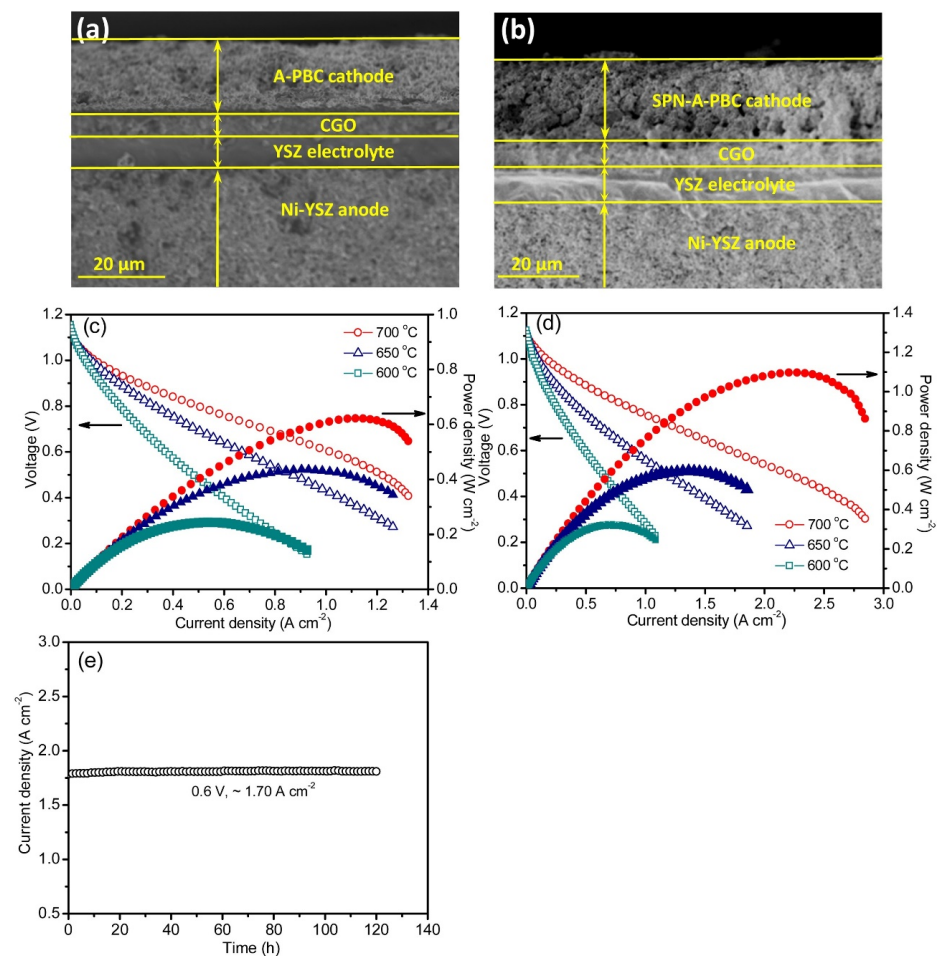


**Figure 6.** Cross-section view of SEM images of the anode-supported single cell with a Ni-YSZ anode, an YSZ electrolyte, a CGO buffer layer and the (a) A-PBC and (b) SPN-A-PBC cathodes. *V–I* and *P–I* curves of the single cells with the (c) A-PBC and (d) SPN-A-PBC cathodes within 873–973 K. (e) Long-term stability test of a single cell with the SPN-A-PBC cathode at a constant loading voltage of 0.6 V at 973 K for 120 h (reproduced with permission from [116]. Copyright 2019, Elsevier).

A partial substitution of barium with smaller strontium or/and calcium in  $LnBaCo_2O_{5+\delta}$  leads to the expected decrease of lattice constants and TEC values [117–120,124] and an increase in the electrical conductivity [118,123,124] and the electrochemical performance of the corresponding materials [117–124].

In [118], a co-doping strategy of both Pr and Ba by Ca in layered  $PrBaCo_2O_{5+\delta}$  cobaltite for improving its properties was used. It was shown that this strategy makes it possible to increase electrical conductivity and thermal stability of the samples as well as to reduce ASR values and enlarge MPD (Table 4). The  $NdBa_{0.5}Sr_{0.25}Ca_{0.25}Co_2O_{5+\delta}$  cathode demonstrated a very low ASR value of  $0.062 \Omega \text{ cm}^2$  at 1073 K and a maximum output power density of  $812 \text{ mW cm}^{-2}$  at 1073 K (Figure 7). This measurement was much higher than for  $NdBa_{0.5}Sr_{0.5}Co_2O_{5+\delta}$ , proving the effectiveness of the co-doping strategy.

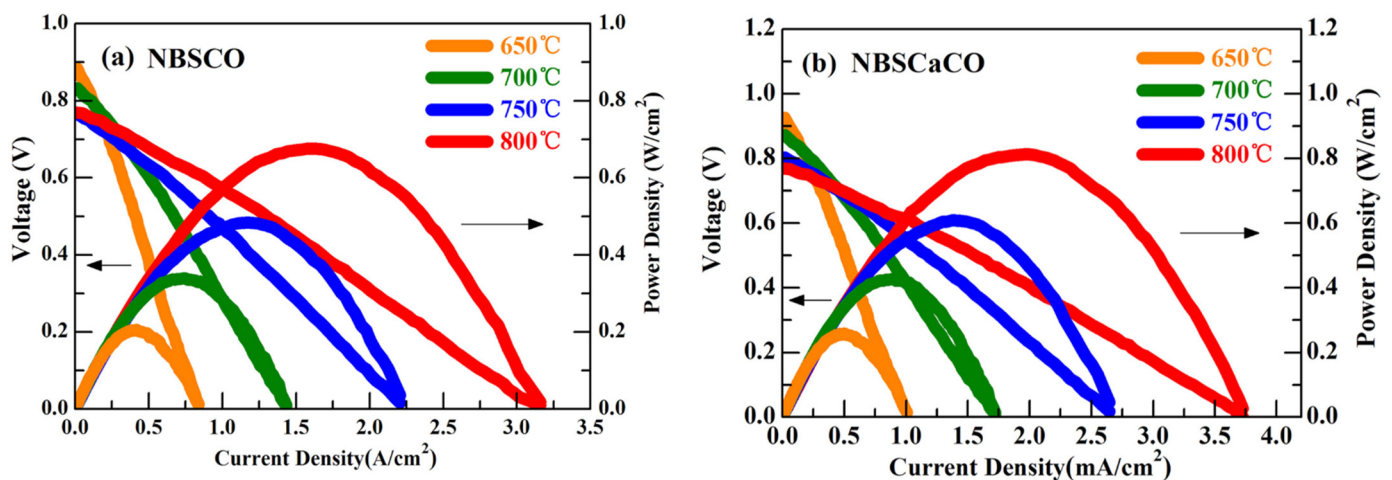


**Figure 7.**  $I$ - $V$  curves and corresponding output power density of (a) NiO-SDC|SDC|NdBa<sub>0.5</sub>Sr<sub>0.5</sub>Co<sub>2</sub>O<sub>5+δ</sub>-SDC and (b) NiO-SDC|SDC|NdBa<sub>0.5</sub>Sr<sub>0.25</sub>Ca<sub>0.25</sub>Co<sub>2</sub>O<sub>5+δ</sub>-SDC single cells at various temperatures (adopted with permission from [120]. Copyright 2018, Elsevier).

Through the electrical conductivity relaxation (ECR) test, the values of chemical bulk diffusion coefficient ( $D_{\text{chem}}$ ) of oxygen in SmBa<sub>0.6</sub>Sr<sub>0.4</sub>Co<sub>2</sub>O<sub>5+δ</sub> were measured from  $1.63 \times 10^{-6} \text{ cm}^2 \text{ s}^{-1}$  at 773 K to  $1.41 \times 10^{-5} \text{ cm}^2 \text{ s}^{-1}$  at 973 K [126]. The temperature dependence of  $D_{\text{chem}}$  in a temperature range of 773–973 K is described by Equation (3):

$$D_{\text{chem}} = 1.77 \times 10^{-5} \cdot \exp[-68.039 \text{ (kJ mol}^{-1}) / (R \cdot T)] \text{ (m}^2 \text{ s}^{-1}) \quad (3)$$

The oxygen transport properties of SmBa<sub>0.5</sub>Sr<sub>0.5</sub>Co<sub>2</sub>O<sub>5+δ</sub> as a potential cathode material for IT-SOFCs were investigated in [127]. The  $D_{\text{chem}}$  values for SmBa<sub>0.5</sub>Sr<sub>0.5</sub>Co<sub>2</sub>O<sub>5+δ</sub> were equal to  $2.6 \times 10^{-6}$ ,  $9.1 \times 10^{-6}$ , and  $1.8 \times 10^{-5} \text{ cm}^2 \text{ s}^{-1}$  at 773, 873, and 973 K, respectively. The activation energy of  $D_{\text{chem}}$  within 773–973 K was  $\sim 58 \text{ kJ mol}^{-1}$ . Oxygen permeation flux for the SmBa<sub>0.5</sub>Sr<sub>0.5</sub>Co<sub>2</sub>O<sub>5+δ</sub> membrane with a thickness of 1.00 mm increased from  $0.143 \text{ mL min}^{-1} \text{ cm}^{-2}$  at 773 K to  $0.406 \text{ mL min}^{-1} \text{ cm}^{-2}$  at 1073 K under synthetic air at a flow rate of  $50 \text{ mL min}^{-1}$  and helium at a rate of  $25 \text{ mL min}^{-1}$ . The activation energies of oxygen permeation for a high-temperature region (973–1073 K) and a low-temperature region (773–923 K) were equal to  $\sim 24$  and  $7 \text{ kJ mol}^{-1}$ , respectively, suggesting that the oxygen diffusion in the high-temperature and low-temperature ranges occurred via surface exchange and bulk diffusion mechanisms, respectively.

#### 4.3. B-Site Deficient and B-Site Substituted $LnBaCo_2O_{5+\delta}$ Layered Perovskites

Co-deficient PrBaCo<sub>2-x</sub>O<sub>6-δ</sub> ( $0 \leq x \leq 0.1$ ) perovskites were prepared and investigated in [128]. It was found that increasing the concentration of the vacancies in the Co-sublattice led to an increase in lattice constants and oxygen nonstoichiometry ( $\delta$ ), additionally, the electrical conductivity decreased and electrochemical performance of PrBaCo<sub>2-x</sub>O<sub>6-δ</sub> cath-



odes improved. The minimum value of ASR and the maximum value of MPD were found for  $\text{PrBaCo}_{1.94}\text{O}_{6-\delta}$ , they were  $0.059 \Omega \text{ cm}^2$  at 973 K and  $889 \text{ mW cm}^{-2}$  at 923 K, respectively. This was 16% lower and higher, respectively, than for the cation-stoichiometric  $\text{PrBaCo}_2\text{O}_{6-\delta}$  phase. The thermal stability of the samples did not change due to the formation of Co-deficiency. Table 5 shows some typical results concerning the electrochemical performance of SOFCs with a B-site substituted REE-barium layered cobaltites as cathodes.

A partial substitution of cobalt in  $\text{LnBaCo}_2\text{O}_{5+\delta}$  perovskites by low-valence Ni- [129–131], Zn- [132], or Cu- [86,131,133–135] ions led to a slight increase in their lattice constants [131] and a decrease in oxygen content ( $\delta$ ) [131,132], TEC [129,130,134,135], and electrical conductivity values [86,129–131,134]. In some cases, such a substitution improved the electrochemical performance of the derived cathode materials [129,130,132,134]. For Cu-doped  $\text{SmBa}_{0.5}\text{Sr}_{0.5}\text{Co}_{1.5}\text{Cu}_{0.5}\text{O}_{5+\delta}$  and  $\text{YBaCoCuO}_{5+\delta}$  perovskites, the ASR values were larger and the maximum power density were smaller than for their Cu-free  $\text{SmBa}_{0.5}\text{Sr}_{0.5}\text{Co}_2\text{O}_{5+\delta}$  and  $\text{YBaCo}_2\text{O}_{5+\delta}$  counterparts. Moreover, Cu-doped materials showed better long-term stability [86,133,134].

In [136], it was found that a partial substitution of cobalt with high-valence tantalum in  $\text{PrBa}_{0.94}\text{Co}_2\text{O}_{5+\delta}$  stabilizes the A-site-ordered layered perovskite structure, slightly increases TEC and electrical conductivity of the samples, and improves catalytic activity towards ORR. The optimal composition,  $\text{PrBa}_{0.94}\text{Co}_{1.96}\text{Ta}_{0.04}\text{O}_{5+\delta}$ , exhibits the lowest polarization resistance ( $0.020 \Omega \text{ cm}^2$  at 973 K) and the highest power density of  $1050 \text{ mW cm}^{-2}$  at 973 K and is operated steadily at a loading voltage of 0.6 V over 100 h at 923 K. The  $\text{PrBa}_{0.94}\text{Co}_{1.96}\text{Ta}_{0.04}\text{O}_{5+\delta}$  cathode showed excellent tolerance to  $\text{CO}_2$ , as evidenced by its durable polarization resistance of  $0.061 \Omega \text{ cm}^2$  at 973 K in air with 10 vol.% of  $\text{CO}_2$ . A partial substitution of cobalt by high-valence molybdenum ions in  $\text{PrBaCo}_{2-x}\text{Mo}_x\text{O}_{5+\delta}$  almost did not affect the crystal structure of the parent oxide but decreased its TEC and electrical conductivity values [137]. The polarization resistance of the  $\text{PrBaCo}_{1.97}\text{Mo}_{0.03}\text{O}_{5+\delta}$  (PBCM–0.03) cathode was  $0.067 \Omega \text{ cm}^2$  at 973 K, which was slightly higher than for the pristine  $\text{PrBaCo}_2\text{O}_{5+\delta}$  cathode (PBCO) ( $0.060 \Omega \text{ cm}^2$  at 973 K). The maximum power density of the single cells containing the PBCM–0.03 and PBCO cathodes at 973 K attained 343 and  $339 \text{ mW cm}^{-2}$ , respectively. It was also found in [137] that trace amounts of high-valence Mo-doping in the  $\text{PrBaCo}_2\text{O}_{5+\delta}$  cathode improved its electrochemical stability. So, generally, the results obtained in [137] showed that  $\text{PrBaCo}_{2-x}\text{Mn}_x\text{O}_{5+\delta}$  solid solutions are attractive for applications as SOFCs cathodes.

The isovalent Co-by-Mn substitution in LODPs was studied in [138–141]. It was found that the TEC and electrical conductivity of  $\text{SmSrCo}_{2-x}\text{Mn}_x\text{O}_{5+\delta}$  ( $0 \leq x \leq 1$ ) perovskites decreased with increasing  $x$ . The electrochemical performance of  $\text{SmSrCo}_2\text{O}_{5+\delta}$  slightly decreased after Mn-doping; however, reduced TEC and good chemical compatibility with GDC indicate that these materials may be used as SOFCs cathodes. Similar results were observed in another work [139], where  $\text{GdBaCo}_{2-x}\text{Mn}_x\text{O}_{5+\delta}$  ( $0 \leq x \leq 2$ ) was formed within the whole studied composition region. Mn-doped oxides showed lower electrical conductivity and increased polarization resistance. Nevertheless, these materials exhibited an increased oxygen content ( $\delta$ ) and reduced TEC values. Moderate TEC values and good catalytic activity in ORR were found for the  $\text{LnBaCo}_{2-x}\text{Mn}_x\text{O}_{5+\delta}$  perovskites [140,141].

The effect of the partial substitution of cobalt with iron in layered perovskites of REE and barium and their A-site-deficient and A-site-substituted derivatives was intensively studied in a number of works [86,131,135,142–158]. It was found that Fe-doping results in an increase of lattice constants [131,143–145,147,148,151,153,154,157] and oxygen contents [131,146]. Electrical conductivity of such Fe-doped cobaltites decreases with Fe-doping [143,145–147,153,154,157]. TECs also decreased [143,147,153], though some works reported an inverse tendency [131,144]. The Fe-doping usually improved the electrochemical performance of the layered cobaltites as SOFCs cathodes, but, in a number of works, increased polarization resistances [144,145] or reduced power densities [142,144] were reported, showing that the final properties of materials depend on both chemical compositions of LODPs and the prehistory of their preparation.

**Table 5.** Performance (ASR: area specific resistance, MPD: maximal power density) of SOFCs based on B-site substituted REE–barium layered double cobaltites.

Cathode	Electrolyte	ASR, $\Omega \text{ cm}^2$ (T, K)	MPD, $\text{m W cm}^{-2}$ (T, K)	Refs.
PrBaCo <sub>1.6</sub> Ni <sub>0.4</sub> O <sub>5+<math>\delta</math></sub>	Ce <sub>0.8</sub> Sm <sub>0.2</sub> O <sub>1.9</sub>	0.018 (1073)	732 (1073)	[129]
PrBa <sub>0.5</sub> Sr <sub>0.5</sub> Co <sub>1.9</sub> Ni <sub>0.1</sub> O <sub>5+<math>\delta</math></sub>	YSZ	0.297 (1073)	120 (1073)	[130]
PrBa <sub>0.9</sub> Ca <sub>0.1</sub> Co <sub>1.85</sub> Zn <sub>0.15</sub> O <sub>5+<math>\delta</math></sub>	BZCYYb	0.04 (1023) *	876 (1023) *	[132]
SmBa <sub>0.5</sub> Sr <sub>0.5</sub> Co <sub>1.5</sub> Cu <sub>0.5</sub> O <sub>5+<math>\delta</math></sub>	GDC	0.201 (873)	1760 (923)	[133]
YBaCo <sub>1.4</sub> Cu <sub>0.6</sub> O <sub>5+<math>\delta</math></sub>	La <sub>0.9</sub> Sr <sub>0.1</sub> Ga <sub>0.8</sub> Mg <sub>0.2</sub> O <sub>3–<math>\delta</math></sub>	0.076 (1023)	815 (1123)	[134]
YBaCoCuO <sub>5+<math>\delta</math></sub>	La <sub>0.9</sub> Sr <sub>0.1</sub> Ga <sub>0.8</sub> Mg <sub>0.2</sub> O <sub>3–<math>\delta</math></sub>	0.138 (973)	543 (1073)	[86]
PrBa <sub>0.94</sub> Co <sub>1.96</sub> Ta <sub>0.4</sub> O <sub>5+<math>\delta</math></sub>	GCO	0.020 (973)	1050 (973)	[136]
PrBaCo <sub>1.97</sub> Mo <sub>0.03</sub> O <sub>5+<math>\delta</math></sub>	Sm <sub>0.2</sub> Ce <sub>0.8</sub> O <sub>1.9</sub>	0.067 (973)	339 (973)	[137]
SmSrCo <sub>0.8</sub> Mn <sub>0.2</sub> O <sub>5+<math>\delta</math></sub>	Ce <sub>0.9</sub> Gd <sub>0.1</sub> O <sub>1.95</sub>	0.078 (973)	–	[138]
GdBaCo <sub>1.8</sub> Mn <sub>0.2</sub> O <sub>5+<math>\delta</math></sub>	Ce <sub>0.9</sub> Gd <sub>0.1</sub> O <sub>2–<math>\delta</math></sub>	0.078 (92)	–	[139]
GdBaCo <sub>1.5</sub> Mn <sub>0.5</sub> O <sub>5+<math>\delta</math></sub>	LSGM	0.040 (1123)	–	[140]
PrBaFe <sub>2</sub> O <sub>5+<math>\delta</math></sub>	Sm <sub>0.2</sub> Ce <sub>0.8</sub> O <sub>1.9</sub>	0.18 (973)	–	[143]
YBaCo <sub>1.8</sub> Fe <sub>0.2</sub> O <sub>5+<math>\delta</math></sub>	La <sub>0.8</sub> Sr <sub>0.2</sub> Ga <sub>0.8</sub> Mg <sub>0.115</sub> Co <sub>0.085</sub> O <sub>2.85</sub>	0.13 (973)	768 (1073)	[145]
PrBaCo <sub>1.6</sub> Fe <sub>0.4</sub> O <sub>5+<math>\delta</math></sub>	Ce <sub>0.8</sub> Sm <sub>0.2</sub> O <sub>2–<math>\gamma</math></sub>	0.13 (973)	446.4 (973)	[145]
PrBaCoFeO <sub>5+<math>\delta</math></sub>	YSZ	–	720 (973) **	[146]
PrBaCo <sub>1.5</sub> Fe <sub>0.5</sub> O <sub>5+<math>\delta</math></sub>	La <sub>0.8</sub> Sr <sub>0.2</sub> Ga <sub>0.83</sub> Mg <sub>0.17</sub> O <sub>2.815</sub>	0.07 (1123)	697 (1123)	[147]
NdBa <sub>0.5</sub> Sr <sub>0.5</sub> Co <sub>1.5</sub> Fe <sub>0.5</sub> O <sub>5+<math>\delta</math></sub>	Nd <sub>0.1</sub> Ce <sub>0.9</sub> O <sub>2–<math>\delta</math></sub>	–	1010 (923) #	[151]
GdBaCo <sub>1.4</sub> Fe <sub>0.6</sub> O <sub>5+<math>\delta</math></sub>	Ce <sub>0.9</sub> Gd <sub>0.1</sub> O <sub>2–<math>\delta</math></sub>	0.096 (923)	–	[153]
PrBa <sub>0.5</sub> Sr <sub>0.5</sub> Co <sub>1.8</sub> Fe <sub>0.2</sub> O <sub>5+<math>\delta</math></sub>	ScSZ	0.012 (973)	1350 (973)	[154]
NdBaCo <sub>1.6</sub> Fe <sub>0.4</sub> O <sub>5+<math>\delta</math></sub>	Gd <sub>0.1</sub> Ce <sub>0.9</sub> O <sub>2</sub>	0.17 (973)	–	[155]
NdBa <sub>0.9</sub> Co <sub>1.9</sub> Fe <sub>0.1</sub> O <sub>5+<math>\delta</math></sub>	Ce <sub>0.9</sub> Gd <sub>0.1</sub> O <sub>2–<math>\delta</math></sub>	0.14 (973)	–	[157]
PrBaCo <sub>0.2</sub> Fe <sub>1.8</sub> O <sub>5+<math>\delta</math></sub>	La <sub>0.9</sub> Sr <sub>0.1</sub> Ga <sub>0.8</sub> Mg <sub>0.2</sub> O <sub>3</sub>	–	735 (1123)	[158]
PrBaCo <sub>2/3</sub> Fe <sub>2/3</sub> Cu <sub>2/3</sub> O <sub>5+<math>\delta</math></sub>	Ce <sub>0.9</sub> Gd <sub>0.1</sub> O <sub>1.95</sub>	0.038 (1073)	659 (1073)	[159]
NdBaCo <sub>2/3</sub> Fe <sub>2/3</sub> Cu <sub>2/3</sub> O <sub>5+<math>\delta</math></sub>	La <sub>0.9</sub> Sr <sub>0.1</sub> Ga <sub>0.8</sub> Mg <sub>0.2</sub> O <sub>3–<math>\delta</math></sub>	0.023 (1073)	719 (1073)	[160]
PrBaCo <sub>2/3</sub> Fe <sub>2/3</sub> Mn <sub>1/2</sub> O <sub>5+<math>\delta</math></sub>	Sm <sub>0.2</sub> Ce <sub>0.8</sub> O <sub>1.9</sub>	0.028 (1073)	588 (1073)	[161]

\* For the composite PrBa<sub>0.9</sub>Ca<sub>0.1</sub>Co<sub>1.85</sub>Zn<sub>0.15</sub>O<sub>5+ $\delta$</sub> +BZCYYb (6:4 weight ratio) cathode. \*\* For the composite PrBaCoFeO<sub>5+ $\delta$</sub> +YSZ. # For the composite NdBa<sub>0.5</sub>Sr<sub>0.5</sub>Co<sub>1.5</sub>Fe<sub>0.5</sub>O<sub>5+ $\delta$</sub> +Nd<sub>0.1</sub>Ce<sub>0.9</sub>O<sub>2– $\delta$</sub> .

Lee et al. [151] compared the electrochemical performance of the Ba<sub>0.5</sub>Sr<sub>0.5</sub>Co<sub>0.8</sub>Fe<sub>0.2</sub>O<sub>3– $\delta$</sub>  single perovskite and the NdBa<sub>0.5</sub>Sr<sub>0.5</sub>Co<sub>1.5</sub>Fe<sub>0.5</sub>O<sub>5+ $\delta$</sub>  double perovskite when operated in single cells at different conditions (Figure 8) and demonstrated excellent stability of double perovskite in harsh SOFC environments, including high humidity and low flow rate of air.

In [149,152] it was found that a partial Fe-to-Co substitution in layered cobaltites increases the oxygen-ion diffusion coefficient (Table 6), which should improve the electrochemical activity of these compounds in terms of ORR.

A suspension plasma-sprayed PrBa<sub>0.5</sub>Sr<sub>0.5</sub>Co<sub>1.6</sub>Fe<sub>0.4</sub>O<sub>5+ $\delta$</sub>  (PBSCF) cathode operating in a symmetrical cell of PBSCF|ScSZ|PBSCF (ScSZ—scandia stabilized zirconia) and a single cell of Ni–GDC|ScSZ|PBSCF showed good electrochemical performance with as low a ASR value as 0.074  $\Omega \text{ cm}^2$  and 0.012  $\Omega \text{ cm}^2$  at 873 K and 973 K, respectively, peak power densities of 370, 800, and 1350  $\text{mW cm}^{-2}$  at 773 K, 873 K, and 973 K, respectively, as well as excellent long-term stability (its polarization resistance remained practically constant during isothermal dwelling at 973 K for 300 h) [154].

In [158], a symmetrical SOFC with LSGM and PrBaCo<sub>0.2</sub>Fe<sub>1.8</sub>O<sub>5+ $\delta$</sub>  (PBCF) as a cathode was prepared and tested during its operation with different fuels. According to X-ray diffractometry (XRD) and energy dispersive spectroscopy (EDS) results, the PrBaCo<sub>0.2</sub>Fe<sub>1.8</sub>O<sub>5+ $\delta$</sub>  compound had good chemical compatibility with the LSGM electrolyte. At 1073 K, the polarization resistance values of the PBCF symmetrical electrodes were 0.026 and 0.319  $\Omega \text{ cm}^2$  in air and H<sub>2</sub>, respectively. The output performances of the electrolyte-supported single cell with the PBCF symmetrical electrodes were 735, 626, and 268  $\text{mW cm}^{-2}$  at 1123 K under H<sub>2</sub>, liquefied petroleum gas (LPG), and C<sub>2</sub>H<sub>5</sub>OH fuel, respectively. This cell showed long-term stability at 1023 K for 40 h and 60 h with H<sub>2</sub> and LPG as the fuel, respectively.

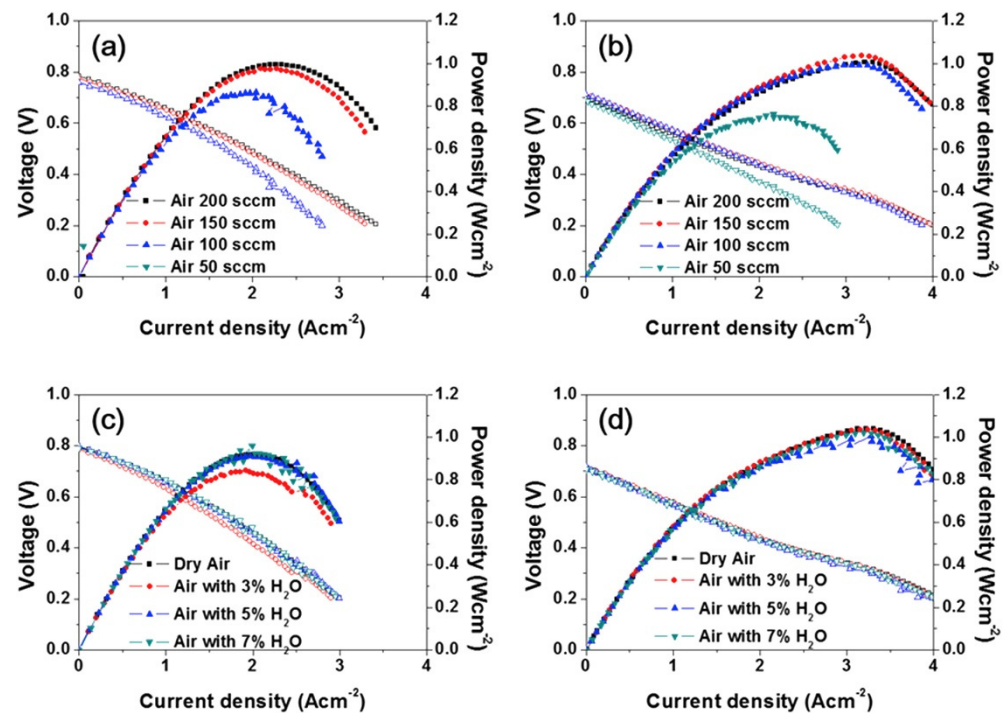


**Figure 8.**  $I$ – $V$  curves and corresponding power densities of test cells with different cathodes (a,c)  $\text{Ba}_{0.5}\text{Sr}_{0.5}\text{Co}_{0.8}\text{Fe}_{0.2}\text{O}_{3-\delta}\text{--Nd}_{0.1}\text{Ce}_{0.9}\text{O}_{2-\delta}$  and (b,d)  $\text{NdBa}_{0.5}\text{Sr}_{0.5}\text{Co}_{1.5}\text{Fe}_{0.5}\text{O}_{5+\delta}\text{--Nd}_{0.1}\text{Ce}_{0.9}\text{O}_{2-\delta}$  under various cathode air flow rates (a,b) and humidities (c,d). The single cells were operated at 923 K with humidified  $\text{H}_2$  (3vol.%  $\text{H}_2\text{O}$ ) as the fuel and ambient air as the oxidant. (a,b) air flow rate change: 50, 100, 150, and 200 sccm. (c,d) air humidity change: dry, 3 vol.%, 5vol.%, and 7vol.%  $\text{H}_2\text{O}$  (reproduced with permission from [151]. Copyright 2016, Elsevier).

**Table 6.** Oxygen anion diffusion coefficients and activation energies calculated using molecular dynamics for REE–barium layered double cobaltites.

Material Composition	Diffusion Coefficient ( $\text{cm}^2 \text{s}^{-1}$ )	$T$ , K	Activation Energy ( $\text{kJ mol}^{-1}$ )	Refs.
$\text{PrBaCo}_2\text{O}_{5+\delta}$	$3.0 \cdot 10^{-8}$	873	40.5	[149]
$\text{PrBa}_{0.5}\text{Sr}_{0.5}\text{Co}_2\text{O}_{5+\delta}$	$8.33 \cdot 10^{-8}$	873	28.9	[149]
$\text{PrBaCo}_{1.5}\text{Fe}_{0.5}\text{O}_{5+\delta}$	$8.0 \cdot 10^{-8}$	873	24.12	[149]
$\text{PrBa}_{0.5}\text{Sr}_{0.5}\text{CoFeO}_{5+\delta}$	$5.50 \cdot 10^{-8}$	873	41.6	[152]
$\text{PrBa}_{0.5}\text{Sr}_{0.5}\text{Co}_{1.5}\text{Fe}_{0.5}\text{O}_{5+\delta}$	$1.18 \cdot 10^{-7}$	873	30.9	[149]
$\text{GdBa}_{0.5}\text{Sr}_{0.5}\text{Co}_2\text{O}_{5+\delta}$	$4 \cdot 10^{-8}$	923	47.2	[152]
$\text{GdBa}_{0.5}\text{Sr}_{0.5}\text{Co}_{1.5}\text{Fe}_{0.5}\text{O}_{5+\delta}$	$3.0 \cdot 10^{-8}$	873	34.7	[149]
$\text{GdBa}_{0.5}\text{Sr}_{0.5}\text{Co}_{1.5}\text{Fe}_{0.5}\text{O}_{5+\delta}$	$5.13 \cdot 10^{-8}$	923	40.6	[152]
$\text{GdBa}_{0.5}\text{Sr}_{0.5}\text{CoFeO}_{5+\delta}$	$7.5 \cdot 10^{-8}$	923	44.9	[149]
$\text{NdBa}_{0.5}\text{Sr}_{0.5}\text{Co}_2\text{O}_{5+\delta}$	$4 \cdot 10^{-8}$	873	28.7	[152]
$\text{NdBa}_{0.5}\text{Sr}_{0.5}\text{Co}_{1.5}\text{Fe}_{0.5}\text{O}_{5+\delta}$	$5.16 \cdot 10^{-8}$	873	48.0	[149]
$\text{NdBa}_{0.5}\text{Sr}_{0.5}\text{CoFeO}_{5+\delta}$	$3.8 \cdot 10^{-8}$	873	28.6	[152]

The co-doping strategy was used in [159–161] to improve the electrochemical performance of  $\text{LnBaCo}_2\text{O}_{5+\delta}$  cathodes. The XPS results showed that REE and transition metal (TM) ions in  $\text{PrBaCo}_{2/3}\text{Fe}_{2/3}\text{Cu}_{2/3}\text{O}_{5+\delta}$  (PCFC) exist in two different valence states ( $\text{Pr}^{3+}/\text{Pr}^{4+}$ ,  $\text{Co}^{3+}/\text{Co}^{4+}$ ,  $\text{Fe}^{3+}/\text{Fe}^{4+}$ , and  $\text{Cu}^+/\text{Cu}^{2+}$ ). The TEC value of this compound was equal to  $16.6 \times 10^{-6} \text{ K}^{-1}$ , which was much smaller than that of the unsubstituted layered cobaltite. The polarization resistance values of the PCFC cathode on the SDC and GDC electrolytes were 0.144 and 0.038  $\Omega \text{ cm}^2$  at 1073 K, respectively. The maximum power density of a single cell with PCFC on a 300  $\mu\text{m}$ -thick GDC electrolyte reached 659  $\text{mW cm}^{-2}$  at 1073 K [159]. Similar results were obtained for the  $\text{NdBaCo}_{2/3}\text{Fe}_{2/3}\text{Cu}_{2/3}\text{O}_{5+\delta}$  (NBCFC) double perovskite, the TEC of which was  $15.7 \times 10^{-6} \text{ K}^{-1}$  within a temperature range of

303–1123 K. The values of the polarization resistance of NBCFC were 0.056 and 0.023  $\Omega \text{ cm}^2$  at 1073 K with the  $\text{Ce}_{0.9}\text{Gd}_{0.1}\text{O}_{1.9}$  and  $\text{La}_{0.9}\text{Sr}_{0.1}\text{Ga}_{0.8}\text{Mg}_{0.2}\text{O}_{3-\delta}$  electrolytes, respectively [160]. Co-substitution with Fe and Mn sharply decreased the TEC from  $21.5 \cdot 10^{-6} \text{ K}^{-1}$  for  $\text{PrBaCo}_2\text{O}_{5+\delta}$  to  $17.8 \times 10^{-6} \text{ K}^{-1}$  for  $\text{PrBaCo}_{2/3}\text{Fe}_{2/3}\text{Mn}_{1/2}\text{O}_{5+\delta}$  (PBCFM) at a temperature range of 303–1273 K [161]. When using 300  $\mu\text{m}$ -thick  $\text{Sm}_{0.2}\text{Ce}_{0.8}\text{O}_{1.9}$  (SDC) as an electrolyte, the ASR and maximum power density values were equal to 0.028  $\Omega \text{ cm}^2$  and 588  $\text{mW cm}^{-2}$  at 1073 K, respectively. The SDC-impregnated PBCFM composite cathode showed improved electrochemical characteristics; its ASR and peak power density were 0.23  $\Omega \text{ cm}^2$  and 621  $\text{mW cm}^{-2}$  at 1073 K, respectively.

#### 4.4. Composites Based on $\text{LnBaCo}_2\text{O}_{5+\delta}$ Layered Perovskites

Composites of layered cobaltites with different solid electrolytes were extensively studied as possible cathode materials for SOFCs based on both oxygen-ion [87,162–169] and proton-conducting solid electrolytes (SE) [170,171], as well as oxygen separation membranes [172,173]. The addition of SE to the layered cobaltites lowers their TEC values [87,162,164–166], making them more chemically and thermomechanically compatible with electrolytes; it also considerably improves the electrochemical performance of composite cathodes in comparison with the single-phase ones due to the enlarging active zones at which ORR can occur [162,163,165,166,168–171].

The addition of 20 wt.% of  $\text{Bi}_2\text{O}_3$  to  $\text{LaBaCo}_2\text{O}_{5+\delta}$  resulted in the lowest ASR value (0.020  $\Omega \text{ cm}^2$  at 1073 K in air), which was about a seventh of that of the  $\text{LaBaCo}_2\text{O}_{5+\delta}$  cathode in the same conditions [163]. At a current density of 0.2  $\text{A cm}^{-2}$ , the cathodic overpotential of  $\text{LaBaCo}_2\text{O}_{5+\delta} + 20 \text{ wt.}\% \text{Bi}_2\text{O}_3$  was approximately 12.6 mV at 973 K, while the corresponding value for  $\text{LaBaCo}_2\text{O}_{5+\delta}$  was 51.0 mV.

In [165], the  $\text{EuBa}_{0.98}\text{Co}_2\text{O}_{5+\delta} + x \text{ wt.}\% \text{Ce}_{0.9}\text{Sm}_{0.1}\text{O}_{1.9}$  (EBCO- $x$ SDC) ( $0 \leq x \leq 40$ ) composites were systematically studied as cathode materials for SOFCs. It was found that EBCO- $x$ SDC materials had excellent electrocatalytic ORR activity due to the synergistic effects of the high electronic-conducting EBCO phase and ionic-conducting SDC electrolyte. The best cathode performance among the studied composites was exhibited by the EBCO-20SDC material (0.028  $\Omega \text{ cm}^2$  at 973 in air), when tested in a single-cell Ni-YSZ|YSZ|CGO|EBCO-20SDC (Figure 9). A high power density of 980  $\text{mW cm}^{-2}$  at 973 K was achieved, which was approximately two times higher than that for the EBCO cathode-based fuel cell. The results of electrochemical impedance spectroscopy (EIS) showed that the charge transfer was the rate-limiting step at the cathode interface. The addition of SDC to the EBCO improved both the charge transfer reaction and the gas diffusion process due to the high oxygen-ion conductivity and large surface of the SDC electrolyte.

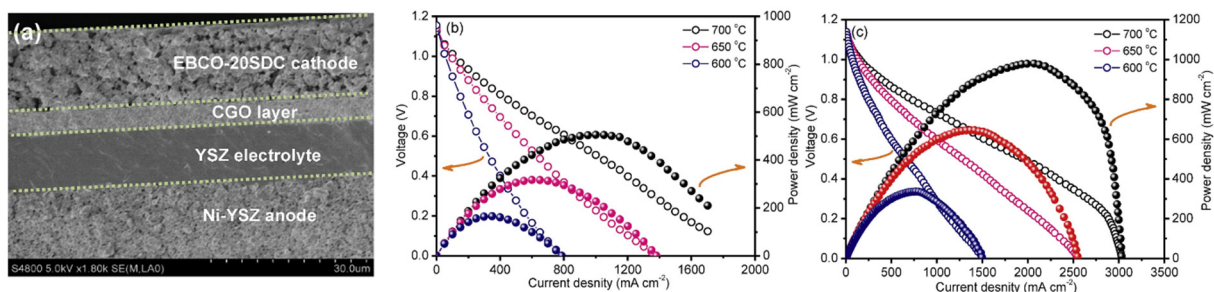


**Figure 9.** (a) Cross-section view of SEM micrograph of the Ni-YSZ|YSZ|CGO|EBCO-20SDC cell. The  $V$ - $I$  and  $P$ - $I$  curves of the Ni-YSZ|YSZ|CGO|EBCO- $x$ SDC cells from 873 K to 973 K at (b)  $x = 0$  and (c)  $x = 20$  (adopted with permission from [165]. Copyright 2019, Elsevier).

Idrees et al. [168], using a facile and effective one-pot sol-gel method, prepared a  $\text{PrBa}_{0.92}\text{Co}_2\text{O}_{6-\delta} - 40 \text{ wt.}\% \text{Ce}_{0.8}\text{Sm}_{0.2}\text{O}_{1.9}$  (OPCC) composite cathode material and comparatively studied its electrochemical performance in tandem with a composite cathode with the same composition which was synthesized by means of a traditional ball-milling method



(BMCC), as well as with the single-phase  $\text{PrBa}_{0.92}\text{Co}_2\text{O}_{6-\delta}$  cathode. Among the three studied cathodes, OPCC showed the lowest ASR ( $0.015 \Omega \text{ cm}^2$  at 1023 K), indicating the highest ORR catalytic activity. The OPCC-based anode-supported single cell demonstrated the highest peak power densities, with a typical value of  $1011 \text{ mW cm}^{-2}$  at 1023 K in contrast to  $783 \text{ mW cm}^{-2}$  for the BMCC-based cell and  $574 \text{ mW cm}^{-2}$  for the  $\text{PrBa}_{0.92}\text{Co}_2\text{O}_{6-\delta}$ -based cell. The OPCC-based cell also showed stable performance without obvious degradation over 100 h at 973 K.

In [169], the  $\text{Pr}_{0.95}\text{BaCo}_2\text{O}_{6-\delta-x}\text{Ce}_{0.8}\text{Sm}_{0.2}\text{O}_{1.9}$  ( $x = 0, 30, 40, 50$ ) composites (PBCO- $x$ SDC) were successfully prepared and investigated. It was found that the addition of SDC to the  $\text{Pr}^{3+}$ -deficient perovskite decreased its TEC and electrical conductivity values but enhanced its catalytic activity over ORR. The best electrochemical performance was shown by the PBCO-40SDC cathode, for which ASR was  $0.005 \Omega \text{ cm}^2$  at 1023 K. An anode-supported single cell with this cathode demonstrated high peak power densities, such as  $1171 \text{ mW cm}^{-2}$  at 1023 K and  $917 \text{ mW cm}^{-2}$  at 973 K.

Electrical conductivity and oxygen permeability of the  $\text{Ce}_{0.8}\text{Gd}_{0.2}\text{O}_{2-\delta}$ - $\text{GdBaCo}_2\text{O}_{5+\delta}$  (CGO-GBCO) and  $\text{Ce}_{0.8}\text{Gd}_{0.2}\text{O}_{2-\delta}$ - $\text{PrBaCo}_2\text{O}_{5+\delta}$  (CGO-PBCO) dual-phase composites were studied in [172,173]. The thermally activated oxygen permeation flux reached  $0.28 \text{ mL min}^{-1} \text{ cm}^{-2}$  at air/He condition for the 0.62 mm-thick CGO-GBCO specimen at 1223 K, which was an order of magnitude larger than that of the GBCO specimen at the same conditions [172]. For the CGO-PBCO (6/4) membrane with 0.6 mm in thickness, oxygen flux was as large as  $2.38 \cdot 10^{-7} \text{ mol cm}^{-2} \text{ s}^{-1}$  at 1198 K [173]. It was found that the CGO and PBCO phases exhibited good chemical compatibility and structural stability.

In [174], the  $\text{Nd}_{1-x}\text{BaCo}_2\text{O}_{5+\delta+x/2}\text{Bi}_2\text{O}_3$  ( $x = 0.05, 0.1$ ) composites were synthesized via a glycine-nitrate process. The addition of bismuth oxide to the  $\text{Nd}^{3+}$ -deficient ceramics effectively increased their electrical conductivity and reduced TEC. Polarization resistance and the maximum power density of the  $\text{Nd}_{0.95}\text{BaCo}_2\text{O}_{5+\delta+0.125}\text{Bi}_2\text{O}_3$  composite cathode at 1073 K were  $0.026 \Omega \text{ cm}^2$  and  $720 \text{ mW cm}^{-2}$ , respectively.

$\text{NdSrCo}_2\text{O}_{5+\delta}$  (NSCO) perovskite was used as a cathode material for the  $\text{Ce}_{0.8}\text{Gd}_{0.2}\text{O}_{2-\delta}$  (GDC)-supported microtubular solid oxide fuel cells (MT-SOFCs) [175]. The MT-SOFC with an outer tube diameter of 1.86 mm, an electrolyte thickness of 180  $\mu\text{m}$ , and an NSCO-GDC (1:1) composite cathode presented the best electrochemical performance. The flexural strength of this cell was 177 MPa, ohmic and polarization resistance values of the cell were 0.15 and  $0.03 \Omega \text{ cm}^2$  at 1073 K, and its maximum power density reached  $0.67 \text{ W cm}^{-2}$  at 1073 K.

#### 4.5. $\text{LnBaMe}'\text{Me}''\text{O}_{5+\delta}$ Layered Perovskites and Their Solid Solutions

$\text{LnBaMe}'\text{Me}''\text{O}_{5+\delta}$  are LODPs, the B-sites of which are occupied by two transition metals (usually 3d-metals) taken in the same quantities. These phases, similar to layered cobaltites of REE and barium, were intensively studied as possible cathode materials for SOFCs [176–190]. Some typical results demonstrating their electrochemical performance are collected in Table 7. As can be seen from these data,  $\text{LnBaMe}'\text{Me}''\text{O}_{5+\delta}$  phases may be used as SOFCs cathodes with both oxygen-ion conducting ( $\text{Ce}_{0.8}\text{Sm}_{0.2}\text{O}_{1.9}$ ,  $\text{La}_{0.9}\text{Sr}_{0.1}\text{Ga}_{0.8}\text{Mg}_{0.2}\text{O}_{3-\delta}$ , and  $\text{Gd}_{0.1}\text{Ce}_{0.9}\text{O}_{1.95}$ ) and proton-conducting ( $\text{BaZr}_{0.1}\text{Ce}_{0.7}\text{Y}_{0.2}\text{O}_{3-\delta}$ ) solid electrolytes; at the same time, they demonstrate high electrochemical activity in ORR, which is close to the activity of layered REE-barium cobaltites and their derivatives. The electrochemical performance of  $\text{LnBaMe}'\text{Me}''\text{O}_{5+\delta}$  compounds may be improved by the addition of solid electrolytes with the formation of composites [182,185,186], partial cation substitution [187,190], or creation of A-site deficiency [188].

The  $\text{GdBaFeNiO}_{5+\delta}$  material exhibits good chemical compatibility with the  $\text{Sm}_{0.2}\text{Ce}_{0.8}\text{O}_{1.9}$  electrolyte at temperatures below 1273 K; its ASR value is  $0.219 \Omega \text{ cm}^2$  at 1073 K, and the maximum power density of the  $\text{Ni-Sm}_{0.2}\text{Ce}_{0.8}\text{O}_{1.9} | \text{Sm}_{0.2}\text{Ce}_{0.8}\text{O}_{1.9} | \text{GdBaFeNiO}_{5+\delta}$  single cell reaches  $287 \text{ mW cm}^{-2}$  at 1073 K [185]. The activity and performance of the  $\text{GdBaFeNiO}_{5+\delta}$  cathode can be improved by the impregnation of nano-sized  $\text{Sm}_{0.2}\text{Ce}_{0.8}\text{O}_{1.9}$  particles: the polarization resistance is decreased by more than 14 times (down to  $0.065 \Omega \text{ cm}^2$

at 1073 K), and the maximum power density of the single cell increased by 1.9 times (up to  $515 \text{ mW cm}^{-2}$  at 1073 K).

The  $\text{La}_{1.4}\text{Ca}_{0.6}\text{CoMnO}_{5+\delta}$  (LCCM) material has a monoclinic structure, high structural stability up to 1173 K, and exhibits good chemical compatibility with the  $\text{La}_{0.9}\text{Sr}_{0.1}\text{Ga}_{0.8}\text{Mg}_{0.2}\text{O}_{3-\delta}$  (LSGM) and  $\text{Sm}_{0.2}\text{Ce}_{0.8}\text{O}_{1.9}$  (SDC) electrolytes at temperatures of up to 1273 K. The maximum power density of a NiO–SDC | SDC | LSGM | LCCM single cell reaches  $445 \text{ mW cm}^{-2}$  at 1073 K [186]. The electrochemical performance, thermal expansion behavior, and stability of LCCM improve by adding appropriate amounts of SDC. The LCCM–30 wt.%SDC composite cathode shows the increased electrochemical performance: the ASR is decreased by 68% and the maximum power density is increased by 22%.

**Table 7.** Performance (ASR: area specific resistance, MPD: maximal power density) of SOFCs based on  $\text{LnBaMe}'\text{Me}''\text{O}_{5+\delta}$  compounds.

Cathode	Electrolyte	ASR, $\Omega \text{ cm}^2$ (T, K)	MPD, $\text{mW cm}^{-2}$ (T, K)	Refs.
$\text{LaBaCuFeO}_{5+\delta}$	$\text{Ce}_{0.8}\text{Sm}_{0.2}\text{O}_{1.9}$	0.21 (973)	557 (1073)	[176]
$\text{LaBaCuCoO}_{5+\delta}$	$\text{Ce}_{0.8}\text{Sm}_{0.2}\text{O}_{1.9}$	0.11 (973)	603 (1073)	[176]
$\text{GdBaCuCoO}_{5+\delta}$	$\text{La}_{0.9}\text{Sr}_{0.1}\text{Ga}_{0.8}\text{Mg}_{0.2}\text{O}_{3-\delta}$	0.091 (1023)	545 (1073)	[177]
$\text{GdBaCuCoO}_{5+\delta}$	$\text{Sm}_{0.2}\text{Ce}_{0.8}\text{O}_{1.9}$	0.129 (1023)	528 (1073)	[177]
$\text{SmBaCuCoO}_{5+\delta}$	$\text{BaCe}_{0.7}\text{Zr}_{0.1}\text{Y}_{0.2}\text{O}_{3-\delta}$	0.22 (973)	355 (973)	[178]
$\text{PrBaCuCoO}_{5+\delta}$	$\text{Sm}_{0.2}\text{Ce}_{0.8}\text{O}_{1.9}$	0.047 (973)	791 (973)	[179]
$\text{LaBaCuFeO}_{5+\delta}$	$\text{BaZr}_{0.1}\text{Ce}_{0.7}\text{Y}_{0.2}\text{O}_{3-\delta}$	0.27 (973)	327 (973)	[181]
$\text{LaBaCuCoO}_{5+\delta}$	$\text{BaZr}_{0.1}\text{Ce}_{0.7}\text{Y}_{0.2}\text{O}_{3-\delta}$	0.15 (973)	432 (973)	[181]
$\text{GdBaFeNiO}_{5+\delta}$	$\text{BaZr}_{0.1}\text{Ce}_{0.7}\text{Y}_{0.2}\text{O}_{3-\delta}$	0.15 (973)	456 (973)	[183]
$\text{PrBaCoFeO}_{5+\delta}$	$\text{La}_{0.9}\text{Sr}_{0.1}\text{Ga}_{0.8}\text{Mg}_{0.2}\text{O}_{3-\delta}$	0.049 (1073)	749 (1073)	[184]
$\text{NdBaCoFeO}_{5+\delta}$	$\text{La}_{0.9}\text{Sr}_{0.1}\text{Ga}_{0.8}\text{Mg}_{0.2}\text{O}_{3-\delta}$	0.062 (1073)	669 (1073)	[184]
$\text{La}_{1.4}\text{Ca}_{0.6}\text{CoMnO}_{5+\delta}$	$\text{La}_{0.9}\text{Sr}_{0.1}\text{Ga}_{0.8}\text{Mg}_{0.2}\text{O}_{3-\delta}$	–	445 (1073)	[186]
$\text{NdBa}_{0.7}\text{Ca}_{0.3}\text{CoCuO}_{5+\delta}$	$\text{Gd}_{0.1}\text{Ce}_{0.9}\text{O}_{1.95}$	0.038 (973)	1840 (1073)	[187]
$\text{Y}_{0.93}\text{BaCoCuO}_{5+\delta}$	$\text{La}_{0.9}\text{Sr}_{0.1}\text{Ga}_{0.8}\text{Mg}_{0.2}\text{O}_{3-\delta}$	0.029 (1073)	862 (1123)	[188]
$\text{Pr}_{0.9}\text{Ca}_{0.1}\text{BaCoFeO}_{5+\delta}$	$\text{La}_{0.9}\text{Sr}_{0.1}\text{Ga}_{0.8}\text{Mg}_{0.2}\text{O}_{3-\delta}$	0.027 (1073)	728 (1073)	[190]

A partial substitution of Ba with Ca in  $\text{NdBaCoCuO}_{5+\delta}$  resulted in decreased TEC and oxygen content and increased the electrical conductivity in air [187]. Compared to the parent oxide, the modified sample has a greatly enhanced electrochemical performance. The ASR of  $\text{NdBa}_{1-x}\text{Ca}_x\text{CoCuO}_{5+\delta}$ -based symmetrical cells with a  $\text{Gd}_{0.1}\text{Ce}_{0.9}\text{O}_{1.95}$  electrolyte at 973 K dropped from  $0.062 \Omega \text{ cm}^2$  for  $x = 0$  to  $0.038 \Omega \text{ cm}^2$  for  $x = 0.3$ . The maximum power density for  $\text{NdBa}_{1-x}\text{Ca}_x\text{CoCuO}_{5+\delta}$ -based single cells at 1073 K increased from  $1420 \text{ mW cm}^{-2}$  for  $x = 0$  to  $1840 \text{ mW cm}^{-2}$  for  $x = 0.3$  (Figure 10).

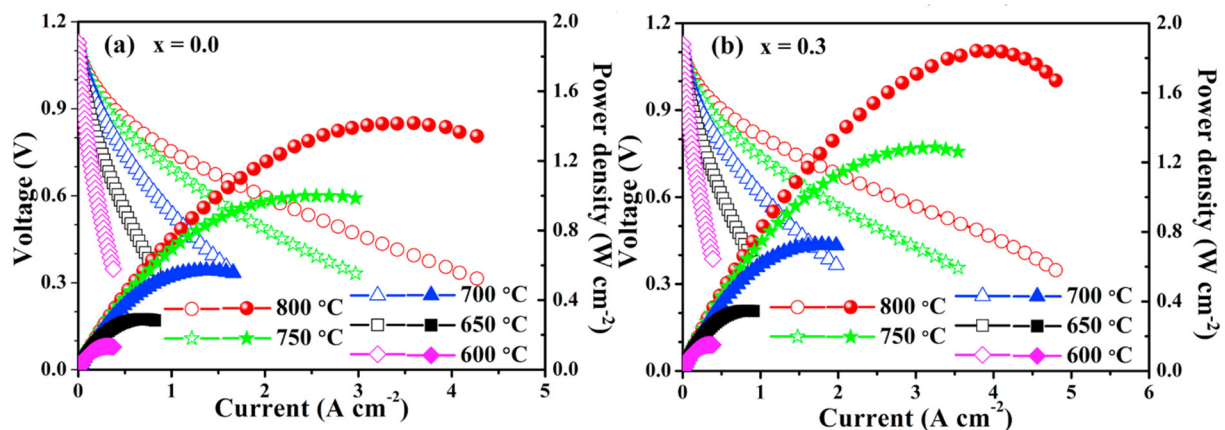


**Figure 10.**  $I$ – $V$  and  $I$ – $P$  curves of  $\text{NdBa}_{1-x}\text{Ca}_x\text{CoCuO}_{5+\delta}$  based single cells at (a)  $x = 0$  and (b)  $x = 0.3$  (adopted with permission from [187]. Copyright 2018, Elsevier).

The  $Y_{1-x}BaCoCuO_{5+\delta}$  ( $x = 0.00, 0.03, 0.05, 0.07, 0.10$ ) layered perovskites with a  $Y^{3+}$ -deficiency were studied as cathodes for SOFCs in work [188]. These compounds crystallize in orthorhombic syngony, and their lattice constants increase with an increasing  $Y^{3+}$  deficiency. The oxygen content and electrical conductivity values of  $Y_{1-x}BaCoCuO_{5+\delta}$  decrease as  $x$  increases. The results of EIS studies indicate that the creation of a  $Y^{3+}$  deficiency reduces the polarization resistance, the lowest value of which was  $0.029 \Omega \text{ cm}^2$  at 1073 K and was observed for the  $Y_{0.93}BaCoCuO_{5+\delta}$  sample. The LSGM electrolyte-supported single cell with the  $Y_{0.93}BaCoCuO_{5+\delta}$  cathode demonstrated the peak power density values of 862, 643, 426, 274, and  $152 \text{ mW cm}^{-2}$  at 1123, 1073, 1023, 973, and 923 K, respectively.

#### 4.6. The Other Layered Oxygen-Deficient Double Perovskites

Layered double cobaltites usually display high electronic and ionic conductivity, as well as high electrocatalytic activity in the ORR, but they have some drawbacks, such as high TEC values (providing relatively low thermomechanical compatibility of layered cobaltites and typical solid electrolytes in SOFCs), high cost, etc. [191]. These disadvantages are overcome in Co-free perovskite cathodes, including double perovskites, such as  $GdBaFeNiO_{5+\delta}$  [183,185] and layered ferrites of REEs and barium [89,158,192–197]. The main advantage of layered ferrites is their high stability levels in both oxidizing and reducing atmospheres [4,191]; this makes them promising electrode materials for A-SOFCs [89,192–194,196], and S-SOFCs [158,195,197] based on oxygen-ion-conducting [158,194–196] and proton-conducting [89,193,197] electrolytes.

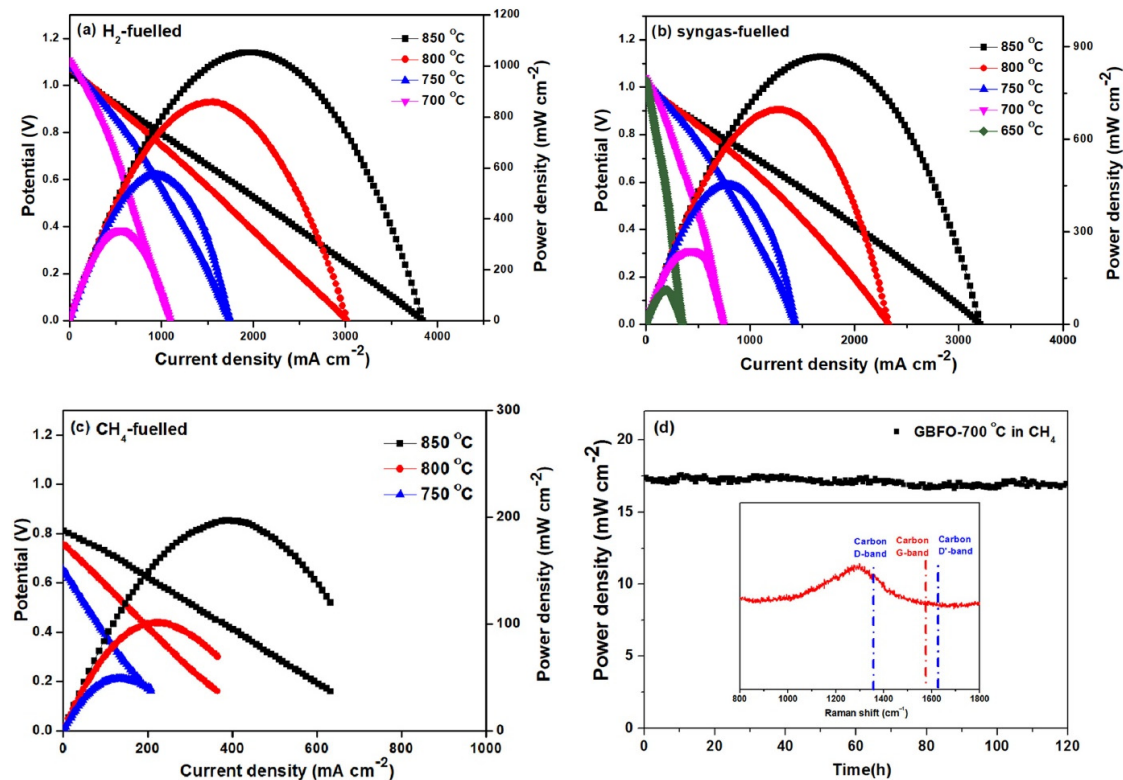
The electrical conductivity and thermal expansion of  $LnBaFe_2O_{5+\delta}$  ( $Ln = La, Pr, Nd, Sm, Gd, \text{ and } Y$ )-layered ferrites decreased at smaller  $Ln^{3+}$  ionic radii; for example, TEC values within 293–1173 K temperature intervals decreased from  $19.4 \times 10^{-6} \text{ K}^{-1}$  for  $Ln = La$  to  $14.6 \times 10^{-6} \text{ K}^{-1}$  for  $Ln = Y$  [192]. The lowest polarization resistance in air under an open circuit voltage was found for the  $SmBaFe_2O_{5+\delta}$  electrode (YSZ as the electrolyte):  $0.043 \Omega \text{ cm}^2$  at 1073 K. The single cell with this material serving as its cathode delivered the highest peak power density of  $1026 \text{ mW cm}^{-2}$  at 1073 K [192]. The  $LaBa_{0.5}Sr_{0.5}Fe_2O_{6-\delta}$  cathode showed a low polarization resistance of  $0.152 \Omega \text{ cm}^2$  at 1023 K and a maximum power density of  $370 \text{ mW cm}^{-2}$  in a  $LaBa_{0.5}Sr_{0.5}Fe_2O_{6-\delta} | SDC | LaBa_{0.5}Sr_{0.5}Fe_2O_{6-\delta}$  S-SOFC [194].

Figure 11 shows the electrochemical performance of the S-SOFC with a  $GdBaFe_2O_{5+\delta} | La_{0.9}Sr_{0.1}Ga_{0.8}Mg_{0.2}O_{3-\delta} | GdBaFe_2O_{5+\delta}$  configuration when using dry  $H_2$ , humidified syngas (61%  $H_2$ , 24%  $CH_4$ , 9.3%  $CO$ , 3.4%  $N_2$ , 2.3%  $CO_2$ , and 5 ppm  $H_2S$ ), and humidified  $CH_4$  (3%  $H_2O$ ) as the fuels and the ambient air as the oxidant. The maximum peak power density of this cell at 1125 K was 1053, 868, and  $197 \text{ mW cm}^{-2}$  for the different fuels, respectively. The observed results indicate that this cell can efficiently operate with complex hydrocarbons fuels. This cell was also tested under a constant potential of 0.35 V with  $CH_4$  as fuel at 973 K for 120 h to assess the carbon tolerance of the  $GdBaFe_2O_{5+\delta}$  anode and the stability of the cell (Figure 11d). No degradation of the cell performance was observed. The Raman spectrum (inset in Figure 11d) shows no peaks corresponding to the carbon deposited on the  $GdBaFe_2O_{5+\delta}$  anode surface, indicating that this material has a high coking tolerance. The peak at ca.  $1300 \text{ cm}^{-1}$  was assigned to  $FeOOH$  and was formed because a small part of exsolved iron nanoparticles reacted with water in humidified  $CH_4$ .

The oxygen transport properties and the chemical stability of  $PrBaFe_2O_{5+\delta}$  (PBF)-layered double perovskite were systematically studied in [198]. The oxygen permeation flux of 0.7 mm-thick samples and the oxygen-ion conductivity were  $4.7 \times 10^{-1} \text{ mL min}^{-1} \text{ cm}^{-2}$  and  $0.12 \text{ Scm}^{-1}$  at 1173 K, respectively. The characteristic thickness estimated from the membrane and conductivity relaxation tests was  $\sim 0.6 \text{ mm}$  at 1173 K. The PBF oxide exhibited superior chemical stability in  $CO_2$ -containing atmosphere.

Layered manganites of barium and REEs (for example,  $PrBaMn_2O_{5+\delta}$ ) have been considered as possible electrode materials both for A-SOFCs and S-SOFCs, as well as for SOECs cathodes [199–201]. The high thermal stability of Fe-doped  $PrBaMn_{2-x}Fe_xO_{6-\delta}$  perovskites both in oxidizing and reducing atmospheres and the moderate TEC values

make these phases good candidates for electrochemical applications [200]. These phases may exchange relatively large amounts of oxygen with the atmosphere, which makes them promising oxygen storage materials as well.



**Figure 11.** Performance of the single cell with  $\text{GdBaFe}_2\text{O}_{5+\delta}$  as its symmetrical electrodes for different fuels: (a)  $\text{H}_2$ , (b) humidified syngas, and (c) humidified  $\text{CH}_4$ . (d) Electrochemical stability test of the cell with humidified  $\text{CH}_4$  as a fuel during a 120 h operation. Inset: Raman spectrum of the anode surface area after stability test (reproduced with permission from [195]. Copyright 2021, Elsevier).

The Sr-deficient  $\text{Sr}_{1.9}\text{FeNb}_{0.9}\text{Mo}_{0.1}\text{O}_{6-\delta}$  double perovskite was prepared via a solid state reaction method and tested as the electrode in S-SOFCs [202]. The electrocatalytic activity of  $\text{Sr}_{1.9}\text{FeNb}_{0.9}\text{Mo}_{0.1}\text{O}_{6-\delta}$  was greatly improved by the impregnation of the solution of  $\text{Pd}(\text{NO}_3)_2$  to form  $\text{Pd-Sr}_{1.9}\text{FeNb}_{0.9}\text{Mo}_{0.1}\text{O}_{6-\delta}$  composite electrodes. The single cell with such symmetrical electrodes after two-time impregnation achieved the peak power densities of 935.4, 196.5, and 11.2  $\text{mW cm}^{-2}$  at 1123 K in dry  $\text{H}_2$ , humidified  $\text{CH}_4$ , and  $17\text{CH}_4-83\text{CO}_2$  mixed gas, respectively, revealing superior performance in different fuels.

In [90], it was shown that  $\text{Sr}_2\text{Co}_{1-x}\text{Nb}_x\text{FeO}_{5+\delta}$  ( $x = 0.0-0.2$ ) double perovskites have good structural stability and chemical compatibility with  $\text{La}_{0.9}\text{Sr}_{0.1}\text{Ga}_{0.8}\text{Mg}_{0.2}\text{O}_{3-\delta}$  and  $\text{Ce}_{0.8}\text{Sm}_{0.2}\text{O}_{1.9}$  electrolytes. The ASR of the  $\text{Sr}_2\text{Co}_{1.9}\text{Nb}_{0.1}\text{FeO}_{5+\delta}$  cathode was  $0.081 \Omega \text{ cm}^2$  at 973 K on the LSGM electrolyte. This cathode showed good electrocatalytic activity for ORR, functional stability, and high electrical conductivity.

The possibility of using  $\text{Sr}_2\text{Sc}_{0.1}\text{Nb}_{0.1}\text{Co}_{1.5}\text{Fe}_{0.3}\text{O}_{6-2\delta}$  thin films as cathodes for IT-SOFCs was tested in [203]. It was found that the film grown along the [110] direction on the YSZ substrate demonstrated lower polarization resistances and smaller activation energy than the film grown along the [100] direction on the SDC/YSZ substrate, indicating better ORR activity. It was also found that the lower Sr-enrichment and higher cobalt-ion oxidation states were beneficial for the ORR.

The La-deficient  $\text{La}_{2-x}\text{CoTiO}_{6-\delta}$  ( $0 \leq x \leq 0.20$ ) double perovskites were chemically stable under oxidizing conditions towards CGO, whereas they reacted with YSZ [204]. The  $\text{La}_{2-x}\text{CoTiO}_{6-\delta}/\text{Ce}_{0.8}\text{Gd}_{0.2}\text{O}_{1.9}$  composites were studied as electrodes of symmetrical cells.



The lowest polarization resistance of  $0.39 \Omega \text{ cm}^2$  at 1073 K was found for materials with  $x = 0.05$ .

#### 4.7. Short Resume

Layered oxygen-deficient double perovskites (primarily cobaltites and their derivatives) are promising cathode materials for IT-SOFCs due to their high electrocatalytic activity in ORR, stability at elevated temperatures and chemical and thermomechanical compatibility with solid electrolytes.

Despite numerous advantages, LODPs have a number of drawbacks in terms of their applications in SOFCs. The literature analyses performed above shows that the main problems are their degradation in  $\text{CO}_2$ -containing atmospheres and relatively large TEC values, as well as chemical expansion at high temperatures due to the loss of weakly-bonded oxygen.

These disadvantages can be eliminated or reduced by tuning the chemical composition of the LODPs or by producing their composites containing different solid electrolytes as a second phase. The electrochemical performance of LODPs can be essentially improved both by the substitution of cations in their A- or/and B-sublattices or by the creation of small cation deficiencies in the A-sublattice (Figure 12). The TEC values and chemical expansion of the LODPs may be reduced by the formation of high-entropy oxides (HEOs) on their base, in which A- or/and B-positions are shared by at least five REEs (as well as alkaline-earth elements) and transition metals, respectively, in equal or near-equal atomic ratios. Such HEOs should be more stable and possess lower polarization resistances compared when with other cathodes based on LODPs. The addition of solid electrolytes to LODPs lowers their TECs and makes them more chemically and thermomechanically compatible with electrolytes and can also improve the electrochemical performance of composite cathodes due to enlarging the zones of the ORRs. The creation of a hierarchical porous microstructure of cathodes also enlarges the areas of the ORRs and improves their electrochemical and electrocatalytic performance.

LODPs based on light REEs have small oxygen deficiencies (large amounts of weakly-bonded oxygen), high values of the Seebeck coefficient, and electrical conductivity, and they also contain transition metal ions in different oxidation states. For these reasons they may be used as high-temperature thermoelectrics, oxygen storage materials, or photocatalysts for the oxidation of organic substances.

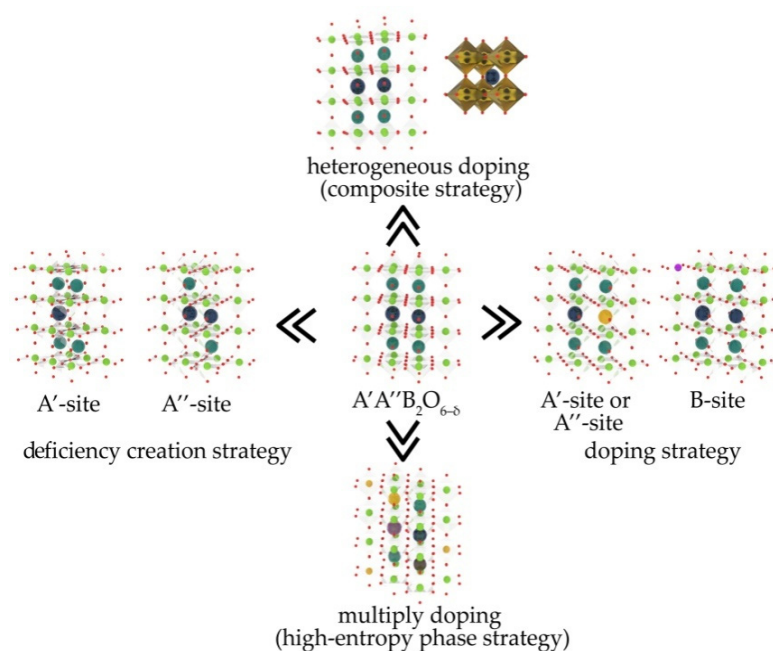


**Figure 12.** Different strategies of improving the performance of  $A'A''B_2O_{6-\delta}$  layered oxygen deficient double perovskites.

## 5. Conclusions

Layered oxygen-deficient perovskites (LODPs) are considered promising candidates for use as cathodes in IT-SOFC applications. In this review, we shortly summarized the available literature data concerning their crystal structure, thermal, and electrotransport and functional, especially electrochemical, properties. The phase transitions of different natures (structural, electric, and magnetic), which take place in LODPs due to the variations of temperature and their chemical composition, were also discussed. The electrochemical performance of materials belonging to different groups of LODPs (cobaltites, ferrites, etc.) in single cells based on both oxygen-ion- and proton-conducting solid electrolytes was found to be quite high for applied purposes. The main focus was on various chemical engineering approaches to improve the electrochemical activity of these materials (creation of cationic deficiencies, doping on different sites, modification by noble metals and solid electrolytes nanoparticles, etc.). It was demonstrated that some LODPs can effectively operate as electrodes of symmetrical SOFCs fueled with hydrogen, methane, or complex hydrocarbons. The other possible areas of usage of these complex oxides (high-temperature thermoelectrics, oxygen storage materials, photocatalysts, etc.) were also finally depicted.

Although this work overviews the last trends in LODPs, a number of recent publications fell within the reviewing procedure. In our opinion, these works [205–211] should be mentioned with no detailed analysis.

**Author Contributions:** Conceptualization: A.I.K. and E.A.C.; formal analysis: A.I.K. and D.S.K.; data curation: E.A.C. and D.S.K.; writing—original draft preparation: A.I.K. and E.A.C.; writing—review and editing: D.S.K. and D.A.M.; visualization: E.A.C. and D.S.K.; supervision: A.I.K. and D.A.M.; project administration: A.I.K. All authors have read and agreed to the published version of the manuscript.

**Funding:** A.I. Klyndyuk thanks to the Ministry of Education of Belarus Republic, contract no. 20062703, and to the Belarusian Republican Foundation for Fundamental Research, grant no. C3M-049. D.A. Medvedev thanks to the Ministry of Education and Science of the Russian Federation, contract no. 075-03-2021-051/5.

**Institutional Review Board Statement:** Not applicable.

**Informed Consent Statement:** Not applicable.

**Data Availability Statement:** Not applicable.

**Conflicts of Interest:** The authors declare no conflict of interest.

## References

1. Lenser, C.; Udomsilp, D.; Menzler, N.H.; Holtappels, P.; Fujisaki, L.; Matsumoto, H.; Sabato, A.G.; Smeacetto, F.; Chrysanthou, A.; Molin, S. Solid oxide fuel and electrolysis cells. In *Advanced Ceramics for Energy Conversion and Storage*; Guillon, O., Ed.; Elsevier: Amsterdam, The Netherlands; Oxford, UK; Cambridge, MA, USA, 2019; pp. 387–547.
2. Lyu, Y.; Xie, J.; Wang, D.; Wang, J. Review of cell performance in solid oxide fuel cells. *J. Mater. Sci.* **2020**, *55*, 7184–7207. [[CrossRef](#)]
3. Filippov, S.P.; Yaroslavtsev, A.B. Hydrogen energy: Development prospects and materials. *Russ. Chem. Rev.* **2021**, *90*, 627–643. [[CrossRef](#)]
4. Istomin, S.Y.; Lyskov, N.V.; Mazo, G.N.; Antipov, E.V. Electrode materials based on complex *d*-metal oxides for symmetrical solid oxide fuel cells. *Russ. Chem. Rev.* **2021**, *90*, 644–676. [[CrossRef](#)]
5. Kharton, V.V.; Marques, F.M.B.; Atkinson, A. Transport properties of solid oxide electrolyte ceramics: A brief review. *Solid State Ion.* **2004**, *174*, 135–149. [[CrossRef](#)]
6. Jacobson, A.J. Materials for Solid Oxide Fuel Cells. *Chem. Mater.* **2010**, *22*, 660–674. [[CrossRef](#)]
7. Irshad, M.; Siraj, K.; Raza, R.; Ali, A.; Tiwari, P.; Zhu, B.; Rafique, A.; Ali, A.; Ullah, M.K.; Usman, A. A Brief Description of High Temperature Solid Oxide Fuel Cell's Operation, Materials, Design, Fabrication Technologies and Performance. *Appl. Sci.* **2016**, *6*, 75. [[CrossRef](#)]
8. da Silva, F.S.; de Souza, T.M. Novel materials for solid oxide fuel cell technologies: A literature review. *Int. J. Hydrogen Energy* **2017**, *42*, 26020–26036. [[CrossRef](#)]
9. Hussain, S.; Yangping, L. Review of solid oxide fuel cell materials: Cathode, anode, and electrolyte. *Energy Transit.* **2020**, *4*, 113–126. [[CrossRef](#)]
10. Vostakola, M.F.; Horri, B.A. Progress in Materials Development for Low-Temperature Solid Oxide Fuel Cells: A Review. *Energies* **2021**, *14*, 1280. [[CrossRef](#)]
11. Dudek, M.; Lis, B.; Lach, R.; Daugela, S.; Šalkus, T.; Kežionis, A.; Mosiałek, M.; Socha, R.; Morgiel, J.; Gajek, M.; et al. Ba<sub>0.95</sub>Ca<sub>0.05</sub>Ce<sub>0.9</sub>Y<sub>0.1</sub>O<sub>3</sub> as electrolyte for proton-conducting ceramic fuel cells. *Electrochim. Acta* **2019**, *304*, 70–79. [[CrossRef](#)]
12. Molenda, J.; Kupecki, J.; Baron, R.; Blesznowski, M.; Brus, G.; Brylewski, T.; Busko, M.; Chmielowec, J.; Cwieka, K.; Gazda, M.; et al. Status report on high temperature fuel cells in Poland—Recent advances and achievements. *Int. J. Hydrogen Energy* **2017**, *42*, 4366–4403. [[CrossRef](#)]
13. Plazaola, A.A.; Labella, A.C.; Liu, Y.; Porras, N.B.; Tanaka, D.A.P.; Annaland, M.V.S.; Gallucci, F. Mixed Ionic–Electronic Conducting Membranes (MIEC) for Their Application in Membrane Reactors: A Review. *Processes* **2019**, *7*, 128. [[CrossRef](#)]
14. Khan, M.S.; Xu, X.; Knibbe, R.; Zhu, Z. Air electrodes and related degradation mechanisms in solid oxide electrolysis and reversible solid oxide fuel cells. *Renew. Sustain. Energy Rev.* **2021**, *143*, 110918. [[CrossRef](#)]
15. Wang, R.-T.; Chang, H.-Y.; Wang, J.-C. An Overview on the Novel Core-Shell Electrodes for solid Oxide Fuel Cell (SOFC) Using Polymeric Methodology. *Polymers* **2021**, *13*, 2774. [[CrossRef](#)]
16. Lu, Y.; Mi, Y.; Li, J.; Qi, F.; Yan, S.; Dong, W. Recent Progress in Semiconductor-Ionic Conductor Nanomaterial as a Membrane for Low-Temperature Solid Oxide Fuel Cells. *Nanomaterials* **2021**, *11*, 2290. [[CrossRef](#)]
17. Kalinina, E.; Pikalova, E. Opportunities, Challenges and Prospects for Electrodeposition of Thin-Film Functional Layers in Solid Oxide Fuel Cell Technology. *Materials* **2021**, *14*, 5584. [[CrossRef](#)]
18. Liu, J.; Ma, J.; Zhang, Z.; Qin, Y.; Wang, Y.-J.; Wang, Y.; Tan, R.; Duan, X.; Tian, T.Z.; Zhang, C.H.; et al. 2021 Roadmap: Electrocatalysis for green catalytic processes. *J. Phys. Mater.* **2021**, *4*, 022004. [[CrossRef](#)]
19. Chen, G.; Feldhoff, A.; Weidenkaff, A.; Li, C.; Liu, S.; Zhu, X.; Sunarso, J.; Huang, K.; Wu, X.-Y.; Ghoniem, A.F.; et al. Roadmap on Sustainable Mixed Ionic-Electronic Conducting Membranes. *Adv. Funct. Mater.* **2021**, *31*, 2105702. [[CrossRef](#)]
20. Kim, S.; Kim, G.; Manthiram, A. A review on infiltration techniques for energy conversion and storage devices: From fundamentals to applications. *Sustain. Energy Fuels* **2021**, *5*, 5024–5037. [[CrossRef](#)]
21. Mendonça, C.; Ferreira, A.; Santos, D.M.F. Towards the Commercialization of Solid Oxide Fuel Cells: Recent Advances in Materials and Integration Strategies. *Fuels* **2021**, *2*, 393–419. [[CrossRef](#)]
22. Hanif, M.B.; Rauf, S.; Motola, M.; Babar, Z.U.D.; Li, C.-J. Recent progress of perovskite-based electrolyte materials for solid oxide fuel cells and performance optimizing strategies for energy storage applications. *Mat. Res. Bull.* **2022**, *146*, 111612. [[CrossRef](#)]
23. Cigolotti, V.; Genovese, M.; Fragiaco, P. Comprehensive Review on Fuel Cell Technology for Stationary Applications as Sustainable and Efficient Poly-Generation Energy Systems. *Energies* **2021**, *14*, 4963. [[CrossRef](#)]
24. Skutina, L.S.; Vylkov, A.A.; Kuznetsov, D.K.; Medvedev, D.A.; Shur, Y. Tailoring Ni and Sr<sub>2</sub>Mg<sub>0.25</sub>Ni<sub>0.75</sub>MoO<sub>6-δ</sub> Cermet Compositions for Designing the Fuel Electrodes of Solid Oxide Electrochemical Cells. *Energies* **2019**, *12*, 2394. [[CrossRef](#)]
25. Skutina, L.; Filonova, E.; Medvedev, D.; Maignan, A. Undoped Sr<sub>2</sub>MMoO<sub>6</sub> Double Perovskite Molybdates (M = Ni, Mg, Fe) as Promising Anode Materials for Solid Oxide Fuel Cells. *Materials* **2021**, *14*, 1715. [[CrossRef](#)] [[PubMed](#)]
26. Klyndyuk, A.I. Layered Perovskite-Like Oxides 0112 Type: Structure, Properties, and Possible Applications. In *Advanced in Chemistry Research*; Taylor, J.C., Ed.; Nova Science Publishers: New York, NY, USA, 2010; pp. 59–105.

27. Sun, C.; Hui, R.; Roller, J. Cathode materials for solid oxide fuel cells: A review. *J. Solid State Electrochem.* **2010**, *14*, 1125–1144. [[CrossRef](#)]
28. Tahir, N.N.M.; Baharuddin, N.A.; Samat, A.A.; Osman, N.; Somalu, M.R. A review on cathode materials for conventional and proton-conducting solid oxide fuel cells. *J. Alloys Compd.* **2021**, *894*, 162458. [[CrossRef](#)]
29. Khan, M.Z.; Song, R.-H.; Mehran, M.T.; Lee, S.-B.; Lim, T.-H. Controlling cation migration and inter-diffusion across cathode/interlayer/electrolyte interfaces of solid oxide fuel cells: A review. *Ceram. Int.* **2021**, *47*, 5839–5869. [[CrossRef](#)]
30. Wang, F.; Kishimoto, H.; Ishihara, T.; Develos-Bagarinao, K.; Yamaji, K.; Horita, T.; Yokokawa, H. A review of sulfur poisoning of solid oxide fuel cell cathode materials for solid oxide fuel cells. *J. Power Source* **2020**, *478*, 228763. [[CrossRef](#)]
31. Shen, M.; Zhang, P. Progress and challenges of cathode contact layer for solid oxide fuel cell. *Int. J. Hydrogen Energy* **2020**, *45*, 33876–33894. [[CrossRef](#)]
32. Aziz, A.J.A.; Baharuddin, N.A.; Somalu, M.R.; Muchtar, A. Review of composite cathodes for intermediate-temperature solid oxide fuel cell applications. *Ceram. Int.* **2020**, *46*, 23314–23325. [[CrossRef](#)]
33. Qiu, P.; Yang, X.; Zhu, T.; Sun, S.; Jia, L.; Li, J. Review on core-shell structured cathode for intermediate temperature solid oxide fuel cells. *Int. J. Hydrogen Energy* **2020**, *45*, 23160–23173. [[CrossRef](#)]
34. Kaur, P.; Singh, K. Review of perovskite-structure related cathode materials for solid oxide fuel cells. *Ceram. Int.* **2020**, *46*, 5521–5535. [[CrossRef](#)]
35. Yattoo, M.A.; Kawale, S.S.; Skinner, S.J. Perovskite and layered oxide materials for intermediate temperature solid oxide fuel cells. In *Intermediate Temperature Solid Oxide Fuel Cells*; Kaur, G., Ed.; Elsevier: Amsterdam, The Netherlands; Oxford, UK; Cambridge, MA, USA, 2020; pp. 315–346.
36. Irvine, J.; Rupp, J.L.M.; Liu, G.; Xu, X.; Haile, S.; Qian, X.; Snyder, A.; Freer, R.; Efrén, D.; Skinner, S.; et al. Roadmap on inorganic perovskites for energy applications. *J. Phys. Energy* **2021**, *3*, 031502. [[CrossRef](#)]
37. Su, C.; Wang, W.; Shao, Z. Cation-Deficient Perovskites for Clean Energy Conversion. *Acc. Mater. Res.* **2021**, *2*, 477–488. [[CrossRef](#)]
38. Nechache, A.; Hody, S. Alternative and innovative solid oxide electrolysis cell materials: A review. *Renew. Sust. Energy Rev.* **2021**, *149*, 111322. [[CrossRef](#)]
39. Hanif, M.B.; Motola, M.; Rauf, S.; Li, C.-J.; Li, C.-X. Recent advancements, doping strategies and the future perspective of perovskite-based solid oxide fuel cells for energy conversion. *Chem. Eng. J.* **2022**, *428*, 132603. [[CrossRef](#)]
40. Gao, Z.; Mogni, L.V.; Miller, E.C.; Railsback, J.C.; Barnett, S.A. A perspective on low-temperature solid oxide fuel cells. *Energy Environ. Sci.* **2016**, *9*, 1602–1644. [[CrossRef](#)]
41. Afroze, S.; Karim, A.H.; Cheok, Q.; Eriksson, S.; Azad, A.K. Latest development of double perovskite electrode materials for solid oxide fuel cells: A review. *Front. Energy* **2019**, *13*, 770–797. [[CrossRef](#)]
42. Bello, I.T.; Zhai, S.; He, Q.; Xu, Q.; Ni, M. Scientometric review of advancements in the development of high-performance cathode for low and intermediate temperature solid oxide fuel cells: Three decades in retrospect. *Int. J. Hydrogen Energy* **2021**, *46*, 26518–26536. [[CrossRef](#)]
43. Kasyanova, A.V.; Tarutina, L.R.; Rudenko, A.O.; Lyagaeva, J.G.; Medvedev, D.A. Ba(Ce,Zr)O<sub>3</sub>-based electrodes for protonic ceramic electrochemical cells: Towards highly compatible functionality and triple-conducting behaviour. *Russ. Chem. Rev.* **2020**, *89*, 667–692. [[CrossRef](#)]
44. Mather, G.C.; Muñoz-Gil, D.; Zamudio-García, J.; Porras-Vázquez, J.M.; Marrero-López, D.; Pérez-Coll, D. Perspectives on Cathodes for Protonic Ceramic Fuel Cells. *Appl. Sci.* **2021**, *11*, 5363. [[CrossRef](#)]
45. Seong, A.; Kim, J.; Jeong, D.; Sengodan, S.; Liu, M.; Choi, S.; Kim, G. Electrokinetic Proton Transport in Triple (H<sup>+</sup>/O<sup>2-</sup>/e<sup>-</sup>) Conducting Oxides as a Key Descriptor for Highly Efficient Protonic Ceramic Fuel Cells. *Adv. Sci.* **2021**, *8*, 2004099. [[CrossRef](#)] [[PubMed](#)]
46. Samat, A.A.; Darus, M.; Osman, N.; Baharuddin, N.A.; Anwar, M. A Short Review on Triple Conducting Oxide Cathode Materials for Proton conducting Oxide Fuel Cell. *AIP Conf. Proc.* **2021**, *2339*, 020233.
47. Wang, N.; Hinokuma, S.; Ina, T.; Zhu, C.; Habazaki, H.; Aoki, Y. Mixed Proton–electron–oxide ion Triple Conducting Manganite as Efficient Cobalt-free Cathode for Protonic ceramic Fuel Cells. *J. Mater. Chem. A* **2020**, *8*, 11043–11055. [[CrossRef](#)]
48. Malyshkin, D.; Novikov, A.; Ivanov, I.; Sereda, V.; Tsvetkov, D.; Zuev, A. The origin of triple conductivity and water uptake in layered double perovskites: A case study on lanthanum-substituted GdBaCo<sub>2</sub>O<sub>6-δ</sub>. *J. Alloys Compd.* **2020**, *845*, 156309. [[CrossRef](#)]
49. Xiang, H.; Xing, Y.; Dai, F.-z.; Wang, H.; Su, L.; Miao, L.; Zhang, G.; Wang, Y.; Qi, X.; Yao, L.; et al. High-entropy ceramics: Present status, challenges, and a look forward. *J. Adv. Ceram.* **2021**, *10*, 385–441. [[CrossRef](#)]
50. Ma, Y.; Ma, Y.; Wang, Q.; Schweider, S.; Botros, M.; Fu, T.; Hahn, H.; Drezesinski, T.; Vreitung, B. High-entropy energy materials: Challenges and new opportunities. *Energy Environ. Sci.* **2021**, *14*, 2883–2905. [[CrossRef](#)]
51. Wright, A.J.; Luo, J. A step forward from high-entropy ceramics to compositionally complex ceramics: A new perspective. *J. Mater. Sci.* **2020**, *55*, 9812–9827. [[CrossRef](#)]
52. Shen, L.; Du, Z.; Zhang, Y.; Dong, X.; Zhao, H. Medium-Entropy perovskites Sr(Fe<sub>α</sub>Ti<sub>β</sub>Co<sub>γ</sub>Mn<sub>ζ</sub>)O<sub>3-δ</sub> as promising cathodes for intermediate temperature solid oxide fuel cell. *Appl. Catal. B. Environ.* **2021**, *295*, 120264. [[CrossRef](#)]
53. Dąbrowa, J.; Olszewska, A.; Falkenstein, A.; Shwab, C.; Szymczak, M.; Zajusz, M.; Moździerz, M.; Mikoła, A.; Zielińska, K.; Berent, K.; et al. An innovative approach to design SOFC air electrode materials: High entropy La<sub>1-x</sub>Sr<sub>x</sub>(Co,Cr,Fe,Mn,Ni)O<sub>3-δ</sub> (x = 0., 0.1, 0.2, 0.3) perovskites synthesized by the sol–gel method. *J. Mater. Chem. A* **2020**, *8*, 24455. [[CrossRef](#)]



54. Dąbrowa, J.; Zielińska, K.; Stepien, A.; Zajusz, M.; Nowakowska, M.; Moździerz, M.; Berent, K.; Szymczak, M.; Świerczek, K. Formation of Solid Solutions and Physicochemical Properties of the High-Entropy  $\text{Ln}_{1-x}\text{Sr}_x(\text{Co,Cr,Fe,Mn,Ni})\text{O}_{3-\delta}$  (Ln = La, Pr, Nd, Sm or Gd) Perovskites. *Materials* **2021**, *14*, 5264. [[CrossRef](#)] [[PubMed](#)]
55. Yang, Q.; Wang, G.; Wu, H.; Bashiwork, B.A.; Tian, D.; Zhu, S.; Yang, Y.; Lu, Y.; Ding, Y.; Ling, Y.; et al. A high-entropy perovskite cathode for solid oxide fuel cells. *J. Alloys Compd.* **2021**, *872*, 159633. [[CrossRef](#)]
56. Bernuy-Lopez, C.; Høydalsvik, K.; Einarsrud, M.-A.; Grande, T. Effect of A-Site Ordering on Chemical Stability, Oxygen Stoichiometry and Electrical Conductivity in Layered  $\text{LaBaCo}_2\text{O}_{5+\delta}$  Double Perovskite. *Materials* **2016**, *9*, 154. [[CrossRef](#)]
57. Malyshkin, D.A.; Novikov, A.Y.; Sereda, V.V.; Ivanov, I.L.; Tsvetkov, D.S.; Zuev, A.Y. In Situ and ex Situ Study of Cubic  $\text{La}_{0.5}\text{Ba}_{0.5}\text{CoO}_{3-\delta}$  to Double Perovskite  $\text{LaBaCo}_2\text{O}_{6-\delta}$  Transition and Formation of Domain Textured Phases with Fast Oxygen Exchange Capability. *Inorg. Chem.* **2018**, *57*, 12409–12416. [[CrossRef](#)] [[PubMed](#)]
58. Tsvetkov, D.S.; Ivanov, I.L.; Malyshkin, D.A.; Sednev, A.L.; Sereda, V.V.; Zuev, A.Y. Double perovskites  $\text{REBaCo}_{2-x}\text{M}_x\text{O}_{6-\delta}$  (RE = La, Pr, Nd, Eu, Gd; M = Fe, Mn) as energy-related materials: An overview. *Pure Appl. Chem.* **2019**, *91*, 923–940. [[CrossRef](#)]
59. Yasodha, P.; Premila, M.; Bharathi, A.; Valsakimar, M.C.; Rajaraman, R.; Sundar, C.S. Infrared spectroscopic study of the local structural changes across the metal insulator transition in nickel-doped  $\text{GdBaCo}_2\text{O}_{5.5}$ . *J. Solid State Chem.* **2010**, *183*, 2602–2608. [[CrossRef](#)]
60. Kundu, A.; Pralong, V.; Raveau, B.; Caignaert, V. Magnetic and electrical properties of ordered 112-type perovskite  $\text{LnBaCoMnO}_{5+\delta}$  (Ln = Nd, Eu). *J. Mater. Sci.* **2011**, *46*, 681–687. [[CrossRef](#)]
61. Konne, J.L.; Davis, S.A.; Glatzel, S.; Hall, S.R. Synthesis of phase pure praseodimium barium copper iron oxide. *Chem. Commun.* **2013**, *49*, 5477. [[CrossRef](#)]
62. Klyndyuk, A.I.; Chizhova, E.A. Synthesis and Properties of  $\text{LnBaFeCoO}_{5+\delta}$  (Ln = Nd, Sm, Gd). *Inorg. Mater.* **2013**, *49*, 319–324. [[CrossRef](#)]
63. Zhuravleva, T.A. Electrophysical Properties of Layered Perovskites  $\text{LnBaCo}_{2-x}\text{Cu}_x\text{O}_{5+\delta}$  (Ln = Sm, Nd) for Solid Oxide Fuel Cells. *Rus. J. Electrochem.* **2011**, *47*, 676–680. [[CrossRef](#)]
64. Cherepanov, V.A.; Aksenova, T.V.; Gavrilova, L.Y.; Mikhaleva, K.N. Structure, nonstoichiometry of the  $\text{NdBa}(\text{Co,Fe})_2\text{O}_{5+\delta}$  layered perovskite. *Solid State Ion.* **2011**, *188*, 53–57. [[CrossRef](#)]
65. Świerczek, K. Physico-chemical properties of  $\text{Ln}_{0.5}\text{A}_{0.5}\text{Co}_{0.5}\text{Fe}_{0.5}\text{O}_{3-\delta}$  (Ln: La, Sm; A: Sr, Ba) cathode materials and their performance in electrolyte-supported Intermediate Temperature Solid Oxide Fuel Cell. *J. Power Source* **2011**, *196*, 7110–7116. [[CrossRef](#)]
66. Szpunar, I.; Strandbakke, R.; Sørby, M.H.; Wachowsky, S.L.; Balaguer, M.; Tarach, M.; Serra, J.M.; Witkowska, A.; Dzik, E.; Norby, T.; et al. High-Temperature Structural and Electrical Properties of  $\text{BaLnCo}_2\text{O}_6$  Perovskites. *Materials* **2020**, *13*, 4044. [[CrossRef](#)]
67. Galeano, V.; Zapata, V.H.; Ostos, C.; Morán, O. On the electrical properties of textured  $\text{YBaCo}_2\text{O}_{5+\delta}$  thin layers tested by means of complex impedance spectroscopy. *Vacuum* **2020**, *181*, 109595. [[CrossRef](#)]
68. Taskin, A.; Lavrov, A. Origin of the large thermoelectric power in oxygen-variable  $\text{RBaCo}_2\text{O}_{5+x}$  (R = Gd, Nd). *Phys. Rev.* **2006**, *73*, 1211101. [[CrossRef](#)]
69. Klyndyuk, A.I.; Chizhova, Y.e.A.; Sazanovich, N.V.; Krasutskaya, N.S. Thermoelectric Properties of Some Perovskite Oxides. *J. Thermoelectr.* **2009**, *3*, 73–80.
70. Klyndyuk, A.I. Thermoelectric Properties of Layered Ferrocuprates  $\text{LnBaCuFeO}_{5+\delta}$  (Ln = La, Pr, Nd, Sm, Gd–Lu). *Phys. Solid State* **2009**, *51*, 250–254. [[CrossRef](#)]
71. Zeng, C.; Liu, Y.; Lan, J.; Ren, G.; Lin, Y.; Li, M.; Nan, C. Thermoelectric properties of  $\text{Sm}_{1-x}\text{La}_x\text{BaCuFeO}_5$  ceramics. *Mat. Res. Bull.* **2015**, *69*, 46–50. [[CrossRef](#)]
72. Zeng, C.; Zhan, B.; Butt, S.; Liu, Y.; Ren, G.; Lin, Y.-H.; Li, M.; Nan, C.-W. Electrical and Thermal Conduction Behaviors in La-Substituted  $\text{GdBaCuFeO}_{5+\delta}$  Ceramics. *J. Am. Ceram. Soc.* **2015**, *98*, 437–442. [[CrossRef](#)]
73. Wu, T.; Gao, P. Development of Perovskite-Type Materials for Thermoelectric Application. *Materials* **2018**, *11*, 999. [[CrossRef](#)]
74. Han, B.; Li, Y.; Chen, N.; Deng, D.; Xinxin, X.; Wang, Y. Preparation and Photocatalytic Properties of  $\text{LnBaCo}_2\text{O}_{5+\delta}$  (Ln = Eu, Gd, and Sm). *J. Mat. Sci. Chem. Eng.* **2015**, *3*, 17–25.
75. Løken, A.; Ricote, S.; Wachowski, S. Thermal and Chemical Expansion in Proton Ceramic Electrolytes and Compatible Electrodes. *Crystals* **2018**, *8*, 365. [[CrossRef](#)]
76. Galin, M.Z.; Ivanov-Schitz, A.K.; Mazo, G.N. Molecular Dynamics Simulation of Structural and Transport Properties of Solid Solutions of Double Perovskites Based on  $\text{PrBaCo}_2\text{O}_{5.5}$ . *Crystallography* **2020**, *65*, 289–296. [[CrossRef](#)]
77. Tsvetkov, D.S.; Ivanov, I.L.; Malyshkin, D.A.; Sereda, V.V.; Zuev, A.Y. Mechano-Chemical Coupling in Double Perovskites as Energy Related Materials. *ECS Transact.* **2016**, *72*, 21–35. [[CrossRef](#)]
78. Klyndyuk, A.I. Thermal and Chemical Expansion of  $\text{LnBaCuFeO}_{5+\delta}$  (Ln = La, Pr, Gd) Ferrocuprates and  $\text{LaBa}_{0.75}\text{Sr}_{0.25}\text{CuFeO}_{5+\delta}$  Solid Solution. *Rus. J. Inorg. Chem.* **2007**, *52*, 1343–1349. [[CrossRef](#)]
79. Klyndyuk, A.I. New Perovskite Oxides  $\text{LaBaMCoO}_{5+\delta}$  (M = Fe, Cu): Synthesis, Structure, and Properties. *Phys. Solid State* **2009**, *51*, 270–274. [[CrossRef](#)]
80. Klyndyuk, A.I.; Chizhova, E.A. Properties of Perovskite-Like Phases  $\text{LnBaCuFeO}_{5+\delta}$  (Ln = La, Pr). *Glass Phys. Chem.* **2008**, *34*, 313–318. [[CrossRef](#)]

81. Zhu, L.; Wei, B.; Lü, Z.; Feng, J.; Xu, L.; Gao, H.; Zhang, Y.; Huang, X. Performance degradation of double-perovskite PrBaCo<sub>2</sub>O<sub>5+δ</sub> oxygen electrode in CO<sub>2</sub>containing atmospheres. *Appl. Surf. Sci.* **2017**, *416*, 649–655. [[CrossRef](#)]
82. Tellez, H.; Druce, J.; Ju, Y.-W.; Kilner, J.; Ushihara, T. Surface chemistry evolution in LnBaCo<sub>2</sub>O<sub>5+δ</sub> double perovskites for oxygen electrodes. *Int. J. Hydrogen Energy* **2014**, *39*, 20856–20863. [[CrossRef](#)]
83. Perry, N.H.; Ishihara, T. Roles of Bulk and Surface Chemistry in the Oxygen Exchange Kinetics and Related Properties of Mixed Conducting Perovskite Oxide Electrodes. *Materials* **2016**, *9*, 858. [[CrossRef](#)]
84. Sadykov, V.A.; Sadovszkaya, E.M.; Eremeev, N.F.; Skriabin, P.I.; Krasnov, A.V.; Bespalko, Y.N.; Pavlova, S.N.; Fedorova, Y.E.; Pikalova, E.Y.; Shlyakhtina, A.V. Oxygen Mobility in the Materials for Solid Oxide Fuel Cells and Catalytic Membranes (Review). *Rus. J. Electrochim.* **2019**, *55*, 701–718. [[CrossRef](#)]
85. Zhang, L.; Chen, G.; Dai, R.; Lv, X.; Yang, D.; Geng, S. A review of the chemical compatibility between oxide electrodes and electrolytes in solid oxide fuel cells. *J. Power Source* **2021**, *492*, 229630. [[CrossRef](#)]
86. Liu, J.; Jin, F.; Yang, X.; Niu, B.; Li, Y.; He, T. YBaCo<sub>2</sub>O<sub>5+δ</sub>-based double-perovskite cathodes for intermediate-temperature solid oxide fuel cells with simultaneously improved structural stability and thermal expansion properties. *Electrochim. Acta* **2019**, *297*, 344–354. [[CrossRef](#)]
87. Tsvetkov, D.; Tsvetkova, N.; Ivanov, I.; Malyshkin, D.; Sereda, V.; Zuev, A. PrBaCo<sub>2</sub>O<sub>6-δ</sub>-Ce<sub>0.8</sub>Sm<sub>0.2</sub>O<sub>1.9</sub> Composite Cathodes for Intermediate-Temperature Solid Oxide Fuel Cells: Stability and Cation Interdiffusion. *Energies* **2019**, *12*, 417. [[CrossRef](#)]
88. Zvonareva, I.; Fu, X.-Z.; Medvedev, D.; Shao, Z. Electrochemistry and energy conversion features of protonic ceramic cells with mixed ionic-electronic electrolytes. *Energy Environ. Sci.* **2021**; in press. [[CrossRef](#)]
89. Mao, X.; Ma, G. Performance of cobalt-free double-perovskite NdBaFe<sub>2-x</sub>Mn<sub>x</sub>O<sub>5+δ</sub> cathode materials for proton-conducting IT-SOFC. *J. Alloys Compd.* **2015**, *637*, 286–296. [[CrossRef](#)]
90. Wang, Y.; Jin, F.; Hao, X.; Niu, B.; Lyu, P.; He, T. B-site-ordered Co-based double perovskites Sr<sub>2</sub>Co<sub>1-x</sub>Nb<sub>x</sub>FeO<sub>5+δ</sub> as active and stable cathodes for intermediate-temperature solid oxide fuel cells. *J. Alloys Compd.* **2020**, *829*, 154470. [[CrossRef](#)]
91. Chang, A.; Skinner, S.J.; Kilner, J.A. Electrical properties of GdBaCo<sub>2</sub>O<sub>5+x</sub> for ITSOFC applications. *Solid State Ion.* **2006**, *177*, 2009–2011. [[CrossRef](#)]
92. Tarancon, A.; Morata, A.; Dezanneau, G.; Skinner, S.J.; Kilner, J.A.; Estradé, S.; Hernández-Ramírez, F.; Peiró, F.; Morante, J.R. GdBaCo<sub>2</sub>O<sub>5+x</sub> layered perovskites as an intermediate temperature solid oxide fuel cell cathode. *J. Power Source* **2007**, *174*, 255–263. [[CrossRef](#)]
93. Zhang, K.; Ge, L.; Ran, R.; Shao, Z.; Liu, S. Synthesis, characterization and evaluation of cation-ordered LnBaCo<sub>2</sub>O<sub>5+δ</sub> as materials of oxygen permeation membranes and cathodes of SOFCs. *Acta Mater.* **2008**, *56*, 4876–4889. [[CrossRef](#)]
94. Kim, J.-H.; Manthiram, A. LnBaCo<sub>2</sub>O<sub>5+δ</sub> Oxides as cathodes for Intermediate-Temperature Solid Oxide Fuel Cells. *J. Electrochem. Soc.* **2008**, *155*, B385–B390. [[CrossRef](#)]
95. Zhu, C.; Liu, X.; Yi, C.; Yan, D.; Su, W. Electrochemical performance of PrBaCo<sub>2</sub>O<sub>5+δ</sub> layered perovskite as an intermediate-temperature solid oxide fuel cell cathode. *J. Power Source* **2008**, *185*, 193–196. [[CrossRef](#)]
96. Gu, H.; Chen, H.; Gao, L.; Zheng, Y.; Zhu, X.; Guo, L. Oxygen reduction mechanism of NdBaCo<sub>2</sub>O<sub>5+δ</sub> cathode for intermediate-temperature solid oxide fuel cells under cathodic polarization. *Int. J. Hydrogen Energy* **2009**, *34*, 2416–2420. [[CrossRef](#)]
97. Liu, Y. YBaCo<sub>2</sub>O<sub>5+δ</sub> as a new cathode material for zirconia-based solid oxide fuel cells. *J. Alloys Compd.* **2009**, *477*, 860–862. [[CrossRef](#)]
98. Jin, M.; Zhang, X.; Qiu, Y.; Sheng, J. Layered PrBaCo<sub>2</sub>O<sub>5+δ</sub> perovskite as a cathode for proton-conducting solid oxide fuel cells. *J. Alloys Compd.* **2010**, *494*, 359–361. [[CrossRef](#)]
99. Pang, S.; Jiang, X.; Li, X.; Su, Z.; Xu, H.; Xu, Q.; Chen, C. Characterization of cation-ordered perovskite oxide LaBaCo<sub>2</sub>O<sub>5+δ</sub> as cathode of intermediate-temperature solid oxide fuel cells. *Int. J. Hydrogen Energy* **2012**, *37*, 6836–6843. [[CrossRef](#)]
100. Kim, J.-H.; Manthiram, A. Layered LnBaCo<sub>2</sub>O<sub>5+δ</sub> Perovskite Cathodes for Solid Oxide Fuel Cells: An Overview and Perspective. *J. Mater. Chem. A* **2015**, *3*, 24195–24210. [[CrossRef](#)]
101. Wang, S.; Zan, J.; Qiu, W.; Zheng, D.; Li, F.; Chen, W.; Pei, Q.; Jiang, L. Evaluation of perovskite oxides LnBaCo<sub>2</sub>O<sub>5+δ</sub> (Ln = La, Pr, Nd and Sm) as cathode material for IT-SOFC. *J. Electroanal. Chem.* **2021**, *886*, 115144. [[CrossRef](#)]
102. Bernuy-Lopez, C.; Rioja-Monnlor, L.; Nakamura, T.; Ricote, S.; O’Hayre, R.; Amezawa, K.; Einarsrud, M.-A.; Grande, T. Effect of Cation Ordering on the Performance and Chemical Stability of Layered Double Perovskite Cathodes. *Materials* **2018**, *11*, 196. [[CrossRef](#)] [[PubMed](#)]
103. Dou, Y.; Xie, Y.; Hao, X.; Xia, T.; Li, Q.; Wang, J.; Huo, L.; Zhao, H. Addressing electrocatalytic activity and stability of LnBaCo<sub>2</sub>O<sub>5+δ</sub> perovskites for hydrogen evolution reaction by structural and electronic features. *Appl. Catal. B Environment.* **2021**, *297*, 120403. [[CrossRef](#)]
104. Jiang, X.; Shi, Y.; Zhou, W.; Li, X.; Su, Z.; Pang, S.; Jiang, L. Effects of Pr<sup>3+</sup>-deficiency on structure and properties of PrBaCo<sub>2</sub>O<sub>5+δ</sub> cathode material—A comparison with Ba<sup>2+</sup>-deficiency case. *J. Power Source* **2014**, *272*, 371–377. [[CrossRef](#)]
105. Yi, K.; Sun, L.; Li, Q.; Xia, T.; Huo, L.; Zhao, H.; Li, J.; Lü, Z.; Bassat, J.-M.; Rougier, A.; et al. Effect of Nd-deficiency on electrochemical properties of NdBaCo<sub>2</sub>O<sub>6-δ</sub> cathode for intermediate-temperature solid oxide fuel cells. *Int. J. Hydrogen Energy* **2016**, *41*, 10228–10238. [[CrossRef](#)]
106. Jiang, X.; Xu, Q.; Shi, Y.; Li, X.; Zhou, W.; Xu, H.; Zhang, Q. Synthesis and properties of Sm<sup>3+</sup>-deficient Sm<sub>1-x</sub>BaCo<sub>2</sub>O<sub>5+δ</sub> perovskite oxides as cathode materials. *Int. J. Hydrogen Energy* **2014**, *39*, 10817–10823. [[CrossRef](#)]

107. Kim, C.G.; Woo, S.H.; Song, K.E.; Baek, S.-W.; Kang, H.; Choi, W.S.; Kim, J.H. Enhanced Electrochemical Properties of Non-stoichiometric Layered Perovskites,  $\text{Sm}_{1-x}\text{BaCo}_2\text{O}_{5+\delta}$ , for IT-SOFC Cathodes. *Front. Chem.* **2021**, *9*, 633868. [[CrossRef](#)] [[PubMed](#)]
108. Pang, S.L.; Jiang, X.N.; Li, X.N.; Xu, H.X.; Jiang, L.; Xu, Q.L.; Shi, Y.C.; Zhang, Q.Y. Structure and properties of layered-perovskite  $\text{LaBa}_{1-x}\text{Co}_2\text{O}_{5+\delta}$  ( $x = 0-0.15$ ) as intermediate-temperature cathode material. *J. Power Source* **2013**, *240*, 54–59. [[CrossRef](#)]
109. Pang, S.; Jiang, X.; Li, X.; Wang, Q.; Su, Z. Characterization of Ba-deficient  $\text{PrBa}_{1-x}\text{Co}_2\text{O}_{5+\delta}$  as cathode intermediate temperature solid oxide fuel cells. *J. Power Source* **2012**, *204*, 53–59. [[CrossRef](#)]
110. Wang, J.; Meng, F.; Xia, T.; Shi, Z.; Lian, J.; Xu, C.; Zhao, H.; Bassat, J.-M.; Grenier, J.-C. Superior electrochemical performance and oxygen reduction kinetics of layered perovskite  $\text{PrBa}_x\text{Co}_2\text{O}_{5+\delta}$  ( $x = 0.90-1.0$ ) oxides as cathode materials for intermediate-temperature solid oxide fuel cells. *Int. J. Hydrogen Energy* **2014**, *39*, 18392–18404. [[CrossRef](#)]
111. Donazzi, A.; Pelosato, R.; Cordaro, G.; Stucchi, D.; Cristiani, C.; Dotelli, G.; Sopra, I.N. Evaluation of Ba deficient  $\text{NdBaCo}_2\text{O}_{5+\delta}$  oxide as cathode material for IT-SOFC. *Electrochim. Acta* **2015**, *182*, 573–587. [[CrossRef](#)]
112. Pang, S.; Yang, G.; Su, Y.; Xu, J.; Shen, X.; Zhu, M.; Wu, X.; Li, S.; Chen, C. A-site cation deficiency tuned oxygen transport dynamics of perovskite  $\text{Pr}_{0.5}\text{Ba}_{0.25-x}\text{Ca}_{0.25}\text{CoO}_{3-\delta}$  for intermediate temperature solid oxide fuel cells. *Ceram. Int.* **2019**, *45*, 14602–14607. [[CrossRef](#)]
113. Yao, C.; Yang, J.; Zhang, H.; Chen, S.; Lang, X.; Meng, J.; Cai, K. Evaluation of A-site Ba-deficient  $\text{PrBa}_{0.5-x}\text{Sr}_{0.5}\text{Co}_2\text{O}_{5+\delta}$  ( $x = 0, 0.4$ , and  $0.08$ ) as cathode material for solid oxide fuel cells. *J. Alloys Compd.* **2021**, *883*, 160759. [[CrossRef](#)]
114. Pang, S.; Wang, W.; Chen, T.; Wang, Y.; Xu, K.; Shen, X.; Xi, X.; Fan, J. The effect of potassium on the properties of  $\text{PrBa}_{1-x}\text{Co}_2\text{O}_{5+\delta}$  ( $x = 0.00-0.10$ ) cathodes for intermediate-temperature solid oxide fuel cells. *Int. J. Hydrogen Energy* **2016**, *41*, 13705–13714. [[CrossRef](#)]
115. Bangwal, A.S.; Jha, P.K.; Chauchan, M.; Singh, S.; Sinha, A.S.K.; Jha, P.A.; Singh, P. Compositional effect on oxygen reduction reaction in Pr excess double perovskite  $\text{Pr}_{1+x}\text{Ba}_{1-x}\text{Co}_2\text{O}_{6-\delta}$  cathode materials. *Int. J. Hydrogen Energy* **2020**, *45*, 23378–23390. [[CrossRef](#)]
116. Lu, F.; Xia, T.; Li, Q.; Wang, J.; Huo, L.; Zhao, H. Heterostructured simple perovskitenanorod-decorated double perovskite cathode for solid oxide fuel cells: Highly catalytic activity, stability and  $\text{CO}_2$ -durability for oxygen reduction reaction. *Appl. Catal. B Environ.* **2019**, *249*, 19–31. [[CrossRef](#)]
117. Azad, A.K.; Kim, J.H.; Irvine, J.T.S. Structure–property relationship in layered perovskite cathode  $\text{LnBa}_{0.5}\text{Sr}_{0.5}\text{Co}_2\text{O}_{5+\delta}$  ( $\text{Ln} = \text{Pr}, \text{Nd}$ ) for solid oxide fuel cells. *J. Power Source* **2011**, *196*, 7333–7337. [[CrossRef](#)]
118. Xia, W.; Liu, X.; Jin, F.; Jia, X.; Shen, Y. Evaluation of calcium codoping in double perovskite  $\text{PrBaCo}_2\text{O}_{5+\delta}$  as cathode for IT-SOFCs. *Electrochim. Acta* **2020**, *464*, 137274. [[CrossRef](#)]
119. Subardi, A.; Liao, K.-Y.; Fu, Y.-P. Oxygen transport, thermal and electrochemical properties of  $\text{NdBa}_{0.5}\text{Sr}_{0.5}\text{Co}_2\text{O}_{5+\delta}$  cathode for SOFCs. *J. Eur. Ceram. Soc.* **2019**, *39*, 30–40. [[CrossRef](#)]
120. Yao, C.; Zhang, H.; Liu, X.; Meng, J.; Zhang, X.; Meng, F.; Meng, J. Investigation of layered perovskite  $\text{NdBa}_{0.5}\text{Sr}_{0.25}\text{Ca}_{0.25}\text{Co}_2\text{O}_{5+\delta}$  as cathode for solid oxide fuel cells. *Ceram. Int.* **2018**, *44*, 12048–12054. [[CrossRef](#)]
121. Yoo, S.; Jun, A.; Ju, Y.-W.; Odkhuu, D.; Hyodo, J.; Jeong, H.Y.; Park, N.; Shin, J.; Ishihara, T.; Kim, G. Development of Double-Perovskite Compounds as Cathode Materials for Low-Temperature Solid Oxide Fuel Cells. *Angew. Chem. Int. Ed.* **2014**, *53*, 13064–13067. [[CrossRef](#)] [[PubMed](#)]
122. Zhang, X.; Jin, M.; Sheng, J. Layered  $\text{GdBa}_{0.5}\text{Sr}_{0.5}\text{Co}_2\text{O}_{5+\delta}$  as a cathode for proton-conducting solid oxide fuel cells with stable  $\text{BaCe}_{0.5}\text{Zr}_{0.3}\text{Y}_{0.16}\text{Zn}_{0.04}\text{O}_{3-\delta}$  electrolyte. *J. Alloys Compd.* **2010**, *496*, 241–243. [[CrossRef](#)]
123. Meng, F.; Xia, T.; Wang, J.; Shi, Z.; Lian, J.; Zhao, H.; Bassat, J.-M.; Grenier, J.-C. Evaluation of layered perovskites  $\text{YBa}_{1-x}\text{Sr}_x\text{Co}_2\text{O}_{5+\delta}$  as cathodes for intermediate-temperature solid oxide fuel cells. *Int. J. Hydrogen Energy* **2014**, *39*, 4531–4543. [[CrossRef](#)]
124. Xue, J.; Shen, Y.; He, T. Performance of double-perovskite  $\text{YBa}_{0.5}\text{Sr}_{0.5}\text{Co}_2\text{O}_{5+\delta}$  as cathode material for intermediate-temperature solid oxide fuel cells. *Int. J. Hydrogen Energy* **2011**, *36*, 6894–6898. [[CrossRef](#)]
125. Woo, S.H.; Song, K.E.; Baek, S.-W.; Kang, H.; Choi, W.; Shin, T.H.; Park, J.-Y.; Kim, J.H. Pr- and Sm-Substituted Layered Perovskite Oxide Systems for IT-SOFC Cathodes. *Energies* **2021**, *14*, 6739. [[CrossRef](#)]
126. Subardi, A.; Cheng, M.-H.; Fu, Y.-P. Chemical bulk diffusion and electrochemical properties of  $\text{SmBa}_{0.6}\text{Sr}_{0.4}\text{Co}_2\text{O}_{5+\delta}$  cathode for intermediate solid oxide fuel cells. *Int. J. Hydrogen Energy* **2014**, *39*, 20783–20790. [[CrossRef](#)]
127. Subardi, A.; Chen, C.-C.; Fu, Y.-P. Oxygen transportation, electrical conductivity and electrochemical properties of layered perovskite  $\text{SmBa}_{0.5}\text{Sr}_{0.5}\text{Co}_2\text{O}_{5+\delta}$ . *Int. J. Hydrogen Energy* **2017**, *42*, 5284–5294. [[CrossRef](#)]
128. Zhang, L.; Li, S.; Xia, T.; Sun, L.; Huo, L.; Zhao, H. Co-deficient  $\text{PrBaCo}_{2-x}\text{O}_{6-\delta}$  perovskites as cathode materials for intermediate-temperature solid oxide fuel cells: Enhanced electrochemical performance and oxygen reduction kinetics. *Int. J. Hydrogen Energy* **2018**, *43*, 3761–3775. [[CrossRef](#)]
129. Che, X.; Shen, Y.; Li, H.; He, T. Assessment of  $\text{LnBaCo}_{1.6}\text{Ni}_{0.4}\text{O}_{5+\delta}$  ( $\text{Ln} = \text{Pr}, \text{Nd}, \text{and Sm}$ ) double-perovskites as cathodes for intermediate-temperature solid-oxide fuel cells. *J. Power Source* **2013**, *222*, 288–293. [[CrossRef](#)]
130. Liu, L.; Guo, R.; Wang, S.; Yang, Y.; Yin, D. Synthesis and characterization of  $\text{PrBa}_{0.5}\text{Sr}_{0.5}\text{Co}_{2-x}\text{Ni}_x\text{O}_{5+\delta}$  ( $x = 0.1, 0.2$  and  $0.3$ ) cathodes for intermediate temperature SOFCs. *Ceram. Int.* **2014**, *40*, 16393–16398. [[CrossRef](#)]
131. Urusova, A.S.; Cherepanov, V.A.; Lebedev, O.I.; Aksanova, T.V.; Gavrilova, L.Y.; Caignaert, V.; Raveau, B. Tuning oxygen content and distribution by substitution at Co site in 112  $\text{YBaCo}_2\text{O}_{5+\delta}$ : Impact on transport and thermal properties. *Chem. Mater. A* **2014**, *2*, 8823. [[CrossRef](#)]



132. Liu, B.; Yang, J.; Yan, D.; Jia, L.; Chi, B.; Pu, J.; Li, J. Novel  $\text{PrBa}_{0.9}\text{Ca}_{0.1}\text{Co}_{2-x}\text{Zn}_x\text{O}_{5+\delta}$  double-perovskite as an active cathode material for high-performance proton-conducting solid oxide fuel cells. *Int. J. Hydrogen Energy* **2020**, *45*, 31009–31016. [[CrossRef](#)]
133. Jun, A.; Shin, J.; Kim, G. High redox and performance stability of layered  $\text{SmBa}_{0.5}\text{Sr}_{0.5}\text{Co}_{1.5}\text{Cu}_{0.5}\text{O}_{5+\delta}$  perovskite cathodes for intermediate-temperature solid oxide fuel cells. *Phys. Chem. Chem. Phys.* **2013**, *15*, 19906–19912. [[CrossRef](#)]
134. Zhang, Y.; Yu, B.; Lü, S.; Meng, X.; Zhao, X.; Ji, Y.; Wang, Y.; Fu, C.; Liu, X.; Li, X.; et al. Effect of Cu doping on  $\text{YBaCo}_2\text{O}_{5+\delta}$  as cathode for intermediate-temperature solid oxide fuel cells. *Electrochim. Acta* **2014**, *134*, 107–115. [[CrossRef](#)]
135. Klyndyuk, A.I.; Mosiałek, M.; Kharitonov, D.S.; Chizhova, E.A.; Zimowska, M.; Socha, R.; Komenda, A. Structural and electrochemical characterization of  $\text{YBa}(\text{Fe},\text{Co},\text{Cu})_2\text{O}_{5+\delta}$  layered perovskites as cathode materials for solid oxide fuel cells. *Int. J. Hydrogen Energy* **2021**, *46*, 16977–16988. [[CrossRef](#)]
136. Lu, F.; Xia, T.; Li, Q.; Sun, L.; Huo, L.; Zhao, H. Ta-doped  $\text{PrBa}_{0.94}\text{Co}_{2-x}\text{Ta}_x\text{O}_{5+\delta}$  as promising oxygen electrodes: A focused study on catalytic oxygen reduction reaction activity, stability and  $\text{CO}_2$ -durability. *J. Power Source* **2019**, *417*, 42–52. [[CrossRef](#)]
137. Xu, J.; Cai, H.; Hao, G.; Zhang, L.; Song, Z.; Long, W.; Zhang, L.; Mang, L. Characterization of high-valence Mo-doped  $\text{PrBaCo}_2\text{O}_{5+\delta}$  cathodes for IT-SOFCs. *J. Alloys Compd.* **2020**, *842*, 155600. [[CrossRef](#)]
138. Wang, Y.; Zhao, X.; Lü, S.; Meng, X.; Zhang, Y.; Yu, B.; Li, X.; Sui, Y.; Yang, J.; Fu, C.; et al. Synthesis and characterization of  $\text{SmSrCo}_{2-x}\text{Mn}_x\text{O}_{5+\delta}$  ( $x = 0.0, 0.2, 0.4, 0.6, 0.8, 1.0$ ) cathode materials for intermediate-temperature solid-oxide fuel cells. *Ceram. Int.* **2014**, *40*, 11343–11350. [[CrossRef](#)]
139. Muñoz-Gil, D.; Urones-Garrote, E.; Pérez-Coll, D.; Amador, U.; García-Martin, S. Crystal structure and compositional effect on the electrical and electrochemical properties of  $\text{GdBaCo}_{2-x}\text{Mn}_x\text{O}_{5+\delta}$  ( $0 \leq x \leq 2$ ) oxides for use as air electrodes in solid oxide fuel cells. *J. Mater. Chem. A* **2018**, *6*, 5452–5460. [[CrossRef](#)]
140. Olszewska, A.; Świerczek, K.  $\text{ReBaCo}_{2-x}\text{Mn}_x\text{O}_{5+\delta}$  (Re: Rare earth element) layered perovskites for application as cathodes in Solid Oxide Fuel Cells. *E3S Web Conf.* **2019**, *108*, 01020. [[CrossRef](#)]
141. Olszewska, A.; Świerczek, K.; Niemczyk, A. Peculiar Properties of Electrochemically Oxidized  $\text{SmBaCo}_{2-x}\text{Mn}_x\text{O}_{5+\delta}$  ( $x = 0; 0.5$  and 1) A-Site Ordered Perovskites. *Crystals* **2020**, *10*, 205. [[CrossRef](#)]
142. Kim, Y.N.; Kim, J.-H.; Manthiram, A. Effect of Fe substitution on the structure and properties of  $\text{LnBaCo}_{2-x}\text{Fe}_x\text{O}_{5+\delta}$  (Ln = Nd and Gd) cathodes. *J. Power Source* **2010**, *195*, 6411–6419. [[CrossRef](#)]
143. Zhao, L.; Shen, J.; He, B.; Chen, F.; Xia, C. Synthesis, characterization and evaluation of  $\text{PrBaCo}_{2-x}\text{Fe}_x\text{O}_{5+\delta}$  as cathodes for intermediate-temperature solid oxide fuel cells. *Int. J. Hydrogen Energy* **2011**, *36*, 3658–3665. [[CrossRef](#)]
144. Xue, J.; He, T. Double-perovskites  $\text{YBaCo}_{2-x}\text{Fe}_x\text{O}_{5+\delta}$  cathodes for intermediate-temperature solid oxide fuel cells. *J. Power Source* **2011**, *196*, 3729–3735. [[CrossRef](#)]
145. Zou, J.; Park, J.; Kwak, B.; Yoon, H.; Chung, J. Effect of Fe doping on  $\text{PrBaCo}_2\text{O}_{5+\delta}$  as cathode for intermediate-temperature solid oxide fuel cells. *Solid State Ion.* **2012**, *206*, 112–119. [[CrossRef](#)]
146. Choi, S.; Shin, J.; Kim, G. The electrochemical and thermodynamic characterization of  $\text{PrBaCo}_{2-x}\text{Fe}_x\text{O}_{5+\delta}$  ( $x = 0, 0.5, 1$ ) infiltrated into yttria-stabilized zirconia scaffold as cathodes for solid oxide fuel cells. *J. Power Source* **2012**, *201*, 10–17. [[CrossRef](#)]
147. Jiang, L.; Wei, T.; Zeng, R.; Zhang, W.-X.; Huang, Y.-H. Thermal and electrochemical properties of  $\text{PrBa}_{0.5}\text{Sr}_{0.5}\text{Co}_{2-x}\text{Fe}_x\text{O}_{5+\delta}$  ( $x = 0.5, 1.0, 1.5$ ) cathode materials for solid-oxide fuel cells. *J. Power Source* **2013**, *232*, 279–285. [[CrossRef](#)]
148. Yoo, C.-Y.; Joo, J.H.; Lee, H.J.; Yu, J.H. The effects of Fe-substitution on the crystal structure and oxygen permeability of  $\text{PrBaCo}_2\text{O}_{5+\delta}$ . *Mat. Lett.* **2013**, *108*, 65–68. [[CrossRef](#)]
149. Anjum, U.; Vashishta, S.; Sinha, N.; Haider, M.A. Role of oxygen anion diffusion in improved electrochemical performance of layered perovskite  $\text{LnBa}_{1-y}\text{Sr}_y\text{Co}_{2-x}\text{Fe}_x\text{O}_{5+\delta}$  (Ln = Pr, Nd, Gd) electrodes. *Solid State Ion.* **2015**, *280*, 24–29. [[CrossRef](#)]
150. Strandbakke, R.; Cherepanov, V.A.; Zuev, A.Y.; Tsvetkov, D.S.; Argirusis, C.; Sourkoni, G.; Prüne, S.; Norby, T. Gd- and Pr-based double perovskitecobaltites as oxygen electrodes for proton ceramic fuel cells and electrolyser cells. *Solid State Ion.* **2015**, *278*, 120–132. [[CrossRef](#)]
151. Lee, T.-H.; Parl, K.-Y.; Kim, N.-I.; Dong, S.-J.; Hong, K.-H.; Ahn, D.; Azad, A.K.; Hwang, J.; Bhattacharjee, S.; Lee, S.-C.; et al. Robust  $\text{NdBa}_{0.5}\text{Sr}_{0.5}\text{Co}_{1.5}\text{Fe}_{0.5}\text{O}_{5+\delta}$  cathode material and its degradation prevention operating logic for intermediate-temperature solid oxide fuel cells. *J. Power Source* **2016**, *331*, 495–506. [[CrossRef](#)]
152. Anjum, U.; Vashishtha, S.; Agarwal, M.; Tiwari, P.; Sinha, N.; Agrawal, A.; Basu, S.; Haider, M.A. Oxygen anion diffusion in double perovskite  $\text{GdBaCo}_2\text{O}_{5+\delta}$  and  $\text{LnBa}_{0.5}\text{Sr}_{0.5}\text{Co}_{2-x}\text{Fe}_x\text{O}_{5+\delta}$  (Ln = Gd, Pr, Nd) electrodes. *Int. J. Hydrogen Energy* **2016**, *41*, 7631–7640. [[CrossRef](#)]
153. Muñoz-Gil, D.; Pérez-Coll, D.; Urones-Garrote, E.; Amador, U.; Garcia-Martin, S. Influence of the synthesis conditions on the crystal structure and properties of  $\text{GdBaCo}_{2-x}\text{Fe}_x\text{O}_{5+\delta}$  oxides as air-electrodes for Intermediate Temperature Solid Oxide Fuel Cells. *J. Mater. Chem. A* **2017**, *5*, 12550–12556. [[CrossRef](#)]
154. Zhang, S.-L.; Chen, K.; Zhang, A.-P.; Li, C.-X.; Li, C.-J. Effect of Fe doping on the performance of suspension plasma-sprayed  $\text{PrBa}_{0.5}\text{Sr}_{0.5}\text{Co}_{2-x}\text{Fe}_x\text{O}_{5+\delta}$  cathodes for intermediate-temperature solid oxide fuel cells. *Ceram. Int.* **2017**, *43*, 11648–11655. [[CrossRef](#)]
155. Cordaro, G.; Donazzi, A.; Pelosato, R.; Cristiani, C.; Dotelli, G.; Sora, I.N. Electrochemical and Chemical Characterization of  $\text{NdBa}_{1-x}\text{Co}_{2-y}\text{Fe}_y\text{O}_{5+\delta}$  Cathodes for IT-SOFCs. *ECS Transact.* **2017**, *78*, 507–520. [[CrossRef](#)]
156. Kim, B.-J.; Fabbri, E.; Castelli, I.E.; Borlaf, M.; Graule, T.; Nachttegaal, M.; Schmidt, T.J. Fe-Doping in Double Perovskite  $\text{PrBaCo}_{2(1-x)}\text{Fe}_x\text{O}_{6-\delta}$ : Insights into Structural and Electronic Effects to Enhance Oxygen Evolution Catalyst Stability. *Catalysts* **2019**, *9*, 263. [[CrossRef](#)]



157. Cordaro, G.; Donazzi, A.; Pelosato, R.; Mastropasqua, L.; Cristiani, C.; Sora, I.N.; Dotelli, G. Structural and Electrochemical Characterization of  $\text{NdBa}_{1-x}\text{Co}_{2-y}\text{Fe}_y\text{O}_{5+\delta}$  as cathode for Intermediate Temperature Solid Oxide Fuel Cells. *J. Electrochem. Soc.* **2020**, *167*, 024502. [CrossRef]
158. Lu, C.; Niu, B.; Yi, W.; Ji, Y.; Xu, B. Efficient symmetrical electrodes of  $\text{PrBaFe}_{2-x}\text{Co}_x\text{O}_{5+\delta}$  ( $x = 0, 0.2, 0.4$ ) for solid oxide fuel cells and solid oxide electrolysis cells. *Electrochim. Acta* **2020**, *358*, 136916. [CrossRef]
159. Jin, F.; Shen, Y.; Wang, R.; He, T. Double-perovskite  $\text{PrBaCo}_{2/3}\text{Fe}_{2/3}\text{Cu}_{2/3}\text{O}_{5+\delta}$  as cathode material for intermediate-temperature solid oxide fuel cells. *J. Power Source* **2013**, *234*, 244–251. [CrossRef]
160. Jin, F.; Li, L.; He, T.  $\text{NdBaCo}_{2/3}\text{Fe}_{2/3}\text{Cu}_{2/3}\text{O}_{5+\delta}$  double perovskites as a novel cathode material for  $\text{CeO}_2$ - and  $\text{LaGaO}_3$ -based solid oxide fuel cells. *J. Power Source* **2015**, *273*, 591–599. [CrossRef]
161. Jin, F.; Li, J.; Wang, Y.; Chu, X.; Xu, M.; Zhai, Y.; Zhang, Y.; Fang, W.; Zou, P.; He, T. Evaluation of Fe and Mn co-doped layered perovskite  $\text{PrBaCo}_{2/3}\text{Fe}_{2/3}\text{Mn}_{1/2}\text{O}_{5+\delta}$  as a novel cathode for intermediate-temperature solid-oxide fuel cell. *Ceram. Int.* **2018**, *44*, 22489–22496. [CrossRef]
162. Lee, S.J.; Kim, D.S.; Muralidharan, P.; Jo, S.H.; Kim, D.K. Improved electrochemical performance and thermal compatibility of Fe- and Cu-doped  $\text{SmBaCo}_2\text{O}_{5+\delta}$ - $\text{Ce}_{0.9}\text{Gd}_{0.1}\text{O}_{1.95}$  composite cathode for intermediate-temperature solid oxide fuel cells. *J. Power Source* **2011**, *196*, 3095–3098. [CrossRef]
163. Li, R.; Wang, D.; Ge, L.; He, S.; Chen, H.; Guo, L. Effect of  $\text{Bi}_2\text{O}_3$  on the electrochemical performance of  $\text{LaBaCo}_2\text{O}_{5+\delta}$  cathode for intermediate-temperature solid oxide fuel cells. *Ceram. Int.* **2014**, *40*, 2599–2603. [CrossRef]
164. Tsvetkov, D.S.; Tsvetkova, N.S.; Ivanov, I.L.; Malyshev, D.A.; Sereda, V.V.; Zuev, A.Y.  $\text{PrBaCo}_2\text{O}_{6-\delta}$ - $\text{Ce}_{0.8}\text{Sm}_{0.2}\text{O}_{1.9}$  Composite Cathodes for Intermediate Temperature Solid Oxide Fuel cells. *ECS Transact.* **2015**, *68*, 965–976. [CrossRef]
165. Li, S.; Zhang, L.; Xia, T.; Li, Q.; Sun, L.; Huo, L.; Zhao, H. Synergistic effect study of  $\text{EuBa}_{0.98}\text{Co}_2\text{O}_{5+\delta}$ - $\text{Ce}_{0.8}\text{Sm}_{0.2}\text{O}_{1.9}$  composite cathodes for intermediate-temperature solid oxide fuel cells. *J. Alloys Compd.* **2019**, *771*, 513–521. [CrossRef]
166. Kim, J.-H.; Irvine, J. Characterization of layered perovskite oxides  $\text{NdBa}_{1-x}\text{Sr}_x\text{Co}_2\text{O}_{5+\delta}$  ( $x = 0$  and  $0.5$ ) as cathode materials for IT-SOFC. *Int. J. Hydrogen Energy* **2012**, *37*, 5920–5929. [CrossRef]
167. Kim, J.-H.; Kim, Y.N.; Bi, Z.; Manthiram, A.; Paranthaman, M.P.; Huq, A. Overcoming phase instability of  $\text{RBaCo}_2\text{O}_{5+\delta}$  ( $R = \text{Y}$  and  $\text{Ho}$ ) by Sr substitution for application as cathodes in solid oxide fuel cells. *Solid State Ion.* **2013**, *253*, 81–87. [CrossRef]
168. Idrees, A.; Jiang, X.; Liu, G.; Luo, H.; Zhang, Q.; Jiang, L.; Li, X.; Xu, B. An optimized synthesis route for high performance composite cathode based on a layered perovskite oxide of  $\text{PrBa}_{0.92}\text{Co}_2\text{O}_{6-\delta}$  with cationic deficiency. *Int. J. Hydrogen Energy* **2019**, *44*, 4271–4280. [CrossRef]
169. Idrees, A.; Jiang, X.; Jiang, L.; Zhang, Q. Properties of composite cathodes composed of  $\text{Pr}^{3+}$ -deficient oxide and ionic conductor  $\text{Ce}_{0.8}\text{Sm}_{0.2}\text{O}_{1.9}$ . *Ceram. Int.* **2020**, *46*, 17532–17539. [CrossRef]
170. Rioja-Monnlor, L.; Ricote, S.; Bernuy-Lopez, C.; Grande, T.; O'Hayre, R.; Einarsrud, M.-A. High-Performance  $\text{La}_{0.5}\text{Ba}_{0.5}\text{Co}_{1/3}\text{Mn}_{1/3}\text{Fe}_{1/3}\text{O}_{3-\delta}$ - $\text{BaZr}_{1-z}\text{Y}_z\text{O}_{3-\delta}$  Cathode Composites via an Exsolution Mechanism for protonic Ceramic Fuel Cells. *Inorg.* **2018**, *6*, 83. [CrossRef]
171. Rioja-Monnlor, L.; Bernuy-Lopez, C.; Fontaine, M.-L.; Grande, T.; Einarsrud, M.-A. Microstructural and compositional optimization of  $\text{La}_{0.5}\text{Ba}_{0.5}\text{CoO}_{3-\delta}$ - $\text{BaZr}_{1-z}\text{Y}_z\text{O}_{3-\delta}$  ( $z = 0, 0.05$  and  $0.1$ ) nanocomposite cathodes for protonic ceramic fuel cells. *J. Phys. Energy* **2020**, *2*, 015001. [CrossRef]
172. Choi, M.-B.; Jeon, S.-Y.; Hwang, H.-J.; Park, J.-Y.; Song, S.-J. Composite of  $\text{Ce}_{0.8}\text{Gd}_{0.2}\text{O}_{2-\delta}$  and  $\text{GdBaCo}_2\text{O}_{5+\delta}$  as oxygen separation membranes. *Solid State Ion.* **2010**, *181*, 1680–1684. [CrossRef]
173. Chen, T.; Zhao, H.; Xie, Z.; Feng, L.; Lu, X.; Ding, W.; Li, F. Electrical conductivity and oxygen permeability of  $\text{Ce}_{0.8}\text{Sm}_{0.2}\text{O}_{2-\delta}$ - $\text{PrBaCo}_2\text{O}_{5+\delta}$  dual-phase composites. *Int. J. Hydrogen Energy* **2012**, *37*, 5277–5285. [CrossRef]
174. Liu, X.; Jin, F.; Sun, N.; Li, J.; Shen, Y.; Wng, F.; Li, J.  $\text{Nd}^{3+}$ -deficiency double perovskite  $\text{Nd}_{1-x}\text{BaCo}_2\text{O}_{5+\delta}$  and performance optimization as cathode materials for intermediate-temperature solid oxide fuel cells. *Ceram. Int.* **2021**, *47*, 33886–33896. [CrossRef]
175. Wang, S.-F.; Hsu, Y.-F.; Liao, Y.-L.; Huang, S.-T.; Jasinski, P. High-performance  $\text{NdSrCo}_2\text{O}_{5+\delta}$ - $\text{Ce}_{0.8}\text{Gd}_{0.2}\text{O}_{2-\delta}$  composite cathodes for electrolyte-supported microtubular solid oxide fuel cells. *Int. J. Hydrogen Energy* **2021**, *46*, 31778–31787. [CrossRef]
176. Zhou, Q.; He, T.; He, Q.; Ji, Y. Electrochemical performances of  $\text{LaBaCuFeO}_{5+x}$  and  $\text{LaBaCuCoO}_{5+x}$  as potential cathode materials for intermediate-temperature solid oxide fuel cells. *Electrochem. Commun.* **2009**, *11*, 80–83. [CrossRef]
177. Zhou, Q.; Zhang, Y.; Shen, Y.; He, T. Layered Perovskite  $\text{GdBaCuCoO}_{5+\delta}$  Cathode Material for Intermediate-Temperature Solid Oxide Fuel Cells. *J. Electrochem. Soc.* **2010**, *157*, B628–B632. [CrossRef]
178. Zhu, Z.; Tao, Z.; Bi, L.; Liu, W. Investigation of  $\text{SmBaCuCoO}_{5+\delta}$  as cathode for proton-conducting solid oxide fuel cells. *Mat. Res. Bull.* **2010**, *45*, 1771–1774. [CrossRef]
179. Zhao, L.; Nian, Q.; He, B.; Lin, B.; Ding, H.; Wang, S.; Peng, R.; Meng, G.; Liu, X. Novel layered perovskite oxide  $\text{PrBaCuCoO}_{5+\delta}$  as a potential cathode for intermediate-temperature solid oxide fuel cells. *J. Power Source* **2010**, *195*, 453–456. [CrossRef]
180. Nian, Q.; Zhao, L.; He, B.; Lin, B.; Peng, R.; Meng, G.; Liu, X. Layered  $\text{SmBaCuCoO}_{5+\delta}$  and  $\text{SmBaCuFeO}_{5+\delta}$  perovskite oxides as cathode materials for proton-conducting SOFCs. *J. Alloys Compd.* **2010**, *492*, 291–294. [CrossRef]
181. Ling, Y.; Lin, B.; Zhao, L.; Zhang, X.; Yu, J.; Peng, R.; Meng, G.; Liu, X. Layered perovskite  $\text{LaBaCuMO}_{5+x}$  ( $M = \text{Fe}, \text{Co}$ ) cathodes for intermediate-temperature protonic ceramic membrane fuel cells. *J. Alloys Compd.* **2010**, *493*, 252–255. [CrossRef]
182. Zhou, Q.; Wei, T.; Guo, S.; Qi, X.; Ruan, R.; Li, Y.; Wu, Y.; Liu, Q. Evaluation of  $\text{GdBaCuCo}_{0.5}\text{Fe}_{0.5}\text{O}_{5+\delta}$  as cathode material for intermediate temperature solid oxide fuel cells. *Ceram. Int.* **2012**, *38*, 2899–2903. [CrossRef]

183. Yang, Z.; Ding, Z.; Xiao, J.; Zhang, H.; Ma, G.; Zhou, Z. A novel cobalt-free layered perovskite-type  $\text{GdBaFeNiO}_{5+\delta}$  cathode material for proton-conducting intermediate-temperature solid oxide fuel cells. *J. Power Source* **2012**, *220*, 15–19. [[CrossRef](#)]
184. Jin, F.; Xu, H.; Long, W.; Shen, Y.; He, T. Characterization and evaluation of double perovskites  $\text{LnBaCoFeO}_{5+\delta}$  (Ln = Pr and Nd) as intermediate-temperature solid oxide fuel cell cathodes. *J. Power Source* **2013**, *243*, 10–18. [[CrossRef](#)]
185. Li, L.; Jin, F.; Shen, Y.; He, T. Cobalt-free double perovskite cathode  $\text{GdBaFeNiO}_{5+\delta}$  and electrochemical performance improvement by  $\text{Ce}_{0.8}\text{Sm}_{0.2}\text{O}_{1.9}$  impregnation for intermediate-temperature solid oxide fuel cells. *Electrochim. Acta* **2015**, *182*, 682–692. [[CrossRef](#)]
186. Li, R.; Jin, F.; Zhang, Y.; Niu, B.; Liu, J.; He, T. Performance and optimization of perovskite-type  $\text{La}_{1.4}\text{Ca}_{0.6}\text{CoMnO}_{5+\delta}$  cathode for intermediate-temperature solid oxide fuel cells. *Int. J. Hydrogen Energy* **2019**, *44*, 8467–8478. [[CrossRef](#)]
187. Pang, S.; Su, Y.; Yang, G.; Shen, X.; Zhu, M.; Wu, X.; Li, S.; Yang, X.; Xi, X. Enhanced electrochemical performance of Ca-doped  $\text{NdBa}_{1-x}\text{Ca}_x\text{CoCuO}_{5+\delta}$  as cathode materials for intermediate-temperature solid oxide fuel cells. *Ceram. Int.* **2018**, *44*, 21902–21907. [[CrossRef](#)]
188. Lü, S.; Meng, X.; Fu, X.; Liu, M.; Sui, Y.; Chen, Y.; Cao, J.; Sun, Y.; Ji, Y.; Yang, L. The evolution of structure and electrochemical properties of Y-site deficiency  $\text{Y}_{1-x}\text{BaCoCuO}_{5+\delta}$  cathode for solid oxide fuel cells. *Int. J. Hydrogen Energy* **2020**, *45*, 23227–23236. [[CrossRef](#)]
189. Costilla-Aquillar, S.U.; Escudero, M.J.; Cienfuegos-Pelaez, R.F.; Aguillar-Martinez, J.A. Double perovskite  $\text{La}_{1.8}\text{Sr}_{0.2}\text{CoFeO}_{5+\delta}$  as a cathode material for intermediate temperature solid oxide fuel cells. *J. Alloys Compd.* **2021**, *862*, 158025. [[CrossRef](#)]
190. Jin, F.; Liu, X.; Chu, X.; Shen, Y.; Li, J. Effect of nonequivalent substitution of  $\text{Pr}^{3+/4+}$  with  $\text{Ca}^{2+}$  in  $\text{PrBaCoFeO}_{5+\delta}$  as cathodes for IT-SOFC. *J. Mater. Sci.* **2021**, *56*, 1147–1161. [[CrossRef](#)]
191. Hashim, S.S.; Liang, F.; Zhou, W.; Sunarso, J. Cobalt-Free Perovskite Cathodes for Solid Oxide Fuel Cells. *Chem. Electro. Chem.* **2019**, *6*, 3549–3569. [[CrossRef](#)]
192. Chen, D.; Wang, F.; Shi, H.; Ran, R.; Shao, Z. Systematic evaluation of Co-free  $\text{LnBaFe}_2\text{O}_{5+\delta}$  (Ln = Lanthanides or Y) oxides towards the application as cathodes for intermediate-temperature solid oxide fuel cells. *Electrochim. Acta* **2012**, *78*, 466–474. [[CrossRef](#)]
193. Li, F.; Tao, Z.; Dai, H.; Xi, X.; Ding, H. A high-performing proton-conducting solid oxide fuel cell with layered perovskite cathode in intermediate temperatures. *Int. J. Hydrogen Energy* **2018**, *43*, 19757–19762. [[CrossRef](#)]
194. Li, H.; Lü, Z. A highly stable cobalt-free  $\text{LaBa}_{0.5}\text{Sr}_{0.5}\text{Fe}_2\text{O}_{6-\delta}$  oxide as a high performance cathode material for solid oxide fuel cells. *Int. J. Hydrogen Energy* **2020**, *45*, 19831–19839. [[CrossRef](#)]
195. Zhang, Y.; Niu, B.; Hao, X.; Wang, Y.; Liu, J.; Jiang, P.; He, T. Layered oxygen-deficient double perovskite  $\text{GdBaFe}_2\text{O}_{5+\delta}$  as electrode material for symmetrical solid-oxide fuel cells. *Electrochim. Acta* **2021**, *370*, 137807. [[CrossRef](#)]
196. Li, H.; Lü, Z. High-performance fluorine-doped cobalt-free oxide as a potential cathode material for solid oxide fuel cells. *Int. J. Hydrogen Energy* **2021**, *46*, 2503–2510. [[CrossRef](#)]
197. Kim, D.; Son, S.J.; Kim, M.; Park, H.J.; Joo, J.H.  $\text{PrBaFe}_2\text{O}_{5+\delta}$  promising electrode for redox-stable symmetrical proton-conducting solid oxide fuel cells. *J. Eur. Ceram. Soc.* **2021**, *41*, 5939–5946. [[CrossRef](#)]
198. Son, S.J.; Kim, D.; Park, H.J.; Joo, J.H. Investigation of oxygen ion transport and surface exchange properties of  $\text{PrBaFe}_2\text{O}_{5+\delta}$ . *J. Eur. Ceram. Soc.* **2021**, *41*, 2691–2698. [[CrossRef](#)]
199. García-García, F.J.; Sayagués, M.J.; Gotor, F.J. Novel, Simple and Highly Efficient Route to Obtain  $\text{PrBaMn}_2\text{O}_{5+\delta}$  Double Perovskite: Mechanochemical Synthesis. *Nanomaterials* **2021**, *11*, 380. [[CrossRef](#)] [[PubMed](#)]
200. Kudryakova, V.S.; Shalamova, A.M.; Chukin, A.V.; Suntsov, A.Y. Enhanced thermal stability and red-ox activity of  $\text{PrBaMn}_{2-x}\text{Fe}_x\text{O}_{6-\delta}$  oxides. *Mat. Res. Bull.* **2021**, *140*, 111309. [[CrossRef](#)]
201. Zhu, J.; Zhang, W.; Li, Y.; Yue, W.; Geng, G.; Yu, B. Enhancing  $\text{CO}_2$  catalytic activation and direct electroreduction on in-situ exsolved  $\text{Fe}/\text{MnO}_x$  nanoparticles from  $(\text{Pr,Ba})_2\text{Mn}_{2-y}\text{Fe}_y\text{O}_{5+\delta}$  layered perovskites for SOEC cathodes. *Appl. Catal. B Environ.* **2020**, *268*, 118389. [[CrossRef](#)]
202. Fu, R.; Jiang, P.; Xu, H.; Niu, B.; Jiang, F.; Yang, L.; Feng, T.; He, T. Performance of Pd-impregnated  $\text{Sr}_{1.9}\text{FeNb}_{0.9}\text{Mo}_{0.1}\text{O}_{6-\delta}$  double perovskite as symmetrical electrodes for direct hydrocarbon solid oxide fuel cells. *Int. J. Hydrogen Energy* **2019**, *44*, 31394–31405. [[CrossRef](#)]
203. Zhu, Z.; Zhou, C.; Zhou, W.; Yang, N. Textured  $\text{Sr}_2\text{Sc}_{0.1}\text{Nb}_{0.1}\text{Co}_{1.5}\text{Fe}_{0.3}\text{O}_{6-2\delta}$  Thin Film Cathodes for IT-SOFCs. *Materials* **2019**, *12*, 777. [[CrossRef](#)]
204. Gómez-Pérez, A.; Azcondo, M.T.; Yuste, M.; Pérez-Flores, J.; Bonanos, N.; Porcher, F.; Muñoz-Noval, A.; Hoelzel, M.; García-Alvarado, F.; Amador, U. The A-cation deficient perovskite series  $\text{La}_{2-x}\text{CoTiO}_{6-\delta}$  ( $0 \leq x \leq 0.20$ ): New components for potential SOFC composite cathodes. *J. Mater. Chem. A* **2016**, *4*, 3386–3397. [[CrossRef](#)]
205. Yue, Z.; Jiang, L.; Ai, N.; Guan, C.; Jiang, S.P.; Sun, X.; Rickard, W.D.A.; Wang, X.; Shao, Y.; Chen, K. Facile co-synthesis and utilization of ultrafine and highly active  $\text{PrBa}_{0.8}\text{Ca}_{0.2}\text{Co}_2\text{O}_{5+\delta}$ - $\text{Gd}_{0.2}\text{Ce}_{0.8}\text{O}_{1.9}$  composite cathodes for solid oxide fuel cells. *Electrochim. Acta* **2022**, *403*, 139673. [[CrossRef](#)]
206. Tolstov, K.Y.; Politov, B.V.; Zhukov, V.P.; Chulkov, E.V.; Kozhevnikov, V.L. The impact of atomic defects on high-temperature stability and electron transport properties in  $\text{Sr}_2\text{Mg}_{1-x}\text{Ni}_x\text{MoO}_{6-\delta}$  solid solutions. *J. Alloys Compd.* **2021**, *883*, 160821. [[CrossRef](#)]
207. Wu, M.; Li, H.; Ma, S.; Chen, S.; Xiang, W. Boosting the surface oxygen activity for high performance Iron-based perovskite oxide. *Sci. Total Environ.* **2021**, *795*, 148904. [[CrossRef](#)]

208. Sednev-Lugovets, A.L.; Sereda, V.V.; Malyshkin, D.A.; Tsvetkov, D.S.; Ivanov, I.L.; Zuev, A.Y.; Maignan, A. Defect chemistry and high-temperature thermodynamics of  $\text{PrBaCo}_2\text{O}_{6-\delta}$ . *J. Chem. Thermodynam.* **2021**, *161*, 106523. [[CrossRef](#)]
209. Gumeci, C.; Parrondo, J.; Hussain, A.M.; Thompson, D.; Dale, N. Praseodymium based double-perovskite cathode nanofibers for intermediate temperature solid oxide fuel cells (IT-SOFC). *Int. J. Hydrogen Energy* **2021**, *46*, 71798–71806. [[CrossRef](#)]
210. Sereda, V.V.; Malyshkin, D.A.; Ivanov, I.L.; Tsvetkov, D.S.; Zuev, A.Y.; Maignan, A. Redox Thermochemistry, Thermodynamics, and Solar Energy Conversion and Storage Capability of Some Double Perovskite Cobaltites. *Inorg. Chem.* **2021**, *60*, 18141–18153. [[CrossRef](#)]
211. Vinoth Kumar, R.; Khandale, A.P. A review on recent progress and selection of cobalt-based cathode materials for low temperature-solid oxide fuel cells. *Renew. Sust. Energy* **2022**, *156*, 111985. [[CrossRef](#)]